Sulphide Self-Heating:
Moisture Content and Sulphur Formation

Sarah Jung

Department of Mining and Materials Engineering

McGill University

Montreal, Canada

July 2012

A thesis submitted to McGill University

in partial fulfillment of the requirements of the degree of

Master of Engineering

Abstract

Spontaneous or self-heating of sulphides can occur under certain conditions of moisture, temperature and oxygen concentration. This can lead to emission of toxic gases such as SO_2 and if uncontrolled, to ignition. Research has established that self-heating divides into three stages: A (below 100 ^oC), B (above 100 ^oC) and C (above 350 ^oC). The understanding is that conditions in stage A promote oxidation of sulphides to elemental sulphur which in stage B oxidizes to SO_2. A standard test based on air injections is used to measure stage A and stage B self-heating.

In this thesis, a mitigation method using hygroscopic reagents to control moisture has been tested on a pyrrhotite-rich material. Water retention capacity was determined to select reagents for application in the standard self-heating test. Tests showed that the water retention capacity correlated with mitigation of self-heating. Two reagents that showed the best mitigating effect were silica gel and poly (acrylic acid sodium salt).

It is hypothesized that temperature and relative humidity have an effect on elemental sulphur production in stage A. To test, pyrrhotite ($Fe_{1-x}S$) samples were exposed (weathered) at temperatures of 40 ^oC and 60 ^oC and relative humidities of 100%, 70% and 30% for 31 days. The weathering apparatus and sulphur analysis method are described. At the end of weathering (31 days), samples were

subjected to stage B self-heating test. Self-heating rate and total number of air injections until heating ceased were determined. Both measurements showed that sulphur formed at 40 ^{o}C in stage A gave higher heating response than sulphur formed at 60 ^{o}C. This observation raises two possibilities that are discussed: there are different types of sulphur formed at the two temperatures; and there is a factor other than just sulphur content that controls stage B self-heating.

Résumé

L'autochauffage spontané des sulfures peut se produire sous certaines conditions d'humidité et d'oxygène. Cela peut entraîner l'émission de gaz toxiques tel que le SO_2. Si l'autochauffage n'est pas contrôlé, la combustion peut se produire spontanément. La recherche a établi que l'autochauffage se divise en trois étapes, soit : l'étape A (en dessous de 100 ^oC), l'étape B (plus de 100 ^oC) et l'étape C (plus de 350 ^oC). Nous comprenons que l'oxydation des sulfures en soufre élémentaire survient lors de l'étape A. Le soufre élémentaire s'oxyde pour produire le SO_2 dans l'étape B. L'autochauffage lors des étapes A et B est mesuré en utilisant un test standard qui injecte l'air dans les échantillons.

Dans ce mémoire, la méthode testée pour l'atténuation des sulfures autochauffantes consistait à contrôler l'humidité en utilisant des produits hygroscopiques sur des échantillons riches en pyrrhotite. Le facteur de sélection des produits hygroscopiques utilisés lors des tests d'autochauffage était leur capacité de rétention d'eau. Les tests ont montré qu'il y a une corrélation entre la rétention d'eau et l'atténuation d'autochauffage. Le gel de silice et le polymère superabsorbant ont montré le meilleur effet d'atténuation.

L'hypothèse émise était que la température et l'humidité relative ont un effet sur la production de soufre élémentaire lors de l'étape A. Pour vérifier l'hypothèse, l'échantillon de pyrrhotite ($Fe_{1-x}S$) était exposé (érodée) à des températures de 40 ^oC et 60 ^oC et à une humidité relative de 100%, 70%, 30% pendant 31 jours.

L'appareil d'érosion et la procédure d'analyse de soufre ont été décrits dans ce document. Suite à l'étape A (31 jours), les échantillons étaient soumis lors de l'étape B à un test d'autochauffage. Le taux d'autochauffage et le nombre total d'injections d'air avant que le chauffage cesse ont été déterminés. Les deux mesures ont démontré que le soufre qui est formé à 40 ^{o}C lors de l'étape A a donné une réponse de chauffage plus élevée que le soufre qui est formé à 60 ^{o}C. Cette observation permet de conclure à deux possibilités qui seront discutées : premièrement, des types de soufre différents se forment aux deux températures et deuxièmement, il y a un autre facteur d'autochauffage que la formation de soufre qui contrôle l'étape B.

Acknowledgements

I would like to thank the following people for their help and support during my time spent at McGill University:

Professor Finch, thank you for giving me the opportunity to work under your supervision, for the encouragement, motivation and inspiration.

Thanks to Mr. Frank Rosenblum, Dr. Jan Nesset, Dr. S. Ramachandra Rao for your support, dedication, patience, discussions and ideas.

To Mr. Ray Langlois, Ms. Monique Riendeau, Mr. Andrew Golsztajn, Mr. Ranjan Roy, thank you for the training, the help in the laboratory and for your ideas.

I would like to thank the sponsors CAMIRO MPD (Vale, Teck, Xstrata Zinc, Xstrata Process Support, Golder Associates and Cytec), NSERC (Natural Sciences and Engineering Research Council of Canada) for supporting this project.

Thanks to the Mineral Processing Group for your friendship and the good times.

To my family and friends, thank you for believing in me and providing me with lots of love and encouragement.

Table of Content

List of Figures

List of Tables

Chapter 1 Introduction

1.1 Sulphide self-heating

In the mining and mineral processing industry, sulphide minerals can spontaneously heat or self-heat (i.e., heat without external heat input) under certain conditions. Self-heating occurs due to exothermic oxidation reactions. In metal sulphides the sulphur is in its lowest oxidation state (S^{2-}). Sulphide minerals, examples being pyrite (FeS_2), pentlandite ($Ni_{4.9}Fe_{4.45}S_8$) and chalcopyrite ($CuFeS_2$), are the major source of base metals. One sulphide in particular, pyrrhotite ($Fe_{1-x}S$), is known to undergo self-heating readily (Rosenblum and Spira 1995). Samples containing more than 10% pyrrhotite are especially prone to self-heating (Somot 2006). Under extreme conditions self-heating can lead to ignition.

Self-heating of sulphides has been observed for centuries and can occur underground, in concentrates and tailings (Ninteman 1978). Toxic gases such as hydrogen disulphide (H_2S) and sulphur dioxide (SO_2) are emitted endangering the lives of workers (Somot and Finch 2010). There have suspected loss of ships due to combustion of sulphide cargo; such a case was documented for a Chilean ship carrying copper ore in 1862 (Kirshenbaum 1967). A widely known Canadian example is the underground fire that occurred at the Sullivan Mine in Kimberly, British Colombia (Good 1977), featured on the front cover of the June 1977 issue of the CIM Bulletin (Figure 1.1).

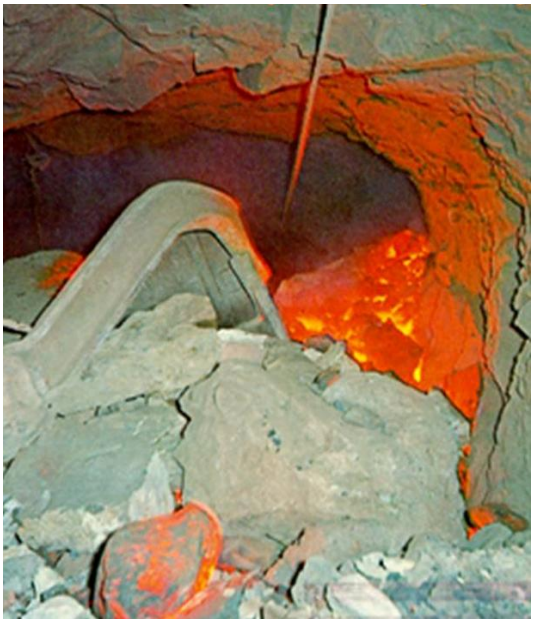

Figure 1.1: Underground sulphide mine fire in Kimberly, BC (CIM Bulletin, 1977)

Different methods of measuring self-heating have been proposed over the years. A self-heating test facility, first developed at Noranda Technology Center by Rosenblum and co-workers (Rosenblum and Spira 1995; Rosenblum et al. 2001), is now established in the Department of Mining and Materials Engineering, McGill University. Self-heating has been determined to be a 3-stage process: stage A (below 100 ^{o}C), stage B (above 100 ^{o}C) and stage C (above 350 ^{o}C) (Rosenblum and Spira 1995; Rosenblum et al. 2001). Reaction mechanisms have been proposed relating self-heating to direct oxidation of sulphides, formation and oxidation of elemental sulphur and formation and reaction of hydrogen sulphide (Somot and Finch 2010).

Research has shown that self-heating is triggered under certain levels of moisture and oxygen. Moisture in the range 3 – 8% appears to give the highest self-heating

response (Rosenblum and Spira 1995). One purpose of this thesis is to determine if self-heating can be mitigated by using hygroscopic agents to control sample moisture. Stage B self-heating is usually associated with elemental sulphur. Thus the second purpose of this thesis is to determine factors leading to sulphur formation in stage A.

1.2 Objectives

This thesis has two objectives:

I. To mitigate self-heating with the addition of hygroscopic reagents to control moisture content.

II. To determine the dependence of sulphur formation in stage A on temperature and sample moisture content, and the dependence of stage B self-heating on sulphur content.

1.3 Thesis organization

The thesis consists of six chapters. Chapter one is an introduction to sulphide self-heating along with the objectives and thesis organization. Chapter two is the literature review where different methods of evaluating self-heating are discussed along with background information. Chapter three describes the experimental methods and how test work was conducted for this thesis work. Chapter four presents the results with discussion in Chapter five. Chapter six is the conclusions and recommendations. Additional figures and tables are shown in the Appendix.

Chapter 2 Literature Review

2.1 Methods for evaluating sulphide self-heating

2.1.1 Good (1977)

Among the first techniques to assess spontaneous heating of sulphides was one developed by Good (1977) for Cominco at the Sullivan Mine in Kimberly, BC. Samples of -200 mesh (0.075mm) were subjected to oxidation and combustion tests. Oxidation was carried out by placing twenty five gram samples on a watch glass and subjecting them to repeated wetting and drying. Color changes observed corresponded with oxidation over time. Combustion tests were carried out by placing two gram samples in an apparatus designed to determine the ignition temperature (Figure 2.1). The sample was heated under a steady stream of oxygen. The sample temperature was monitored by a thermocouple connected to a strip-chart recorder. Sulphur dioxide emissions up to the point of ignition were also monitored. Typical sample heating and corresponding sulphur dioxide emission curves are shown in Figure 2.2. Ignition temperatures ranged from 205 ^{o}C to 515 ^{o}C with most of the samples being in the 385 ^{o}C and 450 ^{o}C range (Good 1977).

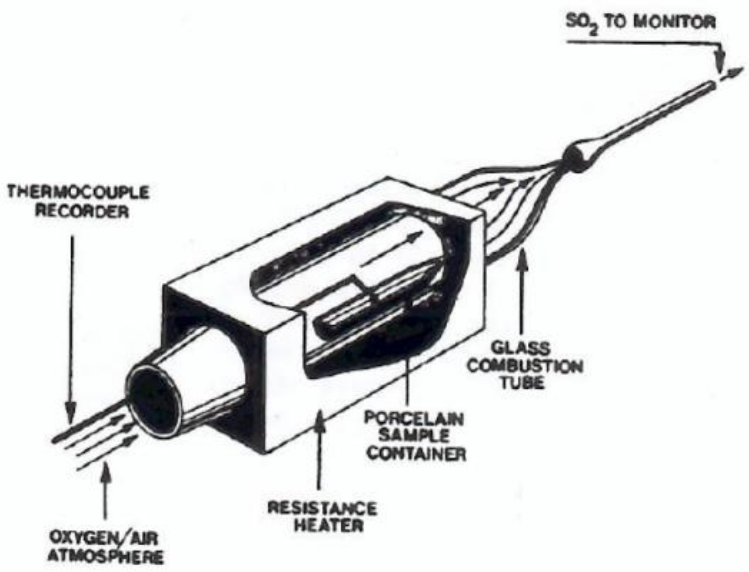

Figure 2.1: Self-heating test apparatus (Good 1977)

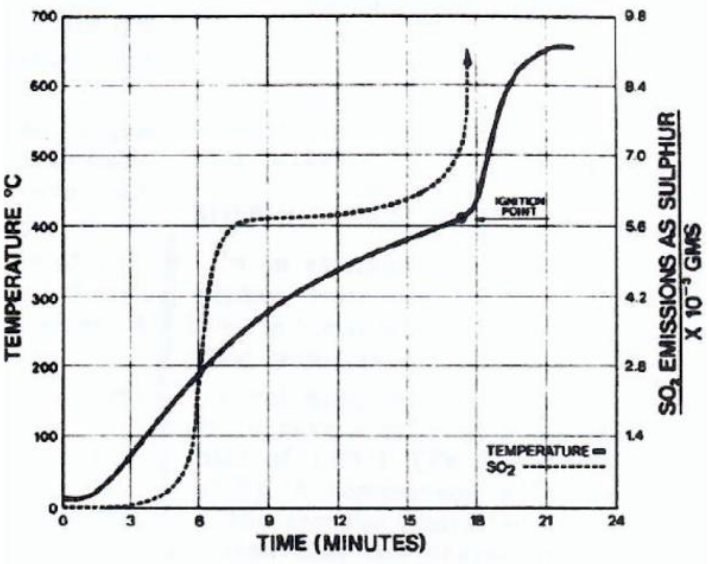

Figure 2.2: Typical heating curve and SO2 emissions from combustion test apparatus (Good 1977)

2.1.2 Wu and Li (2005)

A method for predicting spontaneous sulphide ore combustion at ambient temperature by determining the relationship between sample weight gain and oxygen absorption was described by Wu and Li (2005). For weight gain, samples -40 mesh (0.45mm) were placed in a constant humidity chamber at a temperature of 40 ^{o}C and 90% relative humidity. Samples were weighed periodically over 4 to 10 days. Sulphate and water-soluble iron ions present in the sample were analyzed. For oxygen absorption, 100g samples were placed in a sealed container containing a known volume of air. The container was placed in an isothermal water trough. The amount of oxygen absorbed by the sample was measured periodically. It was found that there was a linear relationship between the oxygen uptake and weight gain in the sample, suggesting a reaction had taken place (Wu and Li 2005). However, while weight increment suggests reactivity, it is not an accurate prediction of spontaneous heating risk as the rate of oxidation is not equivalent to self-heating (Wang 2007).

2.1.3 Iliyas et al. (2011)

A method for analyzing self-heating using thermal methods has been designed by Iliyas et al. (2011). The reactions occurring when sulphide minerals are exposed to oxidising conditions were analysed using differential scanning calorimetry (DSC) (Figure 2.3) and thermal gravimetric analysis (TGA). As an example, ore samples from the Reid Brook deposit (Vale) were exposed to increasing heating

rates of 1, 2, 4 and 8 $^{o}C\ min^{-1}$ and reaction rates were calculated using the advanced thermokinetic software package (AKTS). This information was plotted on a "self-heating diagram" to predict the reaction of the sample at a certain time and on a "safety diagram" to depict safe and unsafe zones (Figure 2.4, Figure 2.5).

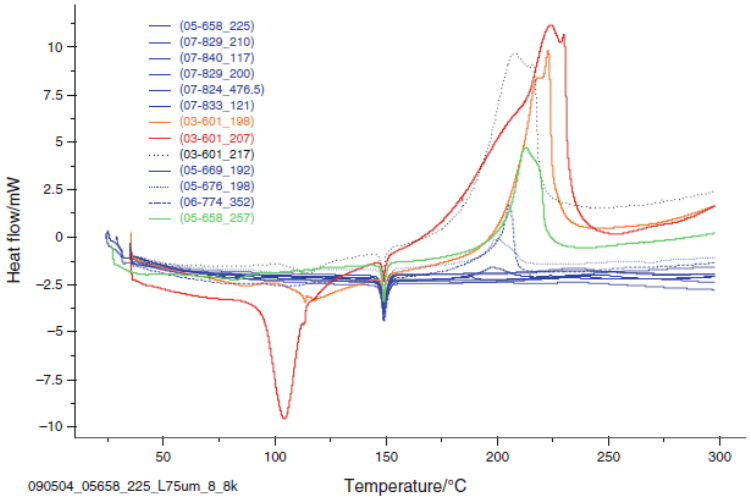

Figure 2.3: Typical DSC signals from oxidized ore samples (Iliyas et al. 2011)

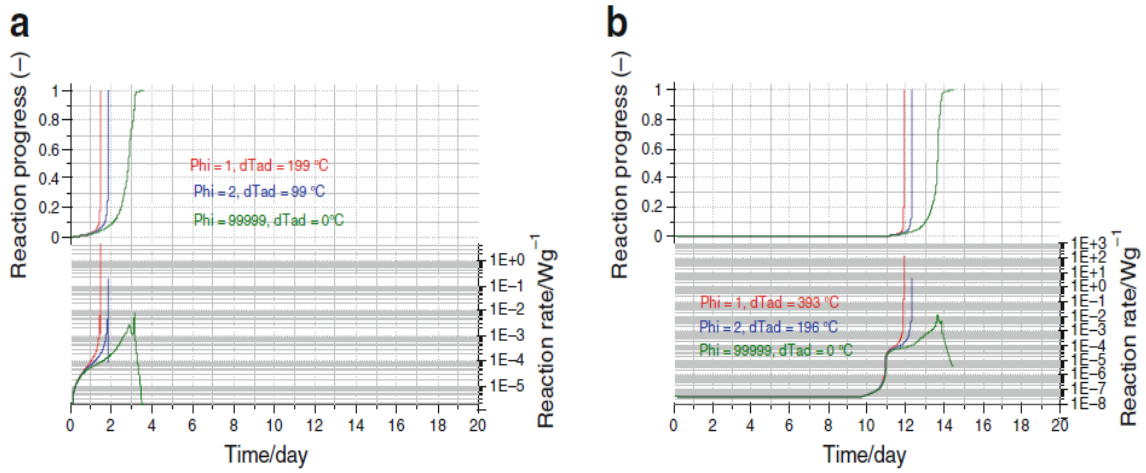

Figure 2.4: Predicted self-heating diagrams of a quick reacting ore sample (a) and delayed reacting ore sample (b) (Iliyas et al. 2011)

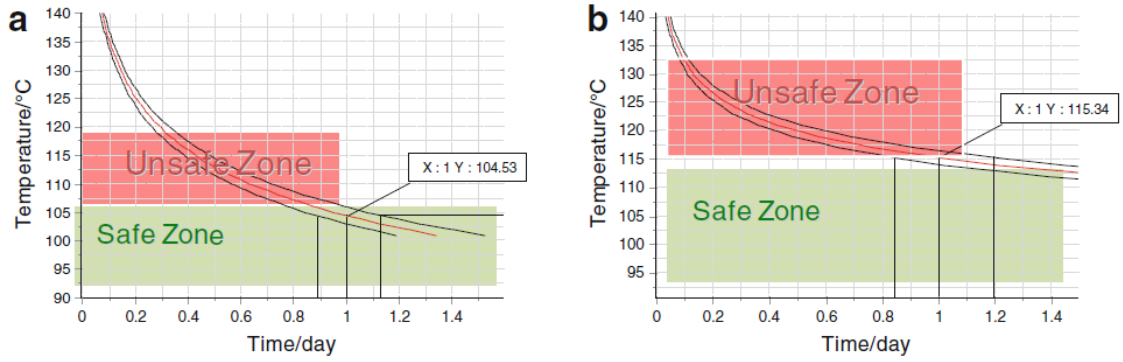

Figure 2.5: Predicted safety diagrams for ore sample a and b (Iliyas et al. 2011)

Another method for determining the thermal stability of a sample is by examining thermal degradation. This is done by determining the self-accelerating decomposition temperature (SADT). Information was obtained using the DSC and the AKTS software and projected a 3D-simulated timeline of a self-heating

material (Figure 2.6). This allowed the prediction of self-heating tendencies of a sample.

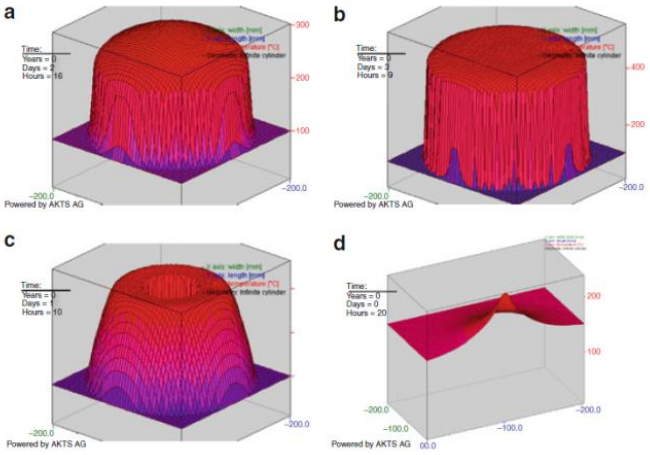

Figure 2.6: 3-D simulations of self-heating in a sample (Iliyas et al. 2011)

2.1.4 Yang et al. (2011)

Self-heating behaviour has been investigated using the crossing-point temperature (CPT) method. Yang et al. (2011) developped a method where a sample of -200 µm held in a cylindrical wire-mesh basket was placed in a chamber with recirculating air at controlled temperatures up to 300 ^{o}C. As shown in Figure 2.7, two thermocouples were inserted in the basket to measure the sample temperature at the center (T1) and at a position 10 mm away from the center (T2). Another thermocouple was placed outside the basket to measure the ambient temperature. The thermocouples were connected to a data logger thermometer which was linked to a computer. The surface of the sample will generally heat faster than the

middle (T2 > T1). If the sample is prone to self-heating, the center and surface will reach equilibrium and the center will eventually surpass the surface temperature. The crossing point temperature is used to indicate self-heating tendency. The self-heating rate is taken as the rate of temperature change with respect to time at the center of the sample (Chen and Chong 1998).

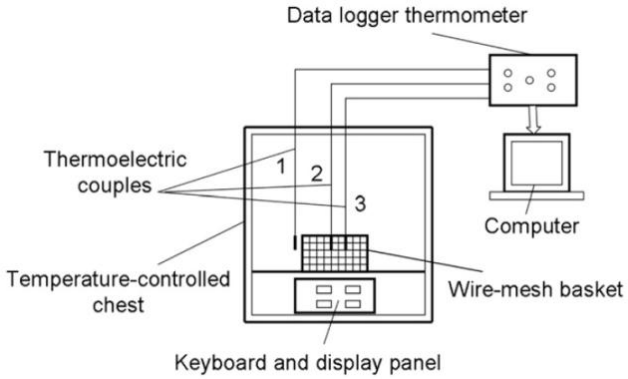

Figure 2.7: Typical experimental set-up for crossing-point temperature (Yang et al. 2011)

2.1.5 Mahadevan-Ramlu (MR) index

A variation on the CPT method is to use the Mahadevan-Ramlu index (MR index). The index takes into account the CPT as well as the inflection-point temperature (IPT), which is the point where temperature begins to increase rapidly with time. The MR index can be defined as (Nelson and Chen 2007):

$$MR\ index = \frac{time\ to\ reach\ CPT}{heating\ rate\ at\ CPT} \times \frac{average\ heating\ rate\ between\ IPT\ and\ CPT}{time\ to\ reach\ IPT} \times 10 \quad (2.1)$$

2.1.6 Feng, Chakravorty, Cochrane (FECC) index

Another variation is to use the FCC (Feng, Chakravorty, Cochrane) index proposed by Feng et al. (1973). The average heating rate of the sample was taken at temperatures between 110 ^{o}C and 220 ^{o}C in order to ensure that all the moisture has evaporated and to limit the evolution of volatile material. The FCC index is defined as (Feng et al. 1973):

$$FCC\ index = \frac{average\ heating\ rate\ between\ 110\ ℃\ and\ 220\ ℃}{CPT} \quad (2.2)$$

2.1.7 WITS-EHAC index

A third variation is the WITS-EHAC (Explosion Hazards Advisory Committee) index proposed by Gouws and Wade (1989). This index takes into account the measured CPT as well as the slope where the temperature difference increases linearly with time and is defined as:

$$WITS - EHAC\ index = 500 \times \frac{\frac{\partial T}{\partial t}\Big|_{T=CPT}}{CPT} \quad (2.3)$$

These three indices (MR, FECC, WITS-EHAC) can be compared with a risk assessment classification (Table 2.1) proposed by Güyagüler et al. (2003).

Table 2.1: Risk classification levels for CPT methods (Güyagüler et al. 2003)

Risk Classification	MR Index	FCC Index	WITS-EHAC Index
Low	0 to 10	0 to 5	0 to 2.5
Medium	10 to 20	5 to 10	2.5 to 5
High	>20	>10	>5

2.1.8 United Nations risk categories

The United Nations (UN) Recommendation on Transport of Dangerous Goods has categorized sulphide materials as Class 4-Flammable solids: substances liable to spontaneous combustion which, in contact with water, emit flammable gases. There are 3 sub-categories: Flammable solids and self-reactive substances (Division 4.1); pyrophoric solids, pyrophoric liquids and self-heating substances (Division 4.2); and substances which in contact with water emit flammable gases (Division 4.3). Sulphide minerals fall in Division 4.2 and are categorized as materials that ignite when in contact with air after long periods of time (hours or days). The basket test is recommended by the UN to classify a material. In the basket test, a powder sample of 100 mm^3 is held in a cubic stainless steel mesh basket and placed in an oven at 140 ^oC for 24 hours. The temperature of the oven and the sample are recorded simultaneously with one thermocouple placed in the center of the sample and another at the oven wall. If the sample temperature is 60

^{o}C higher than that of the oven temperature, this is registered as a positive result for spontaneous combustion. If a positive test is obtained, a 25 mm^3 sample is tested again at 140 ^{o}C for 24 hours. A second positive would result in the sample being assigned to Packaging Group II. A negative test would result in the sample being assigned to Packaging Group III where the sample does not pose a threat (UnitedNations 2011). The methodology is presented in a flow sheet (Figure 2.8).

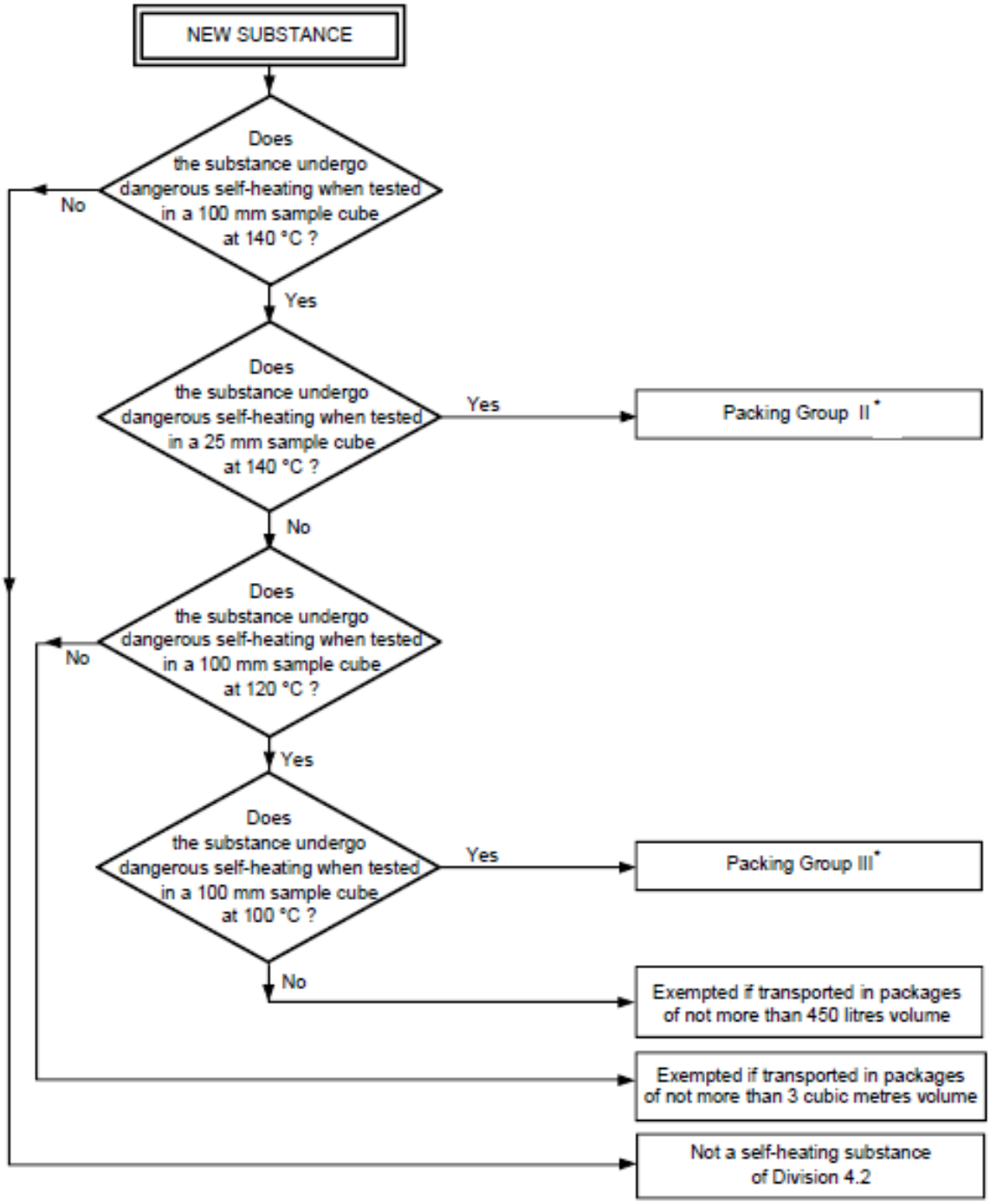

Figure 2.8: Classification of self-heating substances (UnitedNations 2008)

2.1.9 Rosenblum and Spira (1981)

A self-heating test was developed by Rosenblum and Spira (1981) at the Noranda Technology Center (NTC). An apparatus was designed to measure temperature-rise of the sample. This allowed for direct measurement of self-heating under controlled conditions (temperature, oxygen) (Figure 2.9). One kg samples containing approximately 2-15 weight % moisture were held in a one-liter beaker which was placed in a five-liter Dewer flask held inside a Styrofoam block. The vessel was surrounded by a copper shield with a heating coil to maintain a controlled temperature of 40 ± 0.2 ^{o}C at atmospheric conditions. A differential thermocouple was placed in the center of the sample to measure the temperature with reference to the copper shield temperature. The rate of oxygen consumption was measured. Consumed oxygen was replenished by an automatic trigger to restore target conditions. The equilibrium temperature inside the Dewer flask was 38.5 ^{o}C. A sample that maintains this temperature is considered to be an inert sample. If the temperature increases beyond this temperature, the sample is considered to undergo autogeneous heating (self-heating). The temperature rise was measured over time to calculate self-heating rate (^{o}C/hr).

A shortcoming of the method is that the sample must be preheated to 28 ^{o}C before placing in the Dewer flask. The sample mass also affected the self-heating rate. It was found that a 0.5 kg sample gave a higher self-heating rate (by 40%) than a 1 kg sample. This is attributed to the entire bulk of the smaller sample

contributing to the heat production whereas the bottom part of the larger sample acted as a heat sink (Rosenblum and Spira 1981).

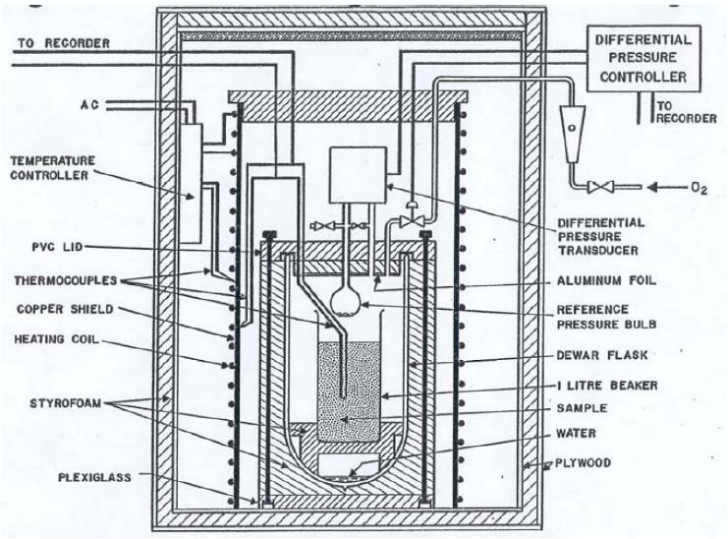

Figure 2.9: Temperature-rise apparatus (Rosenblum and Spira 1981)

Improvements lead to development of the standard self-heating apparatus (Rosenblum and Spira 1995; Rosenblum et al. 2001). Experience had established that self-heating is best considered as a 3-stage process: stage A (below 100 ^{o}C), stage B (above 100 ^{o}C) and stage C (above 350 ^{o}C, equivalent to ignition) and the standard test considered stages A and B. The units built at the NTC were transferred to McGill University in 2003. This set-up is explained in detail in Chapter 3.

2.1.10 Weathering

Weathering is an extended stage A test where moisture, oxygen level and temperature are varied. A weathering test was devised by Wang et al. (2007)

(Figure 2.10). The set-up consisted of a 500 g sample placed inside a reaction vessel sealed with a lid. The chamber was then placed in an oven set at 40 ^{o}C. To vary oxidation level, the lid either had no holes, three holes or 128 holes. The weights of the sample and colour changes were recorded periodically. There was a speculation that self-heating involved formation of hydrogen sulphide (H_2S) (Somot 2006), therefore some tests involved placing a copper piece over the top of the sample to detect H_2S as black Cu_2S (Wang 2007).

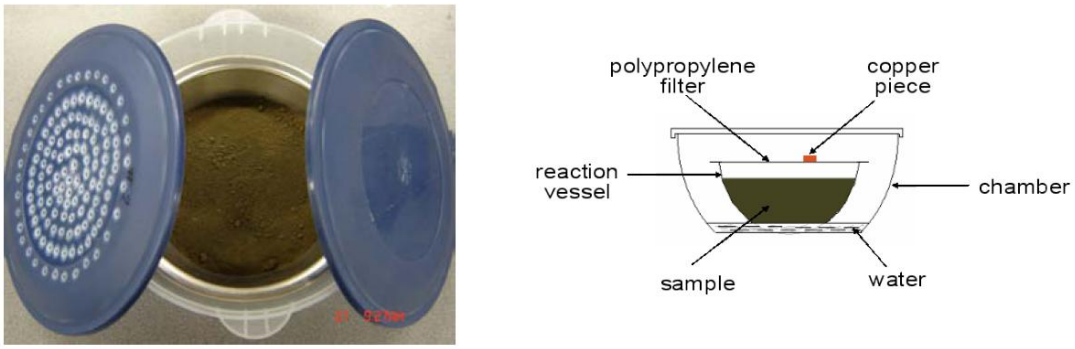

Figure 2.10: Schematic of the weathering test and lid with and without holes (Wang 2007)

Subsequently, a weathering apparatus was built which allowed for control of oxygen content, temperature and relative humidity (Wang et al. 2009). This apparatus is described in Chapter 3.

2.2 Factors affecting self-heating

Studies have shown that there are several factors affecting sulphide self-heating. Some key parameters are: pyrrhotite content in sample, moisture content of sample, oxygen content of air, temperature, particle size, galvanic interactions, presence of bacteria and pH of moisture (Shaw et al. 1998).

2.2.1 Pyrrhotite

Pyrrhotite (Po) is a common iron sulphide mineral (Belzile et al. 2004; Cruz et al. 2005). Sulphide deposits containing pyrrhotite are found in Russia, China, Australia and Canada (Belzile et al. 2004). In the presence of moisture, pyrrhotite is one of the most reactive sulphide minerals (Ninteman 1978). Its reactivity causes many problems in the mining industry such as acid mine drainage (AMD) as well as spontaneous combustion (self-heating). Present in tailings and in concentrates, it can cause problems during storage and transportation.

Pyrrhotite has a non-stoichiometric composition of $Fe_{1-x}S$, where x varies from 0 (FeS) to 0.125 (Fe_7S_8) due to a system of ordered vacancies throughout the Fe lattice (Thomas et al. 2000; Belzile et al. 2004). Pyrrhotite is found in three forms: troilite (seen in certain nickel ore deposits), monoclinic (magnetic) and hexagonal (non-magnetic). Monoclinic and hexagonal pyrrhotites are the more common (Becker et al. 2010). They usually co-exist and pure monoclinic or hexagonal pyrrhotites are rarely found. Monoclinic pyrrhotite is also known as 4C pyrrhotite and has a composition of Fe_7S_8. Non-magnetic pyrrhotite is known

as NC pyrrhotite and has a composition ranging from Fe_9S_{10}, $Fe_{10}S_{11}$ to $Fe_{11}S_{12}$ (Powell et al. 2004; Becker 2009). There is a suggestion that the hexagonal variety oxidizes more readily than the monoclinic (Vaughan et al. 1971; Belzile et al. 2004). Becker et al. (2010), however, found that hexagonal Po is less readily oxidized than monoclinic Po. Some studies have shown there is a greater presence of oxygen-rich phases in monoclinic pyrrhotite indicating a higher oxidation rate (Graham and McKenzie 1987). It is likely that slight variations in the F:S ratio affect the reactivity of the mineral (Ninteman 1978). Microprobe studies have shown that pyrrhotite from Xstrata Nickel's Strathcona mill feed (Sudbury) has a composition ranging from $Fe_{0.85}S$ to $Fe_{0.88}S$, making it mostly monoclinic (Wang 2007).

When pyrrhotite is in an oxidizing environment, a spare sulphur is given off thus acting as a fuel for self-heating (Good 1977). This means that there is an excess of sulphur over iron that can react with oxygen to promote self-heating (Thomas et al. 2000). In comparison to pyrite (FeS_2), the other common iron sulphide, pyrrhotite oxidizes 20-100 times faster (Shaw et al. 1998; Belzile et al. 2004). It is proposed that when pyrrhotite is in an oxidizing environment, Fe diffuses outward to form an iron-oxyhydroxide layer at the air/solid interface (Buckley 1985; Pratt et al. 1994). The depletion of Fe forms a sulphur-rich (polysulphide) layer which contributes to self-heating (Mycroft et al. 1995).

Pyrrhotite can be expressed as $Fe_{n-1}S_n$ where $n \geq 8$ (Fe_7S_8, $Fe_{11}S_{12}$) (Belzile et al. 2004). Due to its non-stoichiometric composition, there is an iron deficiency and the presence of Fe^{3+} is considered to contribute to its high reactivity.

The fundamental mechanism and chemistry of pyrrhotite oxidation is not well understood and speculations have been offered (Mycroft et al. 1995). Pyrrhotite oxidation is discussed further in section 2.5.

2.2.2 Moisture and Oxygen

Studies have shown that reactive sulphide samples exhibit self-heating in the presence of moisture (H_2O) at temperatures < 100 ^oC. The action of moisture could be as a reactant, as a catalyst or because it acts as a solvent to remove reaction products, allowing newly exposed sulphide to undergo further oxidation (Kirshenbaum 1967; Ninteman 1978; Rosenblum et al. 1982).

A certain range of moisture, typically 3 to 8 weight %, gives the highest self-heating response, as shown in Figure 2.11. The decrease in self-heating above this moisture range may be because there is sufficient water to absorb the heat energy by evaporation; at moisture levels below 2 wt %, self-heating may be prevented because the water evaporates too quickly and is lost. Interestingly, it is recommended to store sulphide tailings under water (~1m) to retard oxidation (Tremblay 2011) and at the other extreme it is known that a bone dry material will not exhibit self-heating (Kirshenbaum 1967; Rosenblum et al. 1982).

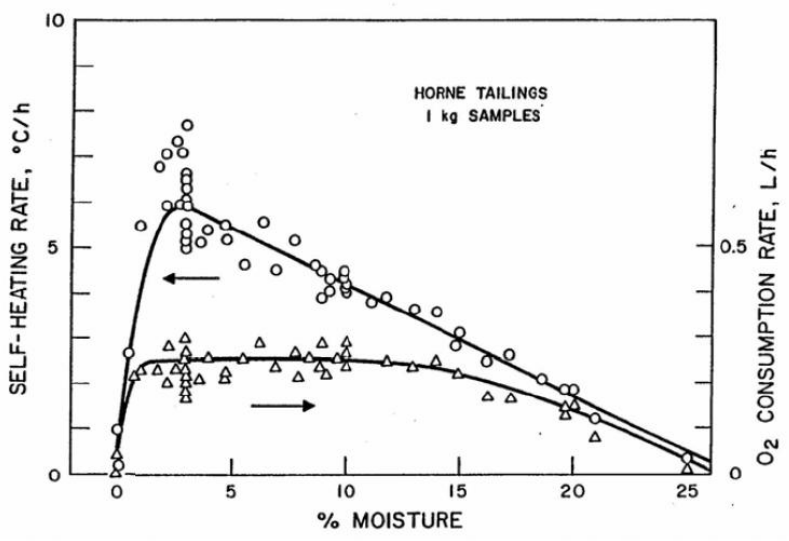

Figure 2.11: Moisture content on self-heating rate and oxygen uptake (Rosenblum et al. 1982)

Oxygen level also has a major impact on self-heating. Studies have shown that there is a direct relationship between self-heating and oxygen consumption in a sample. This is to be expected because the oxidation of a sulphide mineral is exothermic. This can result in oxygen depletion (Rosenblum et al. 1982). Tests have supported this contention, among them being: sulphide samples exposed to nitrogen did not show self-heating; laboratory tests of a reactive concentrate sealed with a plastic sheet showed a decrease in temperature (Rosenblum et al. 2001).

From oxygen uptake rates measured in various backfill tests, Rosenblum et al. (1982) established a hazard ranking criterion (Table 2.2).

Table 2.2: Hazard rating guide for backfill (Rosenblum et al. 1982)

Self-Heating Rate $^{o}C/h$	Oxygen Uptake Rate $m^3/d.m^2$	Rating	Remarks
<1	<0.3	Safe	No heating. Oxygen depletion possible at the upper values of oxygen uptake rate under unfavourable conditions underground.
1-3	0.3-0.9	Possibly Hazardous	Danger of oxygen depletion.
>3	>0.9	Hazardous	Danger of heating, SO_2 generation, combustion, oxygen depletion.

2.2.3 Temperature

A correlation between temperature and oxidation rate has been determined. As temperature increases, the formation of ferric oxides and elemental sulphur increases indicating an increased oxidation rate (Steger 1982). Figure 2.12 shows results from tests performed on sulphide material that indicate a lower self-heating rate at 40 ^{o}C than at 70 ^{o}C, both corresponding to stage A. Experiments have shown that within the range 30 ^{o}C to 60 ^{o}C, oxidation rates doubled with every 10 ^{o}C increment (Ninteman 1978). Under stage B conditions, temperatures up to 143 ^{o}C (just above the melting point of elemental sulphur), again show heating rates increase with increasing temperature (Rosenblum and Spira 1995).

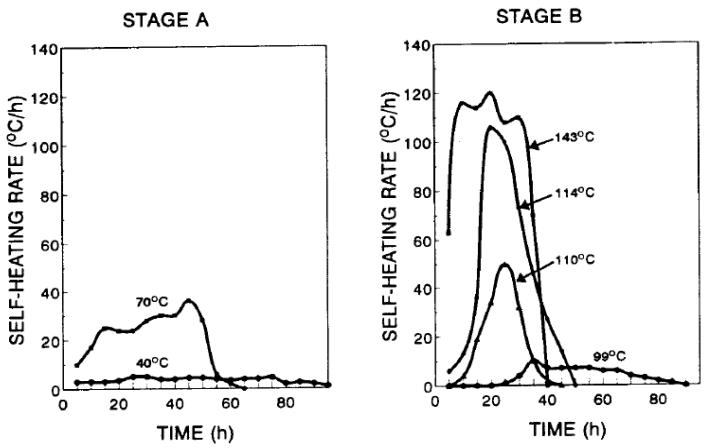

Figure 2.12: Effect of temperature on self-heating rates in stages A and B (Rosenblum and Spira 1995)

The formation of elemental sulphur increases with temperature in stage A (Rosenblum and Spira 1995). Figure 2.13 shows that as temperature is increased, there is an increase in the rate of elemental sulphur formation. The amount of sulphur produced affects self-heating rates in stage B (Rosenblum and Spira 1995).

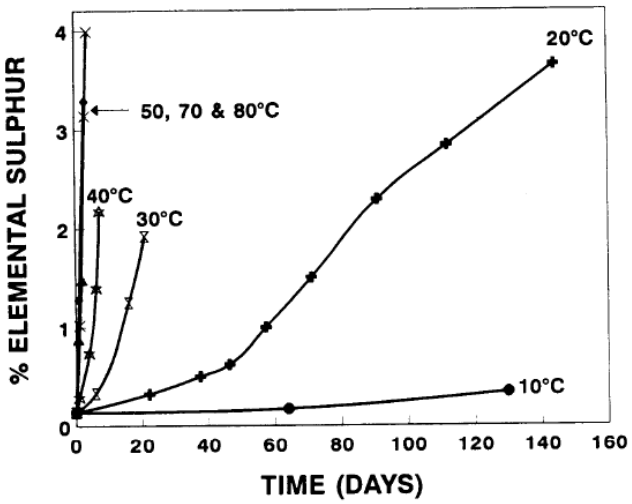

Figure 2.13: Effect of temperature on sulphur formation during weathering in stage A (Rosenblum and Spira 1995)

Although self-heating rate is affected by the temperature, there will be no reaction if moisture and oxygen are not available (Ninteman 1978).

2.2.4 Particle size

The surface area of sulphide particles will affect the self-heating rate. In general, oxidation rate is proportionate to the surface area exposed (Ninteman 1978), i.e. oxidation increases with a decrease in particle size (Farnsworth 1974; Ninteman 1978; Rosenblum and Spira 1981; Payant et al. 2012). Spontaneous combustion can occur after blasting due to the generation of fine particulates (Ninteman 1978). Janzen et Al. (2000) found that surface area is a primary factor governing pyrrhotite reaction kinetics. It is suggested that in order to asses oxidation rates in pyrrhotite containing materials, the particle surface area should be measured (Janzen et al. 2000). Dunn (1997) determined that the ignition temperature occurred at a lower temperature at smaller particles sizes (Figure 2.14).

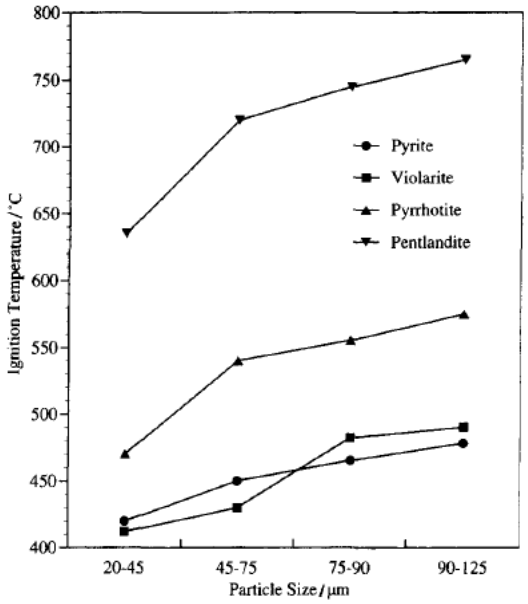

Figure 2.14: Ignition temperature vs. Particle size for sulphide minerals (Dunn 1997)

Along with high reactivity, finer particles were found to have higher levels of elemental sulphur (Good 1977), hence contributing to the stage B self-heating rate.

2.2.5 Galvanic interaction

Galvanic effects occur when two or more minerals that differ in electrochemical properties come in contact with each other in an aqueous electrolyte medium (Rao and Leja 2004). Most sulphide minerals have semiconductor properties. Galvanic effects are important in governing the rate of dissolution of a sulphide mineral (Abraitis et al. 2004). The extent of galvanic interactions depends on the differences in rest potential between the sulphide minerals. In a pair of minerals, the mineral with lower rest potential (E) will act as anode where oxidation will

occur and the mineral with higher rest potential will act as cathode where reduction occurs (Kwong et al. 2003). As the differences between the rest potentials increases, the driving force for galvanic interaction will increase. The rest potential of various sulphide minerals vs. standard hydrogen electrode (S.H.E) at pH 4 is shown in Table 2.3. Since pyrite has the highest rest potential (0.66 V), it will act as a cathode, accepting electrons from a mineral with a lower rest potential (e.g. galena) which acts as the anode (Kocabag and Smith 1985). Pyrrhotite having a low rest potential oxidizes readily (Nowak et al. 1984).

Table 2.3: Rest potential values of various sulphide minerals (Kocabag and Smith 1985)

Mineral	Formula	Rest Potential vs. S.H.E (V)
Pyrite	FeS_2	0.66
Chalcopyrite	$CuFeS_2$	0.56
Sphalerite	ZnS	0.46
Pentlandite	NiFeS	0.35
Pyrrhotite	FeS	0.31
Galena	PbS	0.28

Galvanic interaction is described in equations 2.4, 2.5 and 2.6. Electrons are released from the metal sulphide (MeS) representing the anodic site (equation 2.4) and flow to the cathodic site for either the reduction of oxygen or reduction of

Fe^{3+}, ferric ion being commonly present in sulphide systems (Payant et al. 2012). If oxygen is in limited supply, reduction of Fe^{3+} is favoured.

Anodic (oxidation) half cell reaction:

$$MeS \rightarrow Me^{2+} + S^{o} + 2e^{-} \quad (2.4)$$

Cathodic (reduction) half cell reaction:

$$1)\ 1/2\ O_2 + H_2O + 2e^{-} \rightarrow 2OH^{-} \quad (2.5)$$

$$2)\ Fe^{3+} + e^{-} \rightarrow Fe^{2+} \quad (2.6)$$

An example of galvanic interaction is shown in Figure 2.15. The pyrite is the anodic mineral and hosts Fe^{3+} reduction and chalcopyrite is the cathodic mineral. In this particular reference, the object was for pyrite to enhance dissolution of chalcopyrite, the Galvanox process (Dixon et al. 2008).

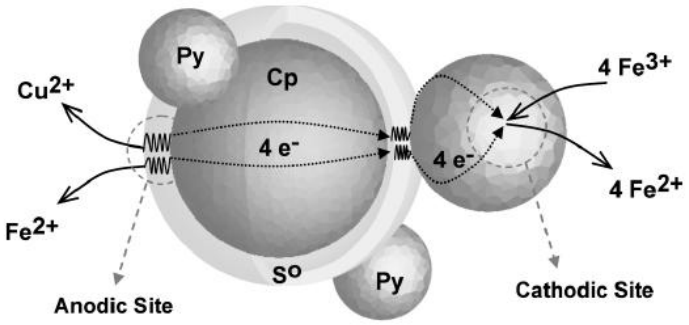

Figure 2.15: Schematic diagram of galvanic interaction between chalcopyrite and pyrite (Dixon et al. 2008)

Tests have shown that self-heating increases in the presence of two sulphide minerals of sufficient difference in rest-potential, $\Delta E > 0.2$ (Payant et al. 2012). The same work also showed that self-heating increases with fineness of the cathodic mineral. Both these observations indicate a galvanic interaction effect promoting self-heating. Payant et al. (2012) suggest that galvanic effects promote the production of H_2S which is suspected of playing a role in self-heating (Somot and Finch 2010).

2.2.6 Bacteria

Certain bacteria promote the oxidation of sulphide minerals. Bacteria such as *Thiobacilli ferrooxidans* and *Acidithiobacillus ferrooxidans* belonging to the acidophilic family can oxidize elemental sulphur compounds to form sulphuric acid (H_2SO_4) and promote oxidation of ferrous iron (Fe^{2+}) to ferric iron (Fe^{3+}) (Suzuki et al. 1994). This was especially apparent at pH below 4 (Mielke et al. 2003) and elevated temperature (45 ^{o}C to 50 ^{o}C) (Norris et al. 1996). Acidophilic bacteria are the most effective in metal sulphide oxidation (Norris et al. 1996). Research has shown that in the presence of this type of bacteria sulphide oxidation kinetics were accelerated 30-300 fold (Nordstrom and Southam 1997). Galvanic interaction between sulphide mixtures (two mineral phase system) were also enhanced in the presence of these bacteria (Mehta and Murr 1983).

Archea microorganisms also have the capability to oxidize sulphide minerals (Rohwerder and Sand 2007). Although bacteria and archea are known to promote

elemental sulphur oxidation, they have different enzymatic reactions resulting in different stoichiometry. Bacteria oxidize elemental sulphur into sulphite using the enzyme sulphur dioxygenase:

$$1/8\ S_8 + O_2 + H_2O \rightarrow SO_3^{2-} + 2\ H^+ \qquad (2.7)$$

Archea oxidizes elemental sulphur into equal amounts of sulphide and sulphite (sulphur disproportionation) using the enzyme sulphur oxygenase reductase (Rohwerder and Sand 2007):

$$1/8\ S_8 + 1/4\ O_2 + H_2O \rightarrow 1/2\ SO_3^{2-} + 1/2\ H_2S + H^+ \qquad (2.8)$$

Although it is evident that bacteria can aid the oxidation process, it is unclear whether they play a significant role in sulphide self-heating. Rosenblum (unpublished work) had previously incorporated bacteriacides into tests and determined that they made no difference in self-heating.

2.3 Mitigation

The self-heating reaction mechanisms are not well understood, which hampers design of mitigation measures. However, knowing some triggers it is possible to delay self-heating. For example, research has shown that self-heating is prompted under certain conditions of moisture and oxygen (Rosenblum and Spira 1995). Therefore, one mitigation method might be to control moisture through the use of

hygroscopic reagents. This will be further discussed in Chapter 4.2. There are reported occasions when ore was blasted and the resulting large surface area exposed to air and moisture quickly caused self-heating. The recommendation is to remove broken ore quickly (Farnsworth 1974). To protect against self-heating, improved ventilation was installed at Inco's (Vale's) underground mine (Stachulak 1994) to cool the reacting area and carry away the gases produced (Ninteman 1978). This method may not be suitable, however, for very active material as ventilation may encourage heating (Rosenblum and Spira 1995). Inco (now Vale) established protocols for fire prevention and early detection (Stachulak 1994). Stockpiles rich in sulphide minerals prone to self-heating have been covered to reduce access to air and suppress oxidation (Tributsch and Gerischer 1976; Rosenblum and Spira 1995).

Chemical agents have been used to suppress self-heating. Wu et al. (2001) used calcium chloride, calcium oxide, magnesium oxides and their mixtures as oxidation suppressants on several types of active sulphide ores. Tests showed a reduction in oxidation rates by 27% to 100% (Wu et al. 2001). Alconox, a laundry detergent, and Marasperse, a commercial lignosulphonate, were tried by Rosenblum and Spira (1995). It was found that when active sulphide material was coated with these reagents, there was a significant decrease in self-heating rates of stages A and B, as shown in Figure 2.16 (Rosenblum and Spira 1995). Lime has also been used as an additive to neutralize the acid (H^+) produced during oxidation which favors a forward reaction that enhances self-heating (Ninteman 1978). Somot and Finch (2010) found that self-heating can be suppressed by

adding sufficient amount of copper sulphate ($CuSO_4$). The suggested explanation was that Cu^{2+} provided a competing reaction for H_2S, that instead of undergoing oxidation and releasing heat, H_2S reacted with Cu^{2+} to form copper sulphide (CuS).

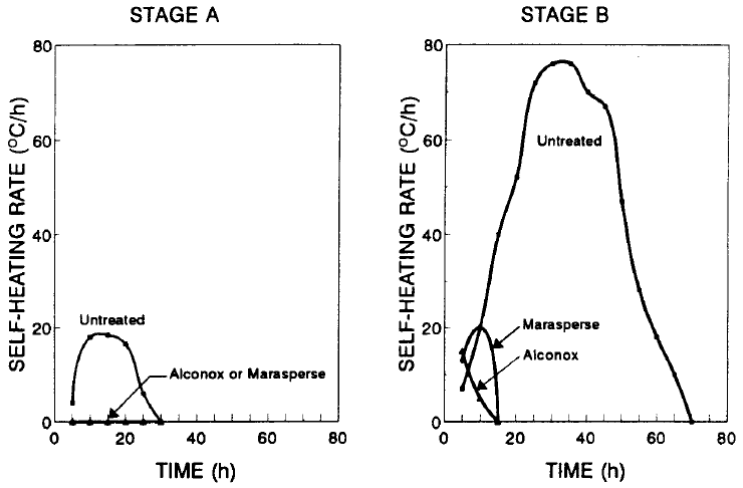

Figure 2.16: Effect of chemical coating on self-heating rate stage A and B (Rosenblum and Spira 1995)

It is important that mitigation methods be cost effective and environmentally acceptable. Given our understanding of self-heating, it is also important that mitigation takes place in stage A to prevent stages B and C from occurring.

2.4 Elemental sulphur analysis

Elemental sulphur has been detected on the surface of sulphide mineral particles in the presence of moisture and oxygen under stage A conditions (Rosenblum and Spira 1995). This sulphur is the fuel for stage B self-heating where temperatures

are above the melting point of sulphur (Figure 2.13). Uncontrolled, sulphur oxidation can lead to the onset of stage C at 300 ^{o}C to 400 ^{o}C (Rosenblum and Spira 1995), ignition being triggered at a critical sulphur content (Good 1977). It is crucial to understand the environmental conditions that promote the formation of elemental sulphur, which demands a reliable S^{o} analysis method. The determination of elemental sulphur can be challenging due to the interference of sulphur compounds such as sulphates, thiosulphates and xanthates (Steger 1976).

Two stable crystalline forms of elemental sulphur exist: rhombic (alpha-sulphur) and monoclinic (beta-sulphur) (Weast and Editor 1984; Shuai and Meisen 1995). Monoclinic sulphur has been found to be 1.28 times more soluble than monoclinic sulphur in solvents such as benzene, diethyl ether and ethanol (Ott and Boerio-Goates 2000). Both forms of sulphur are readily soluble in carbon disulphide (CS_2) (Weast and Editor 1984). Several methods of elemental sulphur analysis exist. X-ray diffraction (XRD), scanning electron microscopy (SEM) and Raman spectroscopy have been used to analyze the mineral surface for sulphur (McGuire and Hamers 2000). X-ray diffraction has been used to determine the bulk sulphur content in a sample before and after oxidation (Yanful and Verma 1999). However, quantification has proved to be a challenge with these methods (McGuire and Hamers 2000).

Steger (1976) separated elemental sulphur from a sample by vaporization in a closed heated tube. The sulphur underwent sublimation and was collected on a cold-finger condenser. Sulphur was extracted from the finger using ethanol and

the UV/vis absorption spectrum analyzed. Another approach was to heat the sample with ethanol under reflux for 4 hours, cool and centrifuge to separate the solid. The concentration in the liquid was then measured by UV/vis spectroscopy in the range 250 nm to 350 nm (Steger 1976). Another method is to extract elemental sulphur using a solvent such as carbon disulphide or acetone and determine the absorbance using spectrophotometric methods. If acetone is used as solvent, thin-layer chromatography could be used (Steger 1976).

X-ray photoelectron spectroscopy (XPS), a surface chemical characterization technique, has been used to analyze polysulphides, elemental sulphur and oxidized iron compounds formed on the surface of pyrrhotite following oxidation (Buckley 1985). Photoelectron spectra of pyrrhotite before and after oxidation show an increasing shift in binding energy (eV) of the S(2P) (Buckley 1985). An issue with this method, is that elemental sulphur is volatile and can be lost to vacuum in the XPS chamber (Pratt et al. 1994).

Elemental sulphur has been extracted from the mineral surface with perchloroethylene, in which it is 50 times more soluble than in methanol (McGuire and Hamers 2000). The liquid phase was extracted and concentration analyzed using high-performance liquid chromatography (HPLC). An issue with this method is that perchloroethylene may lead to further sulphide mineral oxidation. This may be avoided by working with non-elevated temperatures (McGuire and Hamers 2000).

Hampton et al. (2011) used atomic force microscopy (AFM) to analyze the surface topography of a galena sample after oxidation and found evidence of accumulation of reaction products over certain areas of the sample. Raman spectroscopy showed the accumulations to be elemental sulphur. To verify, the results were compared with Raman spectra of elemental sulphur powder (Figure 2.17) (Hampton et al. 2011).

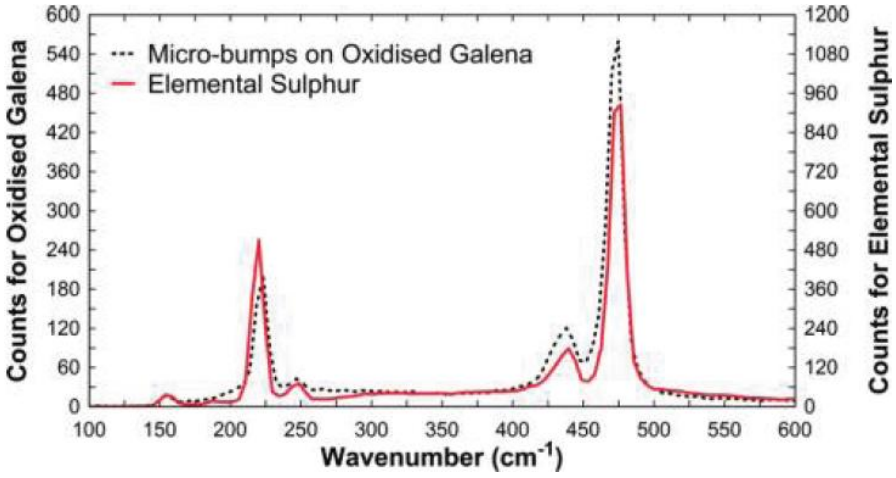

Figure 2.17: Raman spectra of elemental sulphur on galena surface and elemental sulphur powder (Hampton et al. 2011)

Some of these characterization techniques prove to be difficult because elemental sulphur formation is not homogeneously dispersed throughout the sample. Sulphur deposition can be preferred in certain areas of the sample due to impurities and crystal defects (Hampton et al. 2011). In the case of sulphide self-heating, elemental sulphur may form from partial oxidation of H_2S, the gas effectively mobilizing the sulphur throughout the sample.

2.5 Reaction mechanisms

Self-heating reactions are not well understood. A wide range of chemical reactions are possible resulting in dissolved metals, sulphuric acid, sulphates, elemental sulphur etc. Pyrrhotite is known to be active and the following self-heating chemical reactions were proposed by Shaw et al. (1998):

$$Fe_{1-x}S + (2-x/2)O_2 + xH_2O \rightarrow (1-x)Fe^{2+} + SO^{2-}_4 + 2xH^+ \quad (2.9)$$

$$Fe^{2+} + 1/4O_2 + 5/2\ H_2O \rightarrow Fe(OH)_3 + 2H^+ \quad (2.10)$$

$$Fe_{1-x}S + (3-3x)O_2 + (12-12x)H^+ \rightarrow (4-4x)Fe^{3+} + 4S^o + (6-6x)H_2O \quad (2.11)$$

These reactions capture the importance of moisture as well as oxygen. Pyrrhotite oxidizes readily in acidic conditions releasing Fe^{2+} and hydrogen sulphide (H_2S) (Good 1977; Belzile et al. 2004; Gunsinger et al. 2006; Somot and Finch 2010). Acid (H^+) is created from oxidation and hydrolysis of dissolved Fe^{2+} in Equation 2.9. Further oxidation occurs to form elemental sulphur (Equation 2.11). Ferric ions may also act as a secondary oxidant forming sulphate ions if the reaction goes to completion (Equation 2.12). Under low oxygen conditions, ferrous sulphate ($FeSO_4$) and elemental sulphur are principal products whereas at high oxygen conditions, ferric sulphate ($Fe_2(SO_4)_3$ and H_2SO_4 are formed (Lukaszewski 1973). Elemental sulphur is formed if reaction is incomplete (Equation 2.13) (Shaw et al. 1998). At pH below 4, the dominant pyrrhotite oxidant is considered to be Fe^{3+} (Gunsinger et al. 2006). At this low pH, Fe^{3+} does not precipitate whereas at pH above 4, it precipitates as ferric hydroxide

(Janzen et al. 2000). It was found that the most elemental sulphur was formed at low pH (Mycroft et al. 1990).

$$Fe_{1-x}S + (8-2x)Fe^{3+} + 4H_2O \rightarrow (9+3x)Fe^{2+} + SO^{2-}_4 + 8H^+ \quad (2.12)$$

$$Fe_{1-x}S + (2-2x)Fe^{3+} \rightarrow (3-3x)Fe^{2+} + S^o \quad (2.13)$$

Environmental conditions such as temperature and relative humidity affect the oxidation rates. Tests have shown that sulphates are formed at low temperatures (Ninteman 1978; Steger and Desjardins 1978).

Equations 2.9 to 2.13 occur in stage A where temperatures are below 100 ^oC. In this stage, the sample will tend to increase in weight in proportion to the elemental sulphur content (Rosenblum and Spira 1995). At elevated temperatures and relative humidity, there is an increase in ferric oxide (FeO(OH)) and sulphuric acid (H_2SO_4) formation (Equation 2.16) partially due to the increased level of water vapour in the air. Sulphuric acid then reacts with oxygen to increase elemental sulphur formation (Equation 2.17) (Steger 1982).

$$Fe_7S_8 + O_2 \rightarrow xFeS_2O_3 + (1-x)FeSO_4 \quad (2.14)$$

$$2FeSO_4 + (2x+1)H_2O + O_2 \rightarrow 2Fe(OH)(SO_4)\cdot xH_2O \quad (2.15)$$

$$Fe(OH)(SO_4) + H_2O \rightarrow FeO(OH) + H_2SO_4 \quad (2.16)$$

$$Fe_7S_8 + 7H_2SO_4 + O_2 \rightarrow 7FeSO_4 + 7H_2O + 8S^o \quad (2.17)$$

Self-heating as a function of pyrrhotite content was examined by Somot and Finch (2010). It was noted that self-heating rate increased with pyrrhotite content indicating oxidation. However, the sample visibly appeared to be less oxidized (greyer in colour) as pyrrhotite content was increased. It was speculated that this may be because high pyrrhotite content gives a reducing environment favoring H_2S formation. Copper pieces turning black in the presence of H_2S by forming Cu_2S was used to confirm this speculation. They proposed reactions for the formation and the role of H_2S in self-heating:

$$Fe_{1-x}S + 2H^+ \rightarrow (1-x)Fe^{2+} + H_2S \quad (2.18)$$

$$H_2S + 1/2O_2 \rightarrow 2/8S + H_2O \quad (2.19)$$

$$H_2S + O_2 \rightarrow SO + H_2O \quad (2.20)$$

$$H_2S + 3/2O_2 \rightarrow SO_2 + H_2O \quad (2.21)$$

$$H_2S + 2O_2 \rightarrow 2H_2SO_4 \quad (2.22)$$

$$2H_2S + SO_2 \rightarrow 3/8S + 2H_2O \quad (2.23)$$

$$S^o + O_2 \rightarrow SO_2 + Heat \quad (2.24)$$

Equation 2.18 proposes the production of H_2S, where H^+ is present from the moisture which is acidic when in contact with sulphide minerals (Lowson 1982; Somot and Finch 2010). At temperatures below 100^oC, H_2S is completely or partially oxidized depending on the oxygen/H_2S ratio and forms various sulphur compounds as shown in Equations 2.19 to 2.22. This series of reactions composes stage A (Somot and Finch 2010). The sulphur dioxide formed can

further react with H_2S contributing to higher self-heating rates (Equation 2.23) (Pfeiffer et al. ; Somot and Finch 2010). These equations represent exothermic reactions where the enthalpy (ΔH) of Equation 2.19 is -2.6×10^5 J/mol, Equation 2.21 is -5.6×10^5 J/mol and Equation 2.22 is -8.7×10^5 J/mol (Somot and Finch 2010). At temperatures above 100 ^oC, which represents stage B self-heating, elemental sulphur is oxidized to SO_2 (Equation 2.24) (Rosenblum and Spira 1995).

Chapter 3 Experimental method

3.1 Materials and sample preparation

Samples for all the tests contained pyrrhotite (Po) obtained as tailings (ca. 75 weight % Po) from Xstrata's Strathcona mill (Sudbury). Samples under water were shipped to McGill University in sealed plastic bags. Once received, samples were placed in an oven at 40 ^{o}C overnight to eliminate excess water. Once dry, they were mixed and split to homogenize. Samples were divided into 50g lots, placed in plastic bags and stored immediately in a freezer to prevent further oxidation. When ready to use, a sample is removed and vacuum dried to eliminate all free moisture so that it will be "bone dry".

3.2 Apparatus

Two types of test were performed: standard self-heating using the apparatus developed by Rosenblum and co-workers at the Noranda Technology Center (Rosenblum and Spira 1995; Rosenblum et al. 2001); and controlled environment in the weathering apparatus developed at McGill University by Rosenblum (2008).

3.2.1 Standard self-heating

The general self-heating setup is shown in Figure 3.1 with details on the cell in Figure 3.2. The cell has the capacity to hold 500g of sample. The glass cell is placed in the chamber and temperature is controlled by computer to target conditions for the standard self-heating test. The standard test covers stages A and B. The temperature is set to 70 ^{o}C for stage A and 140 ^{o}C for stage B. Air is injected at 100 ml/min for stage A and 250 ml/min for stage B. The air injection period is 15 minutes followed by a 5-hour period without air injection. This process is repeated for 10 cycles for both stage A and stage B. Evaporated water is collected in a separate vessel for possible analysis. The temperature response of the sample is recorded throughout the test.

Figure 3.1: Self-Heating Setup

The sample is placed in a glass cell (Figure 3.2). The seal cover is placed on top to lock in the sample and a thermocouple inserted into the sample.

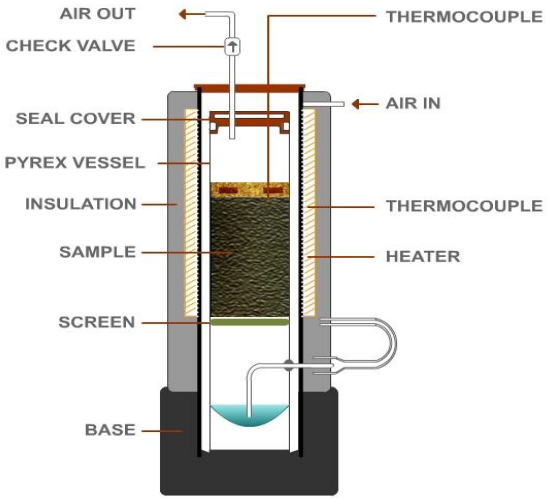

Figure 3.2: Self-Heating Test Cell (Rosenblum et al. 2001)

Figures 3.3 and 3.4 depict example outputs for stages A and B for samples that respond (self-heat) and do not respond, respectively. The x-axis denotes the time in hours. The left-hand y-axis is the temperature in ^{o}C of the sample undergoing the test. The right-hand y-axis is the air flow rate in ml/min. The vertical lines are the air injections for the 10 cycles for stages A and B. If the test requires, air injection cycles may be increased for both stages. In-house software was used to calculate the self-heating rates (^{o}C/hr) for each temperature peak shown in Figure 3.3. The slope of the rising part of each temperature peak is calculated using equation 3.1, where ΔT is the change in temperature and Δt is change in time, to give the self-heating rate (SHR).

$$\frac{\Delta T}{\Delta t} = Slope\ \left(Heating\ rate\ in\ \frac{^{\circ}C}{Hr}\right) \tag{3.1}$$

The heating rates of the temperature peaks are summed for each stage. The self-heating capacity (SHC) (J/g) is then calculated using equation 3.2. The specific heat capacity of sulphides is in the range of 0.5 J/g^{o}C and 0.7 J/g^{o}C over a temperature range of 25 ^{o}C to 500 ^{o}C (Pankratz 1984). As a compromise, the middle value of 0.6 J/g^{o}C was chosen. The air injection time is 0.25 hr (15 minutes).

$$SHC = \sum SHR\ \left(\frac{^{\circ}\mathrm{C}}{Hr}\right) \times Specific\ Heat\ \left(\frac{J}{g^{\circ}\mathrm{C}}\right) \times Air\ Injection\ Time\ (Hr) \tag{3.2}$$

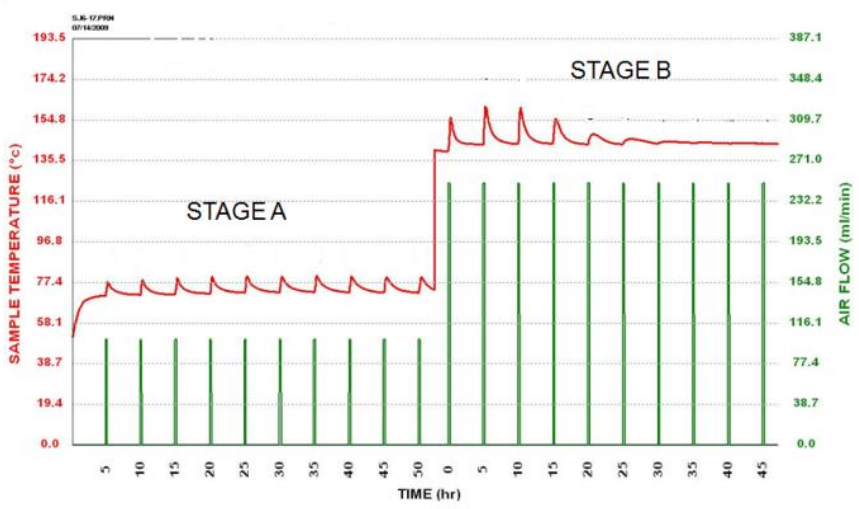

Figure 3.3: Computer output of sample undergoing self-heating

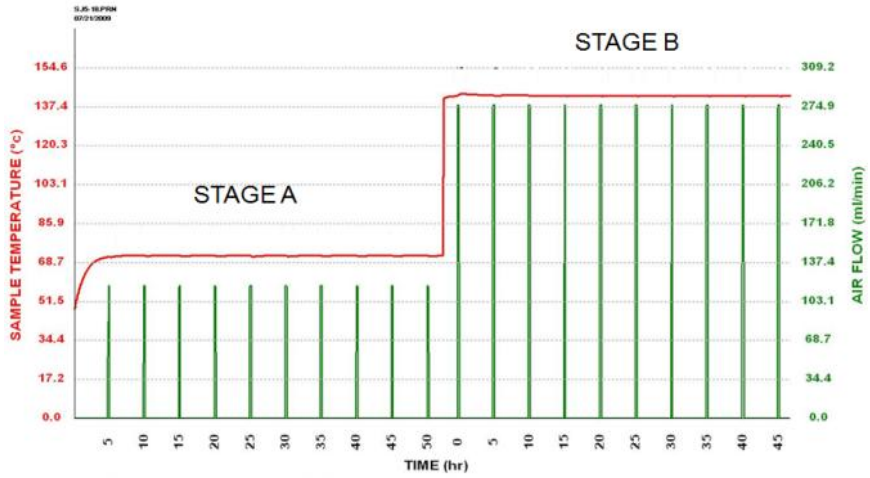

Figure 3.4: Computer output of sample not undergoing self-heating

The risk assessment chart, a plot of self-heating capacity in stage B (y-axis) vs. self-heating capacity in stage A, shown in Figure 3.5, is used to categorize samples. Zone 1 is the safe region where samples are not expected to undergo self-heating. In zone 2, samples are not expected to heat beyond 100 ^{o}C and are not considered to undergo spontaneous combustion. In zone 3, samples should not be exposed to a high heat source due to risk of self-heating. In zone 4, samples are likely to undergo self-heating and monitoring is recommended. In zone 5, samples will self-heat and it is necessary to take preventive action. The risk assessment chart is used to locate the response of the samples in the mitigation study.

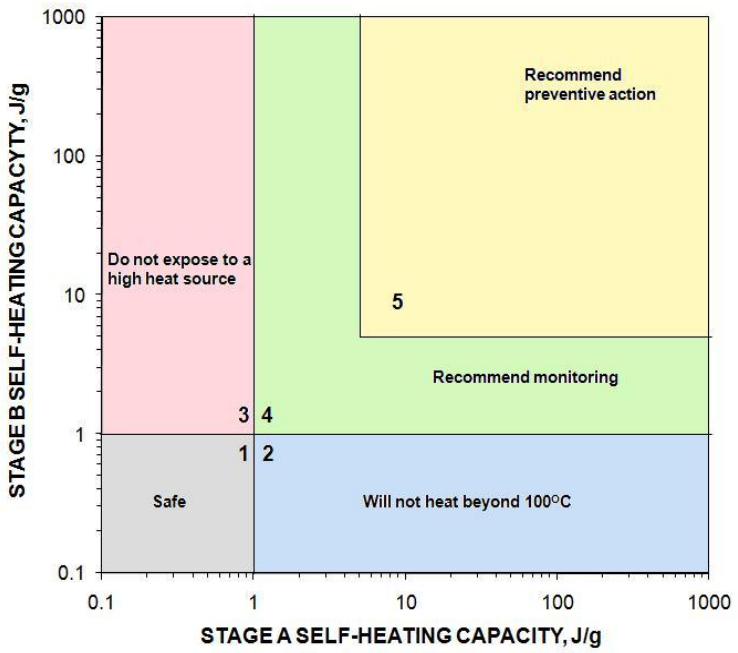

Figure 3.5: Risk Assessment Chart (Rosenblum et al. 2001)

A total of six self-heating units are available. The difference in response between each cell is approximately 20%, not sufficient to confuse the outcomes.

3.2.2 Weathering

The weathering apparatus is an extended stage A where samples are conditioned under controlled environments. The setup of the six available apparatus is shown in Figure 3.6. Samples are weathered at various conditions such as temperature, oxygen level and relative humidity. The apparatus consists of a reaction vessel, chamber and a flask filled half-way with water (Figure 3.7). The reaction vessel has the capacity to hold up to 5 kg of sample. Once the sample is in the chamber, it is sealed from the outside environment. The chamber is fitted with inlet and

outlet ports. The inlet feeds nitrogen and air into the chamber, allowing control of oxygen level. Mass flow controllers control the flow rate. For this thesis, air flow rate was set at 150 ml/min. A thermocouple is inserted into the sample to monitor the temperature throughout the weathering period. The relative humidity and air temperature are monitored with sensors inserted in the chamber. If the relative humidity rises above the set-point, dry air is blown into the chamber; if it falls below the set-point, dry air passes through the flask containing water to moisten the air blown into the chamber. Condensation is collected in a water trap located outside the apparatus.

Figure 3.6: Weathering apparatus setup

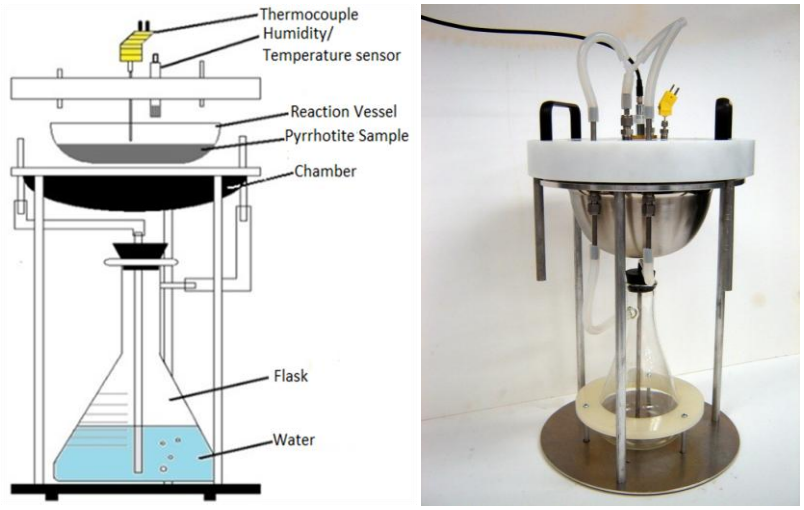

Figure 3.7: Schematic of the weathering apparatus (left) and picture (right)

The temperature of the sample, relative humidity, oxygen, SO_2 and H_2S levels along with experimental parameters such as test duration and set points are monitored by computer and displayed on the screen (Figure 3.8). The duration of the test varies depending on what is required. At the end of a weathering test, the samples are subjected to a stage B test in the standard self-heating apparatus. The hypothesis is that stage B self-heating capacity will be affected by the sample weathering conditions.

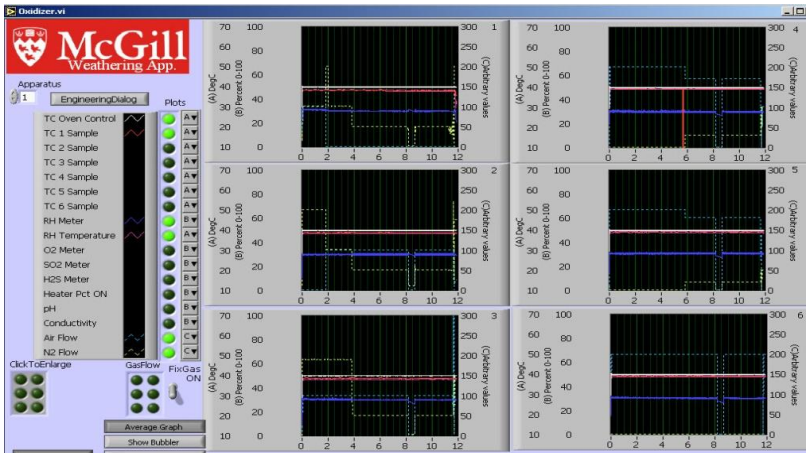

Figure 3.8: Data readout for the six weathering apparatuses (Rosenblum, unpublished work)

3.3 Procedure

3.3.1 Mitigation

Standard self-heating tests were conducted on 500g samples consisting of 50 weight % pyrrhotite tails and 50 weight % coarse quartz sand as an inert diluent. Potential hygroscopic reagents tested were: calcium chloride, calcium oxide, drierite (desiccant), F-150 frother (polyglycol), poly (acrylic acid sodium salt) (super absorbent polymer), silica gel, sodium chloride and sodium hydroxide. Up to 100g of reagent was used, either mixed in or in some cases layered on top of the sample.

Spray tests were conducted on the reagents to determine water retention capacity. De-ionized water was sprayed on to 26.8g of the reagent which was evenly distributed on the bottom of a Petri-dish. Spraying continued until free water was

visible. The reagent was then re-weighed and the water retention capacity (kg water/tonne reagent) determined. Reagents with the highest water retention capacity were selected for the mitigation tests.

Standard self-heating tests were conducted. Bone dry test samples were mixed 50:50 with the sand (i.e. 250g sample, 250g sand) in a plastic bag. De-ionized water was added slowly using a spray bottle and the plastic bag shaken periodically to evenly distribute the moisture. A total of 31.6g water was added to give the standard 6 weight % moisture level. Three samples were prepared for replication purposes. To other samples, the selected hygroscopic reagents were added in an amount and manner depending on the experiment (Table 3.1).

Table 3.1: Quantity and methods of introduction for reagents

Sample Name	Reagent	Quantity of Reagent (g)	Method of Introduction
SJ6-02	Control	N/A	N/A
SJ5-03	Control	N/A	N/A
SJ6-04	Control	N/A	N/A
SJ5-05	Sodium Chloride	9.57	Saturated solution mixed homogenously
SJ6-06	Sodium Chloride	9.57	Mixed homogenously
SJ6-07	Sodium Chloride	50	Mixed homogenously
SJ5-08	Sodium Hydroxide	50	Mixed homogenously
SJ5-10	Sodium Chloride	100	Mixed homogenously
SJ5-11	Calcium Oxide	50	Mixed homogenously
SJ4-12	Silica Gel	50	Mixed homogenously
SJ6-13	Silica Gel	100	Mixed homogenously
SJ5-14	Calcium Oxide	100	Mixed homogenously
SJ4-15	Silica Gel	100	Layered on top
SJ5-16	Poly (acrylic acid sodium salt)	100	Mixed homogenously
SJ6-17	Drierite	100	Mixed homogenously
SJ5-18	Poly (acrylic acid sodium salt)	50	Mixed homogenously
SJ6-19	F-150	50	Mixed homogenously
SJ5-20	F-150	50	Layered on top
SJ6-21	F-150	31.9	Mixed homogenously

3.3.2 Elemental sulphur determination

Weathered samples were subjected to elemental sulphur determination by two methods: cold finger and carbon disulphide (CS_2) analysis.

The cold finger analysis collects elemental sulphur from the sample by sublimation. Half-gram of weathered sample was placed in a flask. A cold finger was inserted into a flask and sealed in place with a cork (Figure 3.10). The flask was placed in a sand bath on top of a hot plate. A temperature probe connected to a controller was inserted into the sand bath to monitor the sample temperature. Nitrogen was flushed through the flask for 15 minutes to eliminate air and prevent further oxidation of the sample. Samples were heated at 130 ^{o}C i.e., above the vaporization point of sulphur (119 ^{o}C) (Currell and Williams 1974) for 5 hours. This specific experimental time was chosen based on literature where Steger (1976) conducted tests determining the fraction of elemental sulphur recovered as a function of the heating period and determined that 5 hour heating was sufficient for 100% recovery at approximately 3% precision. Cold water was re-circulated throughout the cold finger and re-chilled to 5 ^{o}C (Figure 3.9). Once the elemental sulphur has sublimed onto the cold finger, it was placed in a test tube with ethanol and placed in a *Digi*Prep Jr by SCP Science block heater at 70 ^{o}C overnight to dissolve the elemental sulphur. The solution was carefully poured into a cuvette and placed in an UV-vis spectrometer (Evolution 300 UV-Visible Spectrophotometer) scanning in the range of 250 nm to 350 nm to detect the

sulphur and determine concentration using calibration. A calibration curve was first constructed with three ethanol samples.

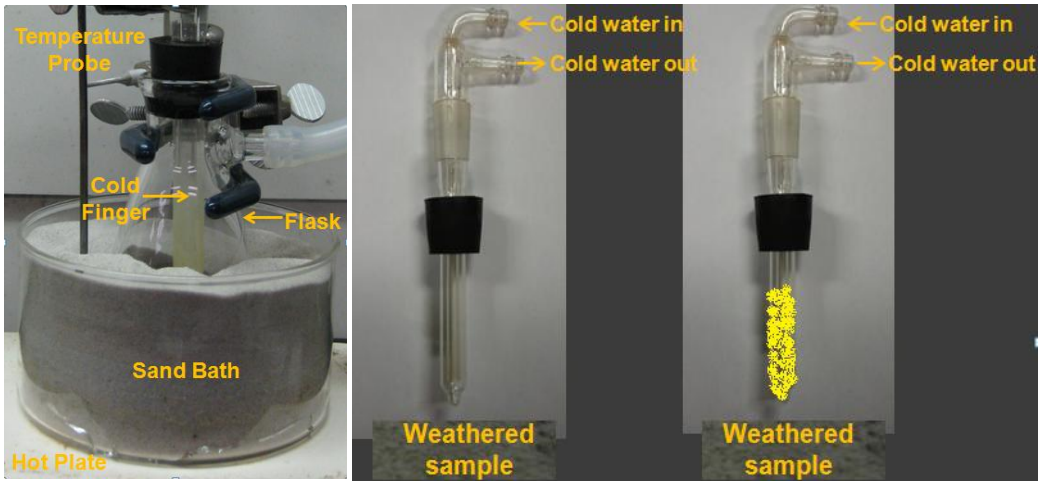

Figure 3.9: Cold finger sulphur analysis set-up

The carbon disulphide method directly brings elemental sulphur into solution from the sample. The chemical used was from Sigma-Aldrich: 99.9% A.C.S reagent grade. Five grams of weathered sample was placed in a 50 mL beaker and 15 mL of carbon disulphide was introduced. The beaker was stirred at one minute intervals with a glass rod for 10 minutes. The solution was then filtered into a 50 mL flask. Five millilitres of carbon disulphide was added to the beaker to further rinse and collect remaining sulphur and the solution re-filtered into the same flask. Air was then blown into the flask to evaporate the carbon disulphide until only elemental sulphur remained. The sulphur and flask is weighed and weight percentage of elemental sulphur in the sample determined (Figure 3.10).

Figure 3.10: Carbon disulphide analysis set-up

3.3.3 Weathering

For each test in the weathering apparatus, 900g of bone dry pyrrhotite samples were weighed out. Moisture was added to the sample with a spray bottle to reach 6 wt. % (i.e., 54 g water) and sample was mixed to homogenize. All six weathering apparatus were employed. Once in the reaction vessel it was sealed. Different experimental parameters for each weathering apparatus were entered into the computer as shown in Table 3.2.

Table: 3.2: Experimental parameters for weathering tests

Sample Name	Weathering Apparatus	Oven Temperature (^{o}C)	Relative Humidity (%)
SJW11-20	1	40	100
SJW22-21	2	60	100
SJW33-22	3	40	30
SJW44-23	4	60	30
SJW55-24	5	40	70
SJW66-25	6	60	70

Samples were weathered for a total duration of 18 days (sulphur analysis by cold finger) and 31 days (sulphur analysis by carbon disulphide). The air rate introduced into each of the chambers was set to 150 ml/min. The chamber was opened periodically throughout the duration of the test for sampling. A sampling probe was used to take 12 g samples both at the center of the reaction vessel (1) and directly under where air is introduced into the chamber (2) (Figure 3.11). Samples were tested for moisture and elemental sulphur content. Moisture analysis was done using a moisture analyzer (Mettler Toledo). A five gram sample was placed on the balance and heated at 100 ^{o}C to evaporate the free moisture. The difference in weight determined the moisture content (percentage) of the sample.

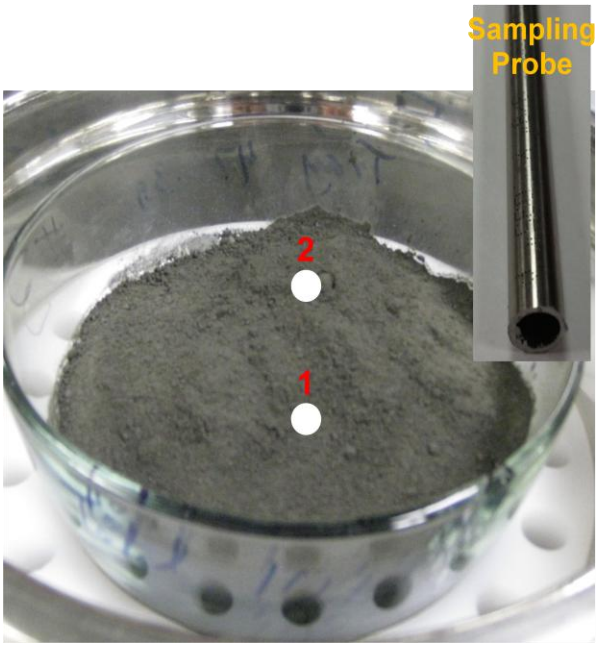

Figure 3.11: Weathering apparatus test sampling locations

After weathering, samples were removed from the chamber and 500 g were weighed out for stage B standard test to indicate reactivity due to weathering. If there was a lack of sample (never more than 5 g), coarse silica sand (80% passing 2.36 mm)-an inert material, was added to make up the weight. Previous tests conducted had shown that addition of up to 50 wt. % silica sand did not affect the self-heating rate of the sample. Samples were then subjected to standard self-heating test for stage B. Air injection cycles were increased from the standard ten to the point when heating peaks were no longer present. Due to lack of standard self-heating cells, samples were stored in freezers to prevent further oxidation while awaiting the test.

3.4 Instrumental analysis

3.4.1 X-ray diffraction

Unweathered pyrrhotite samples were analyzed using a D8 Discovery Bruker XRD with a cobalt anode at a current of 35kV and voltage of 45mA. The software "GADDS: General Area Detector Diffraction System" was used for data acquisition. "MERGE" and "RAW FILE EXCHANGE" program was used for phase analysis.

3.4.2 Ultraviolet-visible spectroscopy

Evolution 300 UV-visible spectrophotometer was used to determine the concentration of elemental sulphur collected in an ethanol solution. "VisionPRO" software was used for quantitative analysis.

Chapter 4 Results

4.1 Sample characterization

X-ray diffraction patterns on as received pyrrhotite tailings from Strathcona Mill indicate the presence of hexagonal pyrrhotite (Reference code: 00-022-1120), magnetite (Fe_3O_4) (Reference code: 01-075-1372) and silicon oxide (SiO_2) (Reference code: 01-073-3461 and 01-073-3470) (Figure 4.1). The X-ray spectra (Figure 4.1) confirmed the composition determined by Wang (2007) on the same material.

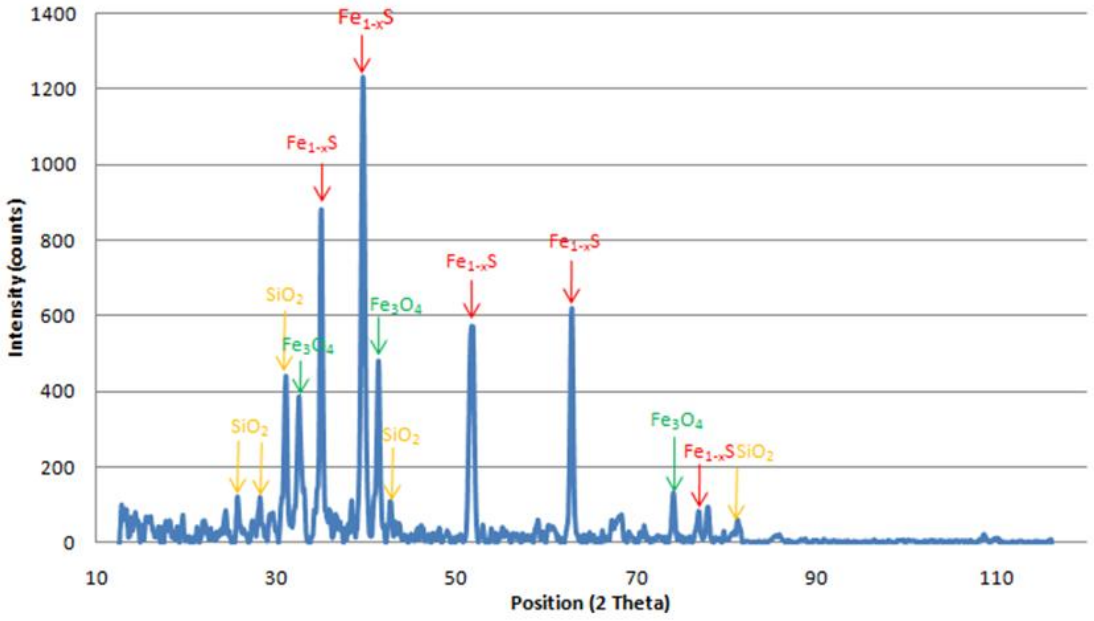

Figure 4.1: XRD analysis of as-received pyrrhotite tailing

4.2 Mitigation

The results are presented on the risk assessment chart. Figure 4.2 gives the results for the three control samples (filled circles), showing excellent repeatability and high self-heating response (zone 5).

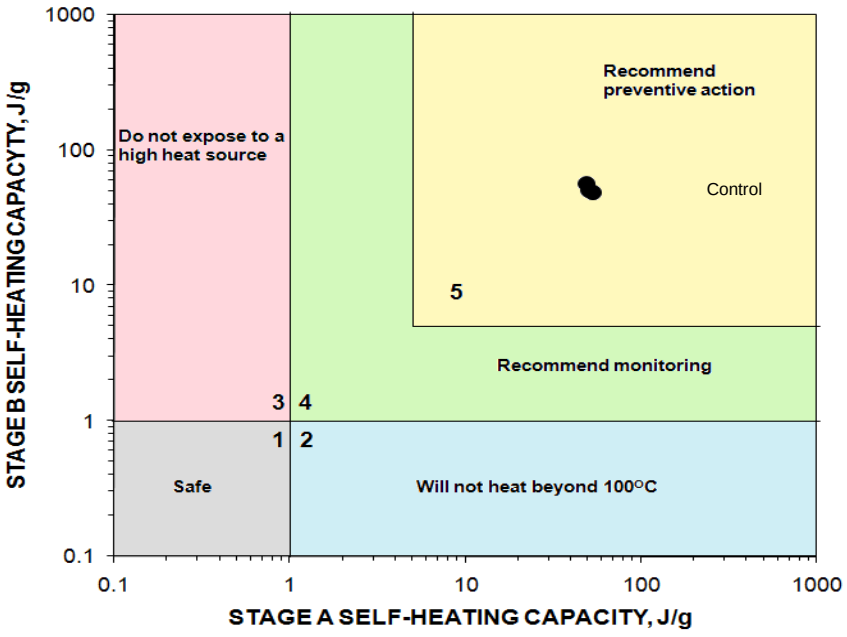

Figure 4.2: Risk Assessment Chart for Controls

To determine which hygroscopic reagents to consider, a spray test was devised to establish water retention capacity. Calcium oxide, poly (acrylic acid sodium salt), silica gel and sodium chloride gave the highest water retention capacities (Table 4.1).

Table 4.1: Water Retention Capacity of Hygroscopic Reagents

Reagent	Water Retention (kg H_2O/tonne reagent)
Calcium Chloride	214.13
Calcium Oxide	1586.56
Drierite	350.32
F-150	N/A
Poly (acrylic acid sodium salt)	691.91
Silica Gel	940.32
Sodium Chloride	720.68
Sodium Hydroxide	158.44

Figure 4.3 includes the results for hygroscopic reagents with low impact on self-heating. Figures 4.4, 4.5, 4.6, 4.7 give the results for sodium chloride, F-150, silica gel, and poly (acrylic acid sodium salt), respectively. Additional detail is provided in Appendix Table A1 and Figures A1 to A19.

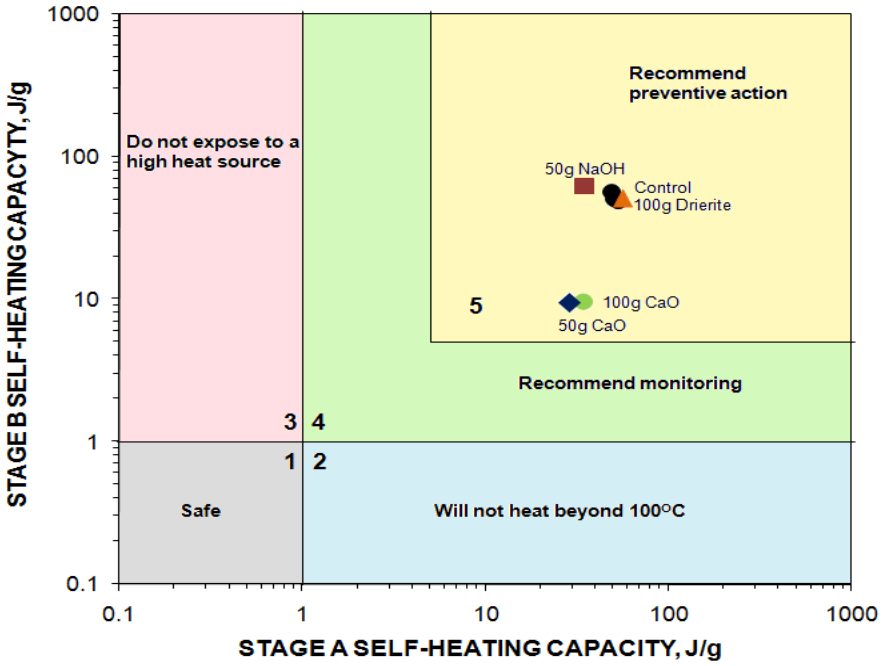

Figure 4.3: Risk Assessment Chart for Hygroscopic Reagents with Low impact on Self-Heating

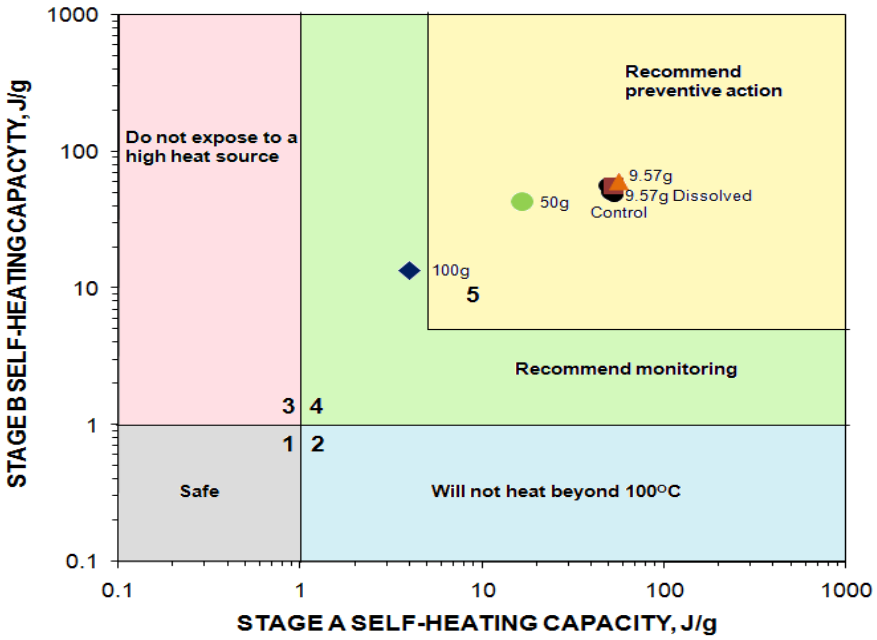

Figure 4.4: Risk Assessment Chart for Sodium Chloride

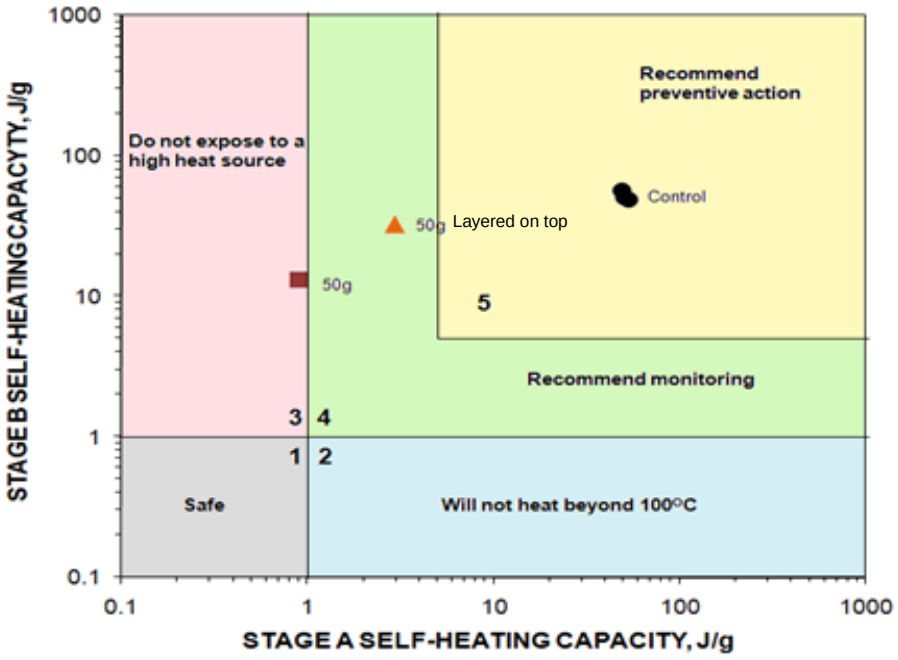

Figure 4.5: Risk Assessment Chart for F-150

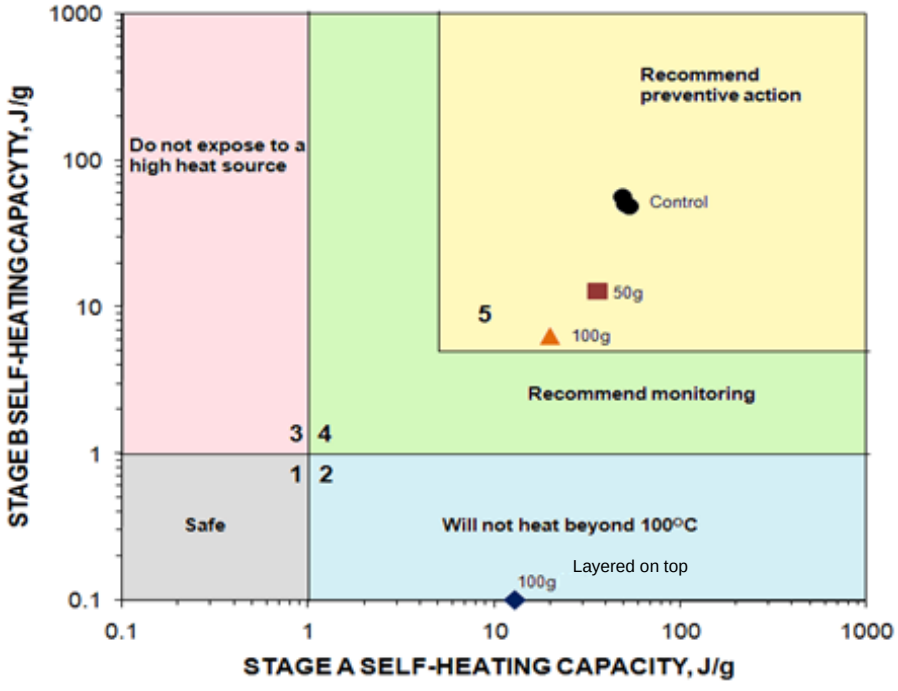

Figure 4.6: Risk Assessment Chart for Silica Gel

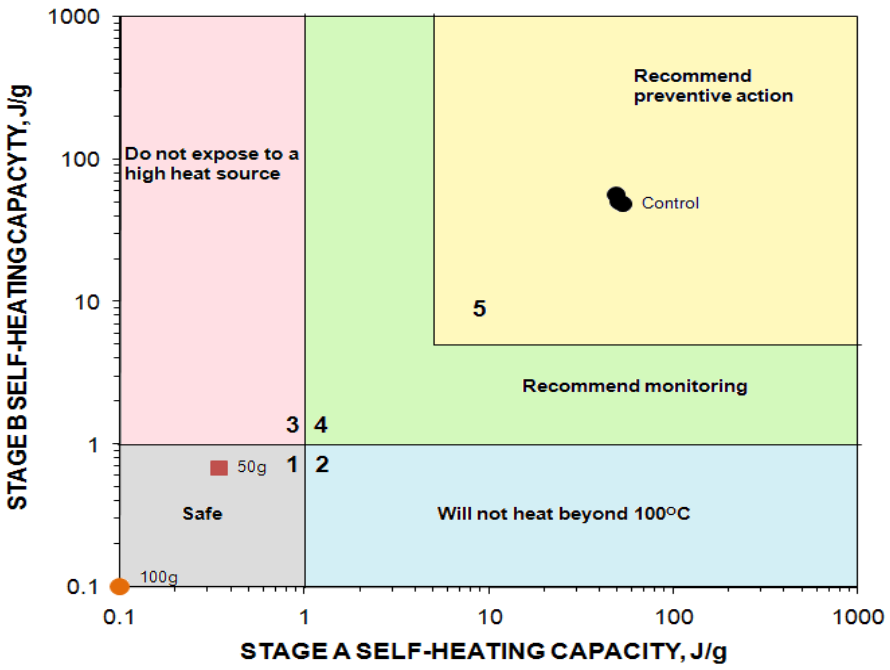

Figure 4.7: Risk Assessment Chart for Poly (acrylic acid sodium salt)

Reagents with low water retention capacities are expected to have low impact on self-heating. This is confirmed in Figure 4.3, where sodium hydroxide and drierite had little to no effect, the samples remaining in the same zone as the control (Zone 5). Although calcium oxide was expected to have a mitigating impact due to its high water retention capacity (Table 4.1), it remains within zone 5 on the risk assessment chart. This unexpected behaviour is not yet understood. Given the results for sodium hydroxide and drierite, calcium chloride with comparable low water retention was not tested.

A summary of the results is given in Table 4.2. As noted, F-150, poly (acrylic acid sodium salt) and silica gel are the most effective mitigating reagents. The latter two in particular merited further investigation. This included examining various methods in which hygroscopic reagents are incorporated into the samples. The excellent results using a layer of silica gel should be followed up by testing layering poly (acrylic acid sodium salt). Layering in recoverable form (e.g. impregnating the reagent into "packets" or "blankets" that can be retrieved) and regenerating the reagents (e.g. by heating) offers some scope for a practical approach to the mitigation of sulphide self-heating by control of moisture.

Table 4.2: Reagents and best mitigation effect

Reagent	Water Retention (kg H_2O/tonne reagent)	Zone on chart (control, zone 5)
Calcium Oxide (50g)	1586.56	Zone 5
Drierite (100g)	350.32	Zone 5
F-150 (50g)	N/A	Zone 3
Poly (acrylic acid sodium salt) (100g)	691.91	Zone 1
Silica Gel (100g Not Mixed)	940.32	Zone 2
Sodium Chloride (100g)	720.68	Zone 4
Sodium Hydroxide (50g)	158.44	Zone 5

4.3 Sulphur analysis

Confirmatory tests for the cold finger analysis using sulphur powder mixed with sand showed 99.05 ± 0.4% recovery (95% confidence interval) from three trials. Using cold finger analysis, the pyrrhotite tailings were weathered for 18 days at 40 ^{o}C and 60 ^{o}C. Elemental sulphur formation increased with increasing weathering time at both temperatures; however a drop in sulphur content was seen on the 18th day attributed to analytical error. Sulphur is dissolved in ethanol for UV-vis analysis and as the amount of sulphur increased, it became difficult to bring all the sulphur into solution due to limited solubility in ethanol. It was not possible to use carbon disulphide as an alternative solvent because the UV-vis instrument could not be moved under the fume hood. Therefore, another analysis method was used namely, direct dissolution in carbon disulphide, which could be done under the fume hood.

Confirmatory tests for carbon disulphide analysis using the sulphur powder mixed with sand showed 98.1 ± 1.98% recovery (95% confidence interval) from three trials. Pyrrhotite tailings were weathered for 31 days and sampled periodically for elemental sulphur by carbon disulphide dissolution and although scatter increased as sulphur content increased, the trends were clear. Consequently, all subsequent tests used the carbon disulphide analysis method.

4.4 Elemental sulphur vs. moisture

An increase in sample moisture content with weathering time was observed when weathered at both 40 ^{o}C and 60 ^{o}C. Samples weathered at 40 ^{o}C, 100% relative humidity gave increasing moisture content but 30% relative humidity moisture content was approximately constant (Figure 4.8). Samples weathered at 60 ^{o}C had a similar pattern as at 40 ^{o}C but with lower moisture content (Figure 4.9) attributed to evaporation at the higher temperature.

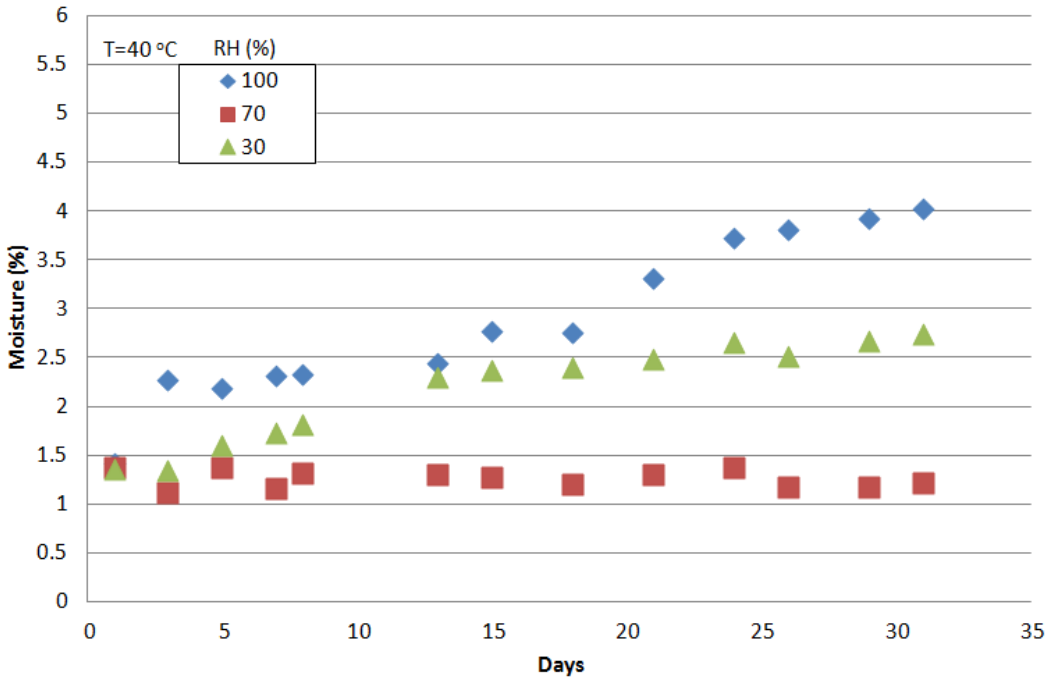

Figure 4.8: Sample moisture as a function of weathering time at 40 ^{o}C

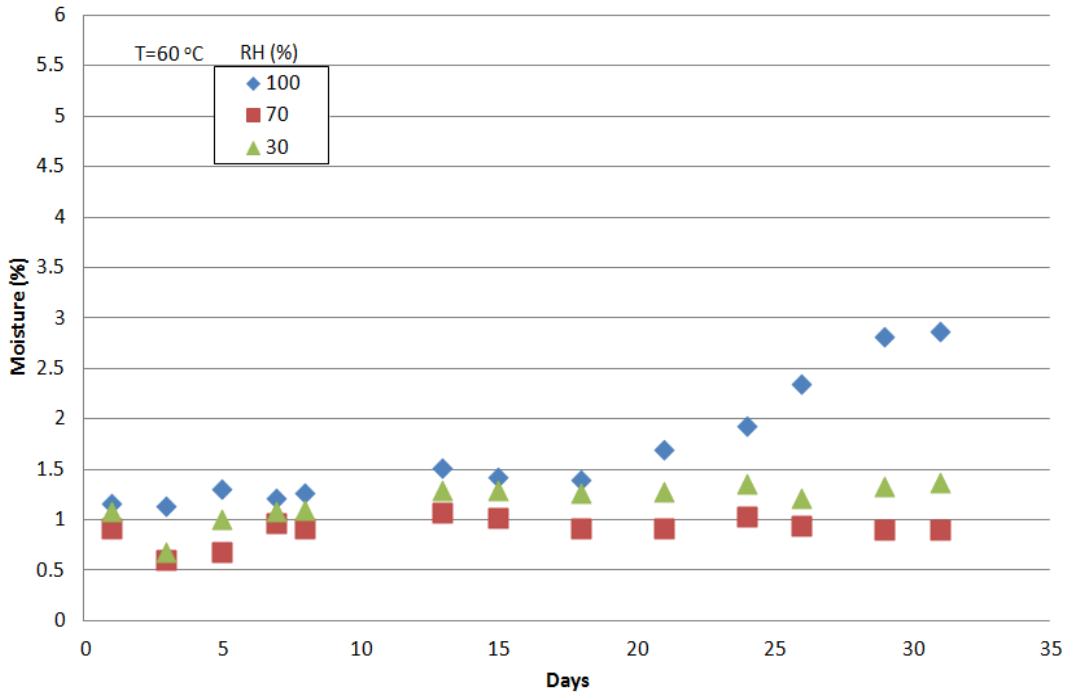

Figure 4.9: Sample moisture as a function of weathering time at 60 ^{o}C

A two-factor with replication ANOVA test was conducted on the moisture data to determine significance (Table 4.3). "Sample" represents the two sampling sites, middle (1) and under the air injection point (2); and "Columns" represent the different weathering conditions. Interactions represent the overall difference between the two sampling sites and weathering conditions. Examining the F, F critical and P-values, the differences between the two sampling sites are not significant. This indicates that the moisture content analysis was representative. A significant difference in moisture content exists between each weathering condition, as expected.

Table 4.3: Two-factor with replication ANOVA on moisture content between samples

Source of Variation	SS	df	MS	F	P-Value	F critical
Sample	6.41E-07	1	6.41E-07	2.74E-06	0.998681	3.906849
Columns	69.50385	5	13.90077	59.42565	2.59E-33	2.277044
Interactions	0.387019	5	0.077404	0.3309	0.893637	2.277044
Within	33.68429	144	0.233919			
Total	103.5752	155				

Elemental sulphur formation increased at both temperatures as weathering time increased (Figure 4.10, Figure 4.11). At both 40 ^{o}C and 60 ^{o}C, samples weathered at the highest relative humidity (100%) had the most sulphur formation and the lowest sulphur formation occurred at the lowest relative humidity (30%). There is some scatter in the data after 15 days attributed to increased uncertainty in dissolution at the higher sulphur levels. The amount of carbon disulphide used to dissolve elemental sulphur seemed adequate initially. However, as the weathering continued and more sulphur was formed, there was a suggestion that more carbon disulphide was required as solvent (i.e., a higher solvent to solids ratio might have reduced the scatter). The same amount of carbon disulphide was kept for each sample for consistency. The trendline, however, remains clear and is used to estimate the most probable sulphur content.

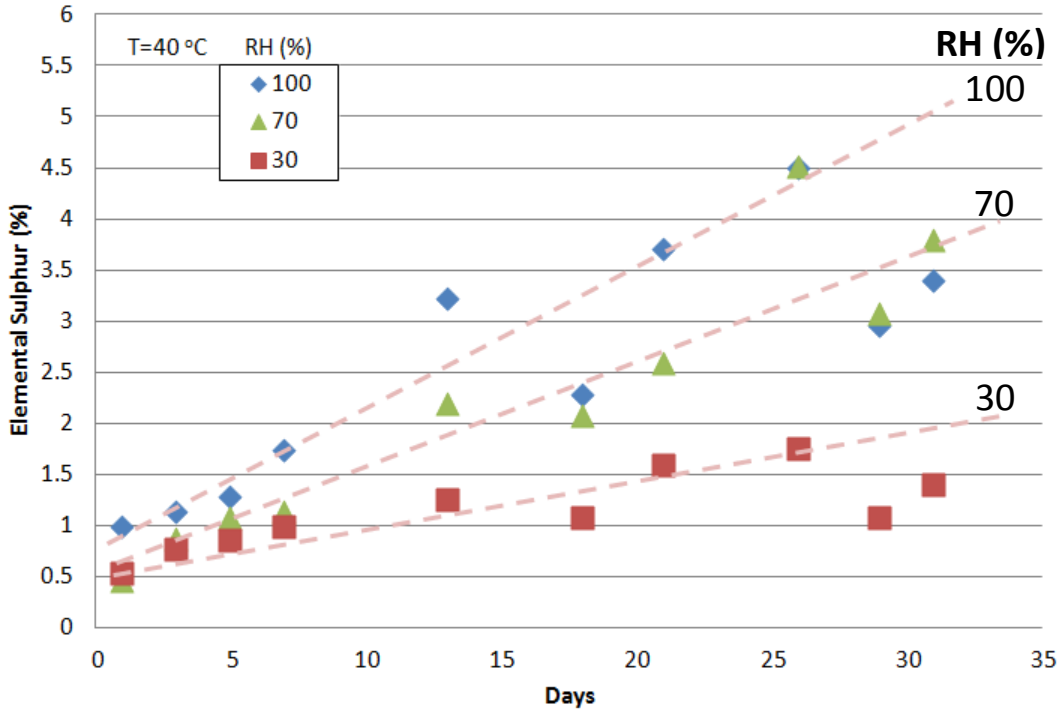

Figure 4.10: Elemental sulphur as a function of weathering time at 40 °C

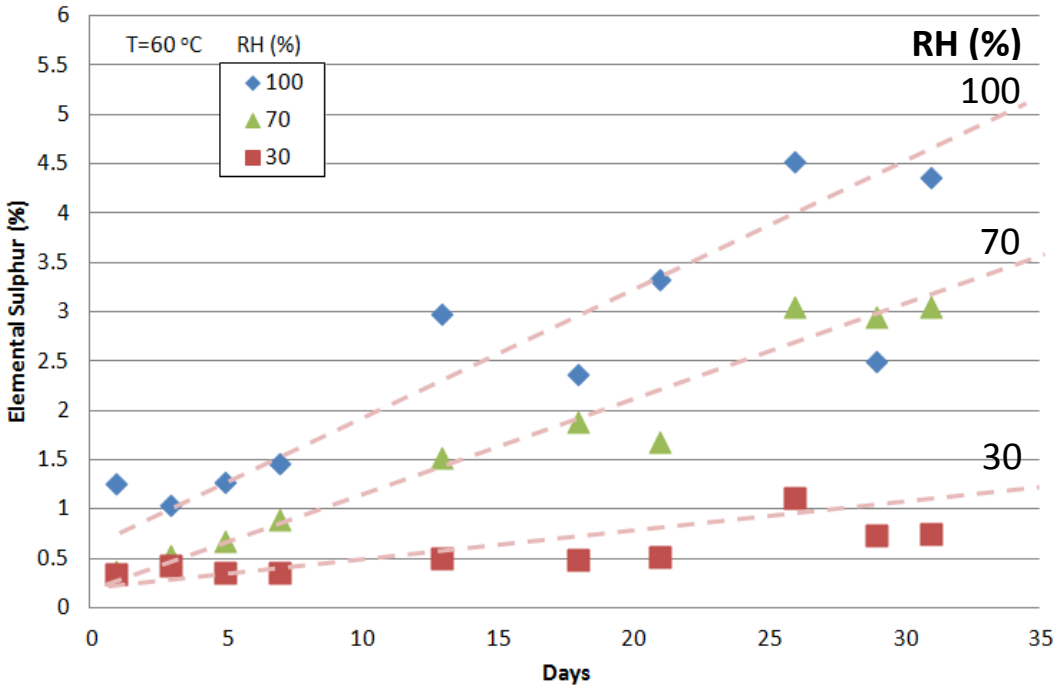

Figure 4.11: Elemental sulphur as a function of weathering time at 60 °C

Combining results from the cold finger analysis (minus the 18th weathering day which gave erroneous sulphur assay) and the carbon disulphide analysis shows that elemental sulphur formation appears to increase linearly with sample moisture content for both temperatures.

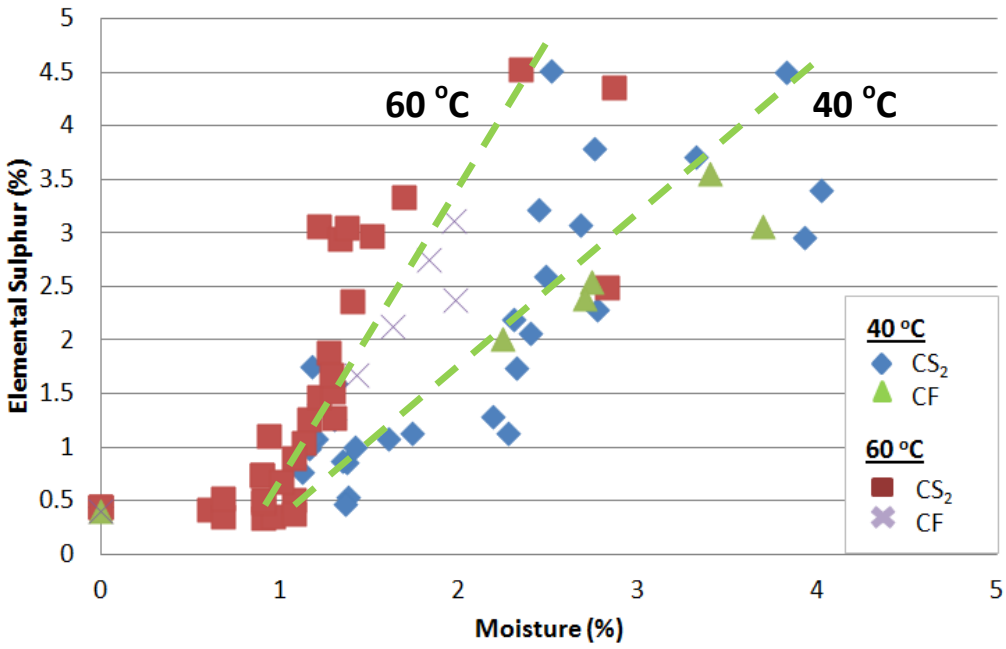

Figure 4.12: Combined carbon disulphide and cold finger analysis for elemental sulphur formation vs. sample moisture at 40 °C and 60 °C (Note: Sulphur at 0% moisture is the initial, i.e., as received, sulphur content, 0.44%)

Elemental sulphur formation on the 31st weathering day was estimated from the trendline in Figure 4.10 and Figure 4.11 and was plotted against moisture content in the sample on the 31st weathering day. Results show a correlation where elemental sulphur formation increases with sample moisture content (Figure

4.13). The data on day 31 are important as this is the sample condition when subjected to the stage B self-heating test.

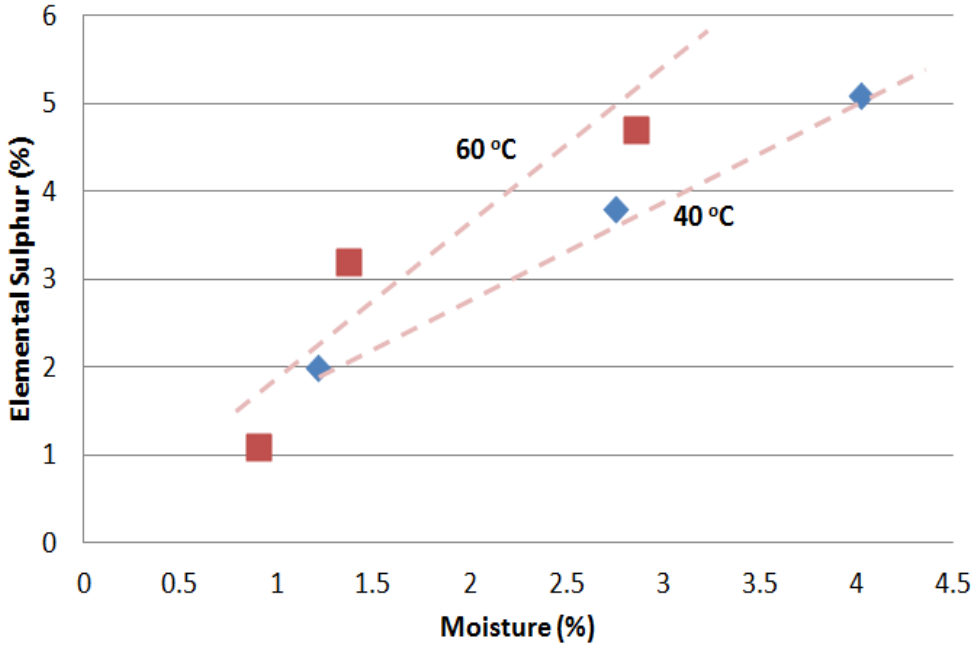

Figure 4.13: Combined carbon disulphide for moisture and elemental sulphur on the 31st weathering day (estimated point) at 40 °C and 60 °C (Note: Elemental sulphur is from trendline, moisture is as measured)

Pictures of the pyrrhotite tailings samples were taken during the periodic sampling (Figure 4.14 – Figure 4.16). It was observed that the color of samples weathered at 30% relative humidity remained more or less constant throughout the entire 31 weathering days (Figure 4.16). Samples weathered at higher relative humidities (70%, 100%) and higher temperatures (60 °C) were visibly more oxidized (Figure 4.14, Figure 4.15).

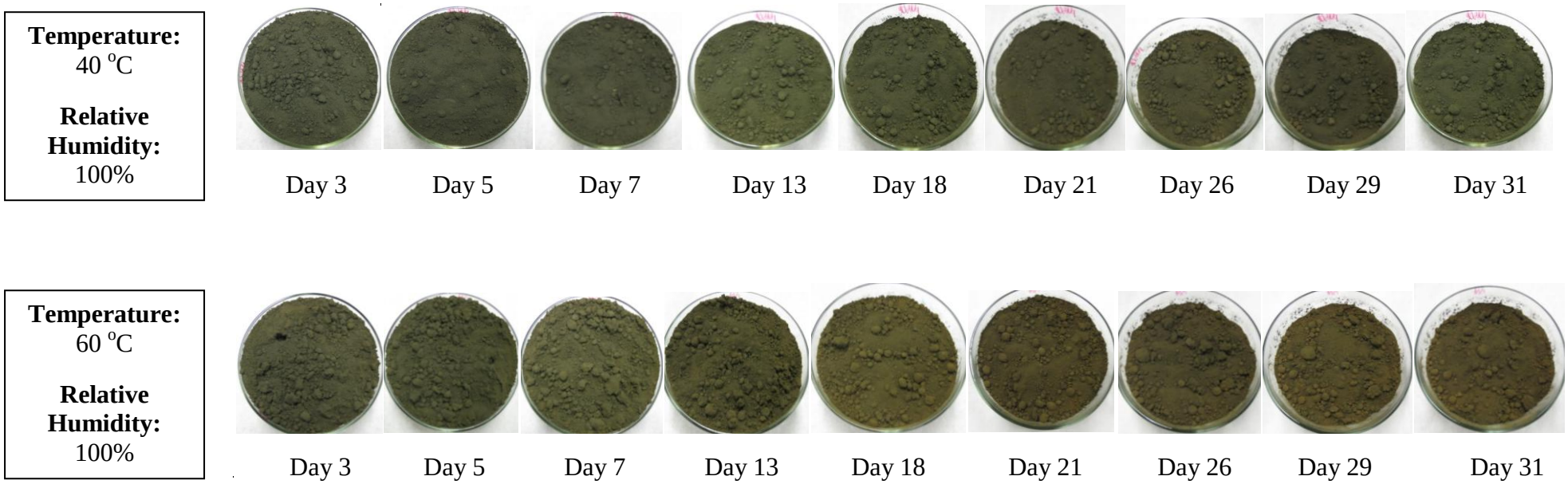

Figure 4.14: Samples weathered for 31 days at temperatures of 40 °C, 60 °C and 100% relative humidity

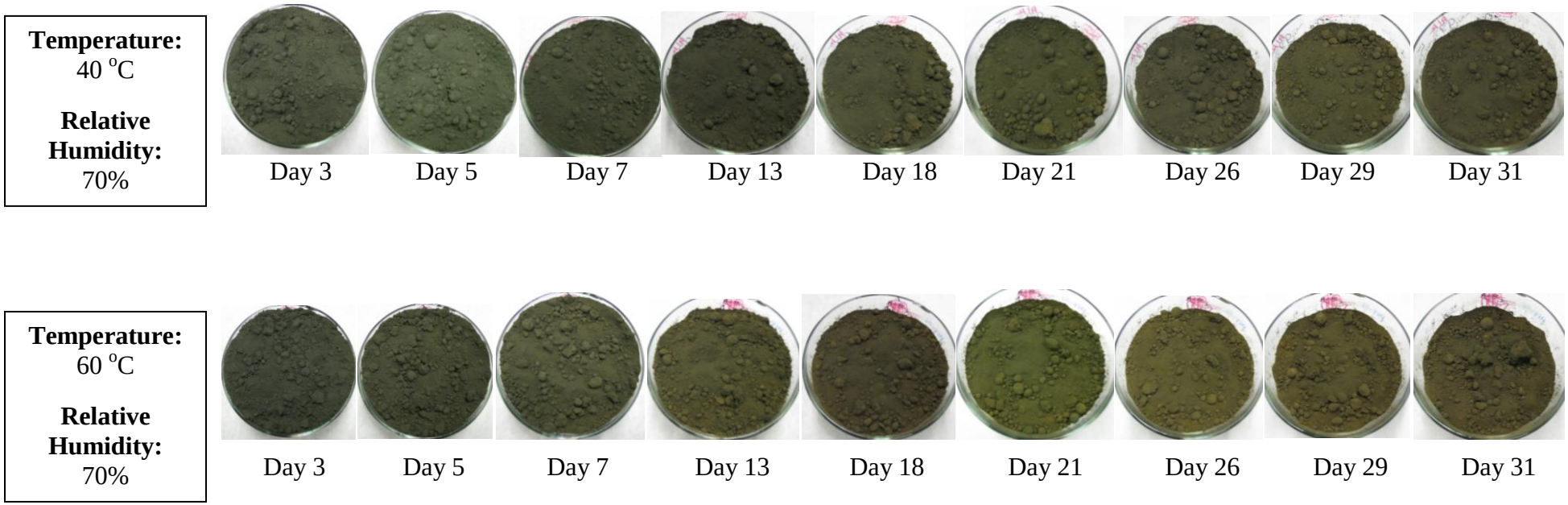

Figure 4.15: Samples weathered for 31 days at temperatures of 40 °C, 60 °C and 70% relative humidity

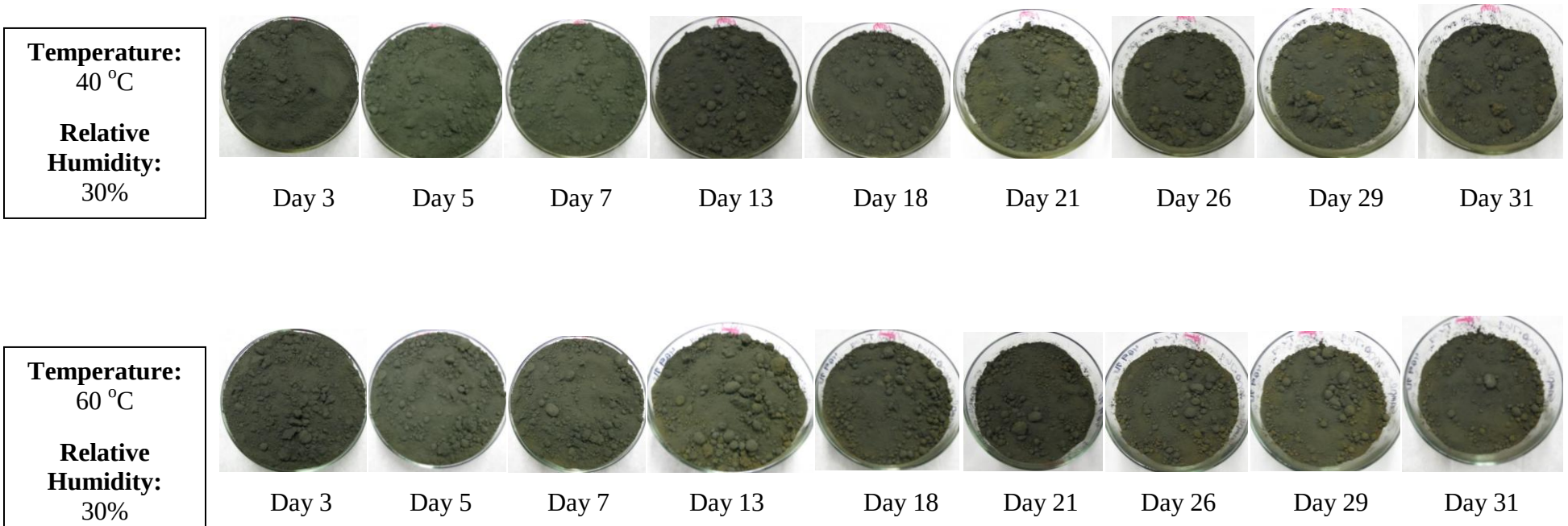

Figure 4.16: Samples weathered for 31 days at temperatures of 40 °C, 60 °C and 30% relative humidity

4.5 Elemental sulphur vs. stage B self-heating rate

Stage B self-heating rates, calculated over the first 10 peaks corresponding to the standard test, were plotted against estimated elemental sulphur at day 31 (Figure 4.17). The figure shows that the amount of self-heating divides into two distinct groups dependent on temperature: 40 ^{o}C and 60 ^{o}C. It is evident that at the lower 40 ^{o}C temperature, samples exhibited higher self heating rates than at the higher 60 ^{o}C temperature. The self-heating rates stayed more or less constant as a function of relative humidity (30%, 70% and 100%) within the temperature group.

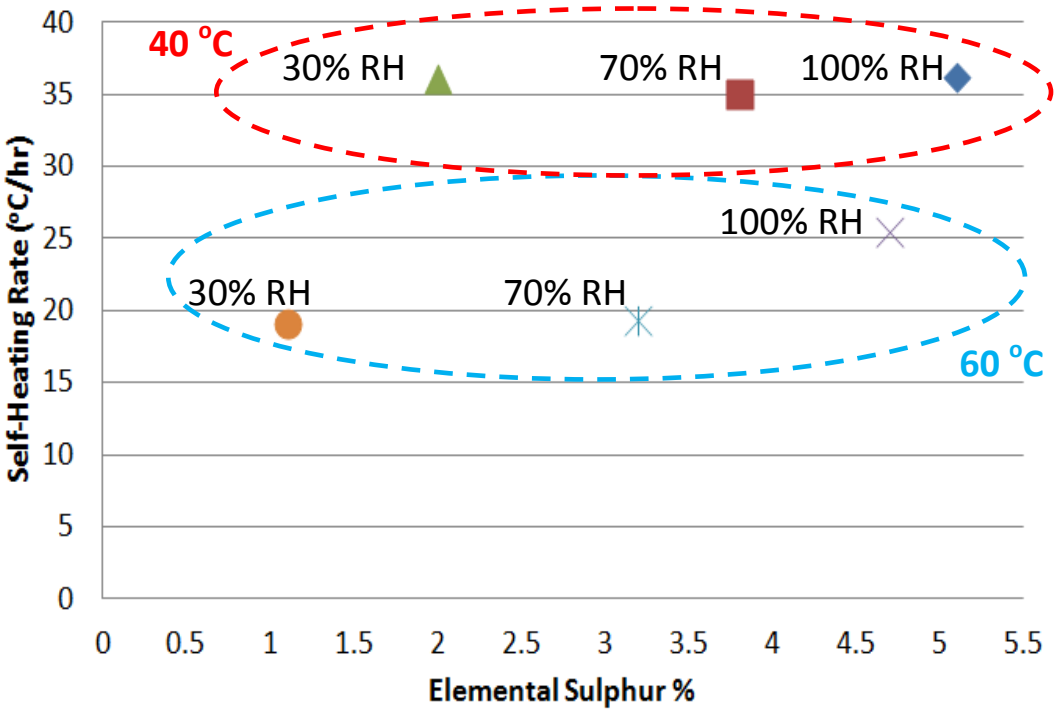

Figure 4.17: Sulphur vs. stage B self-heating rate (standard 10 peaks)

The number of air injections into the sample until heating peaks disappeared also showed the temperature effect. For example, the computer output showed that heating peaks for samples weathered at 40 ^{o}C and 100% relative humidity diminished after 88 air injections (Figure A20a, Figure A20b), while samples weathered at 60 ^{o}C and 100% relative humidity diminished after 69 air injections (Figure A21a, Figure A21b). Figure 4.18 shows that the total number of air injections does increase with elemental sulphur but the division depending on temperature is again observed. Now plotting the total self-heating rate based on all heating peaks, Figure 4.19 does show an increase with sulphur content as well as the temperature effect.

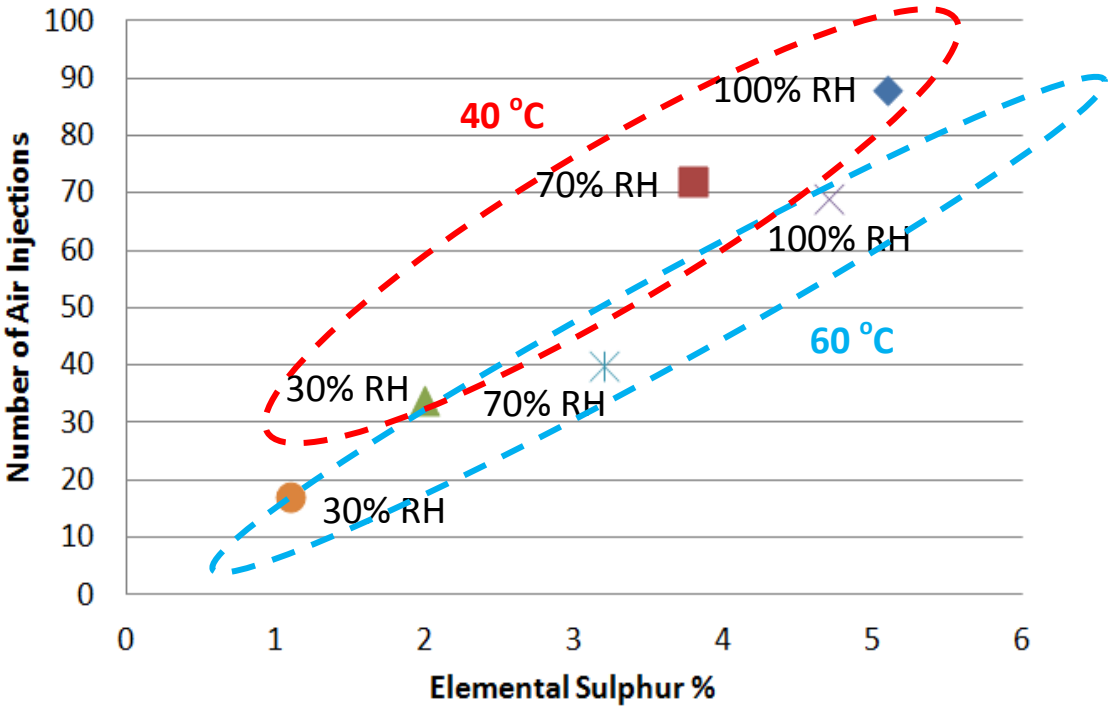

Figure 4.18: Sulphur concentration vs. number of air injections

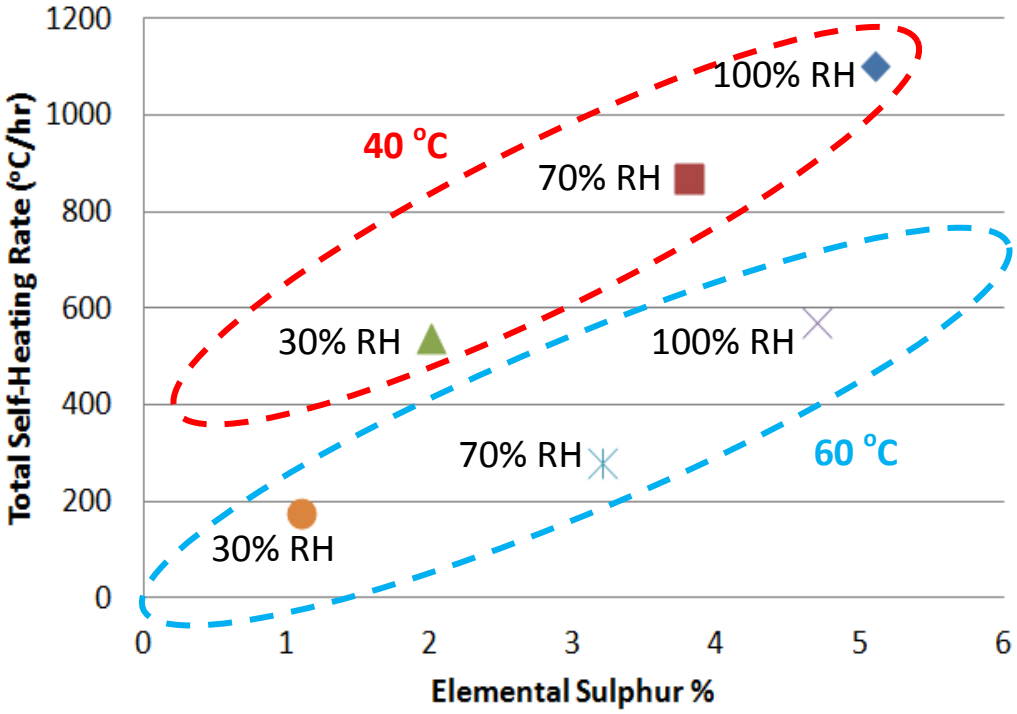

Figure 4.19: Elemental sulphur vs. stage B total self-heating rate

Chapter 5 Discussion

5.1 Mitigation

It has been established that sample moisture plays a role in sulphide self-heating; therefore one approach to mitigation is additives that can control the sample moisture content. Various hygroscopic reagents were chosen, partly dictated by availability. The reagents were screened based on water uptake capacity (hygroscopic strength) and facility to combine with samples in the standard self-heating apparatus. Poly (acrylic acid sodium salt) is a superabsorbent polymer found in baby diapers (Kabiri et al. 2003). Silica gel is often used in packaging to keep humidity low. There are also reports of using sodium chloride to control heating in hay stacks (Johnson 1992).

As seen in Figure 4.4, when saturated sodium chloride solution was substituted for the 6 weight % moisture, there was no mitigation effect. The treated sample remains in the same zone as the control sample and experiences similar self-heating rates for stages A and B as shown in Table A1. The results are the same when 9.57g dry sodium chloride was added to the sample. With 50g sodium chloride, there was still no significant impact but with 100g, there is a decrease in the self-heating rates changing the status to zone 4. However, this is not a practical solution.

Samples treated with F-150 did undergo mitigation (Figure 4.4). The self-heating rates of stage A for both 50g mixed into the sample and 50g layered on top

decreased significantly when compared to the control; the sample status became zone 3. There is mitigation when 50g of F-150 is layered on top, but it is not as efficient as mixing into the sample. The F-150 is liquid and when layered on top, it seeps into the sample and the top layer becomes re-exposed to the atmosphere. There was a question whether F-150 is to be considered "moisture" since it is liquid. A test was conducted where moisture was replaced by F-150 sprayed into the sample. As shown in Figure A19, no self-heating was detected in stage A, therefore F-150 is not considered "moisture". The F-150 is probably effective in moisture control due to its many hydrophilic OH sites which H-bond with water molecules.

With 50g and 100g of silica gel (Figure 4.5), there is a decrease in self-heating rates for stage B and some impact on stage A but the sample remains within zone 5. However, when 100g of silica gel was layered on top of the sample, there was a significant decrease in stage A self-heating and especially in stage B which showed little to no self-heating response. The status changed to zone 2. The layering method of silica gel addition, it is argued, has a superior mitigating effect because it acts as a barrier between the moisture in the atmosphere and the sample. As the sample heats, the 6% moisture originally present starts to evaporate and appears to be replenished from the atmosphere. The silica gel layer intercepts the moisture from the atmosphere, preventing it from replacing the evaporated moisture from the sample.

Silica gel has some attractive features. It possesses high porosity and consequently high specific surface area for water retention (water molecules are

physically adsorbed); and silica gel is widely available and regenerated by heating up to 150 ^{o}C for approximately two hours to drive off the adsorbed water (Weintraub 2002).

The use of poly (acrylic acid sodium salt) as a hygroscopic reagent had a major mitigating effect (Figure 4.6). The self-heating rates of both stage A and B decreased significantly compared with the control, as also shown in Table A1. With 50g poly (acrylic acid sodium salt), the sample status moves to the "safe" zone 1; with 100g it is observed that virtually no self-heating occurs in either stage A or B. Poly (acrylic acid sodium salt) was designed as a super absorbent polymer, classified as a hydrogel, and is used, for example, in baby diapers (Kabiri et al. 2003; Jockusch et al. 2009). It is efficient in moisture control due to the polymer chains being cross-linked by covalent bonds (Jockusch et al. 2009). When in contact with water, the cross-linking causes the polymers to swell, allowing it to trap water molecules. This reagent was expected to have an effect on mitigating self-heating due to its high water retention capacity and this proved to be the case. However, a disadvantage was that after being treated with poly (acrylic acid sodium salt), samples had swelled and were "cemented" and the reagent was difficult to recover for re-use.

5.2 Moisture and elemental sulphur formation in stage A

Sample moisture content increased with time and exposure to higher relative humidity and lower temperatures (Figure 4.8, Figure 4.9). Higher temperatures

retain less humidity in samples due to lower enthalpy of evaporation (ΔH_{vap}). At 40 ^{o}C and 60 ^{o}C, the enthalpies of evaporation are 2406.9 kJ/kg and 2358.6 kJ/kg (Smith et al. 2005), respectively. At both temperatures, samples exposed to 100% relative humidity gained the most moisture whereas moisture in samples exposed to 30% relative humidity remained approximately constant throughout the weathering period.

At both 40 ^{o}C and 60 ^{o}C, there is an increase in elemental sulphur formation with weathering time, samples at 100% relative humidity generally giving higher sulphur levels (Figure 4.10, Figure 4.11). Sulphur formation was least at 60 ^{o}C and 30% relative humidity and remained almost constant over the 31 weathering days. Although there is scatter attributed to dissolution issues at higher sulphur levels, trendlines can be established and clear distinctions between the different relative humidities seen. Combining results obtained from the cold finger and carbon disulphide analysis (Figure 4.12) showed a linear increase in elemental sulphur with the sample moisture content. (This also confirms that the analysis by both methods is in agreement). The linear trend was also observed when combining the estimated sulphur content from the 31st day (from Figure 4.10 and Figure 4.11) (Figure 4.13). The linear correlations confirm that the formation of elemental sulphur is linked with the sample moisture content.

It had previously been determined by Rosenblum and Spira (1995) that elemental sulphur in stage A is formed more readily at higher temperatures and that moisture plays a role in sulphide self-heating. Tests performed in this thesis have shown that temperature and moisture content combine to have an effect on

elemental sulphur formation. Figure 4.12 and Figure 4.13 show that for the same range of sulphur content, less moisture is required for its formation at 60 ^{o}C than at 40 ^{o}C. The next question is how is stage B self-heating related to weathering conditions in stage A, in particular production of sulphur in stage A.

5.3 Stage B self-heating

Results indicate that the combination of temperature and moisture content has an effect on elemental sulphur formation in stage A, therefore likely affecting the self-heating rate in stage B. The anticipated result was that there would be an increase in stage B self-heating correlated with increasing sulphur. However, the results show that self-heating rate was independent of sulphur content but higher for samples exposed to 40 ^{o}C compared to 60 ^{o}C (Figure 4.17). Addressing the first point, it seems possible that provided there is enough sulphur to sustain more than 10 heating peaks that the self-heating rate based upon the first 10 will not differ. This seems born out when using the additional measure, the number of heating peaks until heating stopped, which does show an increase with increasing sulphur (Figure 4.18) and consequently the total self-heating rate increases with increasing sulphur (Figure 4.19).

Regardless of which definition of self-heating rate is used, there is always a division between the two temperatures (40 ^{o}C and 60 ^{o}C). The effect of temperature may be due to the type of sulphur formed. There exist 30 different solid allotropes of sulphur that have been recognized (Steudel and Eckert 2004).

The stability of these sulphurs may vary depending on what temperatures they are formed at. For example, sulphurs may be formed with high bond energies (as high as 430 kJ mol^{-1}) under certain condition whereas some sulphurs may be formed with a lower bond energy (Greenwood and Earnshaw 1984). If higher bond energy sulphur is formed during weathering, it may be more difficult to "burn" this sulphur in stage B, hence resulting in lower self-heating rates. The higher self-heating rate at 40 ^{o}C can also lead to the question of whether self-heating is affected solely by the presence of elemental sulphur or there is another factor.

Another factor may be the reaction giving rise to sulphur. There are various reaction mechanisms that have been proposed for elemental sulphur formation that will depend on temperature. Some of these reactions are described in chapter 2, section 2.5. One sequence of reactions suggests that higher moisture content (i.e., at lower (40 ^{o}C) temperature) promotes formation of H_2S (Equation 2.19 – Equation 2.22) in stage A which contributes to elemental sulphur formation. It is speculated that the amount of H_2S formed and whether it is completely or partially oxidized can affect the type of sulphur produced.

An effect of moisture and temperature during weathering on stage B self-heating is also observed visually (Figure 4.14 – Figure 4.16). Previous tests on similar high pyrrhotite content samples by Somot and Finch (2006) showed similar results where high pyrrhotite samples exhibited high self-heating yet visibly appeared less oxidized. This was also observed by Wang (2007) where samples

with higher access to air visibly appeared less oxidized retaining the original grey color whereas samples exposed to a limited air supply turned a light brown. This led to speculation that the presence of pyrrhotite causes a reducing environment resulting in H_2S formation in stage A. Oxidation of H_2S and self-heating in stage A is attributed to the series of exothermic reactions, Equations 2.19 – Equation 2.23, (Somot 2006).

Chapter 6 Conclusions and recommendations

6.1 Conclusions

A spray test measuring water retention proved effective in identifying hygroscopic reagents for mitigating sulphide self-heating by control of moisture. Poly (acrylic acid sodium salt) was the most efficient mitigating reagent, reducing self-heating in both stage A and B. Silica gel had more influence when layered on top of the sample. This raises the possibility that mitigation by moisture control needs to isolate the sample from atmospheric moisture.

To analyze elemental sulphur content in the sample, the carbon disulphide dissolution method was preferred over the cold finger analysis method especially as sulphur levels rose.

Samples that were weathered at high relative humidity (100%) had higher elemental sulphur formation.

Taking the standard first 10 heating peaks showed stage B self-heating rate remained constant, independent of sulphur but was higher at 40 ^{o}C than at 60 ^{o}C. Taking the total number of peaks until heating ceased showed a dependence on sulphur content but again higher response at 40 ^{o}C than at 60 ^{o}C. An argument is advanced that the type of sulphur formed and thus its oxidation may vary depending on the temperature at which weathering takes place.

6.2 Recommendations

To determine if there is any elemental sulphur remaining after all heating peaks have disappeared. The hypothesis is that sulphur is oxidized during stage B, therefore assaying for remaining sulphur will test the hypothesis.

To weather the sample over a wider range of temperature (i.e., 25 ^{o}C, 30 ^{o}C, 80 ^{o}C) to confirm the temperature effect on stage B self-heating.

To determine the different types of elemental sulphur being formed under various weathering conditions and relate to the effect on stage B self-heating.

A higher volume of carbon disulphide should be used for elemental sulphur analysis to ensure complete solubilisation. For this thesis 15 mL of carbon disulphide was used for 5 g of samples, which may not be sufficient after about 15 weathering days, as suggested by the increased scatter. Future work should consider 20 mL – 25 mL of carbon disulphide for 5 g samples.

References

Abraitis, P. K., R. A. D. Pattrick, et al. (2004). "Acid leaching and dissolution of major sulphide ore minerals: processes and galvanic effects in complex systems." Mineralogical Magazine **68**(2): 343-351.

Becker, M. (2009). The mineralogy and crystallography of pyrrhotite from selected nickel and PGE ore deposits and its effect on flotation performance. Material Science & Metallurgical Engineering. Pretoria, University of Pretoria. **PhD**.

Becker, M., J. d. Villiers, et al. (2010). "The flotation of magnetic and non-magnetic pyrrhotite from selected nickel ore deposits." Minerals Engineering **23**(11–13): 1045-1052.

Belzile, N., Y.-W. Chen, et al. (2004). "A review on pyrrhotite oxidation." Journal of Geochemical Exploration **84**(2): 65-76.

Buckley, A. (1985). "X-ray photoelectron spectroscopy of oxidized pyrrhotite surfaces I. Exposure to aire." Applied Surface Science **22-23**: 280-287.

Chen, X. D. and L. V. Chong (1998). "Several Important Issues Related to the Crossing-Point Temperature (CPT) Method for Measuring Self-Ignition Kinetics of Combustible Solids." Process Safety and Environmental Protection **76**(2): 90-93.

Cruz, R., I. González, et al. (2005). "Electrochemical characterization of pyrrhotite reactivity under simulated weathering conditions." Applied Geochemistry **20**(1): 109-121.

Currell, B. R. and A. J. Williams (1974). "Thermal analysis of elemental sulphur." Thermochimica Acta **9**(3): 255-259.

Dixon, D. G., D. D. Mayne, et al. (2008). "Galvanox™ - A Novel Galvanically-Assisted Atmospheric Leaching Technology for Copper Concentrates." Canadian Metallurgical Quarterly **47**(3): 327-336.

Dunn, J. G. (1997). "The oxidation of sulphide minerals." Thermochimica Acta **300**(1–2): 127-139.

Farnsworth, D. J. M. (1974). "Introduction to and background of sulphide fires in pillar mining at the Sullivan mines." CIM bulletin **70**(782): 65-71.

Feng, K. K., R. N. Chakravorty, et al. (1973). "Spontaneous combustion. Coal mining hazard." CIM (Can. Inst. Mining Met.) Bull. **66**(Copyright (C) 2012 American Chemical Society (ACS). All Rights Reserved.): 75-84.

Good, B. H. (1977). "The oxidation of sulfide minerals in the Sullivan Mine." CIM Bull. **70**(Copyright (C) 2012 American Chemical Society (ACS). All Rights Reserved.): 83-88.

Graham, J. and C. D. McKenzie (1987). "Oxygen in pyrrhotite; 2, Determination of oxygen in natural pyrrhotites." American Mineralogist **2**: 605-609.
Greenwood, N. N. and A. Earnshaw (1984). Chemistry of the elements. Oxford [Oxfordshire]; New York, Pergamon Press.

Gunsinger, M. R., C. J. Ptacek, et al. (2006). "Evaluation of long-term sulfide oxidation processes within pyrrhotite-rich tailings, Lynn Lake, Manitoba." Journal of Contaminant Hydrology **83**(3-4): 149-170.

Güyagüler, T., C. Karpuz, et al. (2003). "The spontaneous combustion characteristics of Turkish lignite and correlation of the self-heating process with the actual fire." CIM Bulletin **96**(1070): 75-79.

Hampton, M. A., C. Plackowski, et al. (2011). "Physical and Chemical Analysis of Elemental Sulfur Formation during Galena Surface Oxidation." Langmuir **27**(7): 4190-4201.

Iliyas, A., K. Hawboldt, et al. (2011). "Kinetics and safety analysis of sulfide mineral self-heating." J. Therm. Anal. Calorim. **106**(Copyright (C) 2012 American Chemical Society (ACS). All Rights Reserved.): 53-61.

Janzen, M. P., R. V. Nicholson, et al. (2000). "Pyrrhotite reaction kinetics: reaction rates for oxidation by oxygen, ferric iron, and for nonoxidative dissolution." Geochimica et Cosmochimica Acta **64**(9): 1511-1522.

Jockusch, S., N. J. Turro, et al. (2009). "Photoinduced surface crosslinking of superabsorbent polymer particles." J. Appl. Polym. Sci. Journal of Applied Polymer Science **111**(5): 2163-2170.

Johnson, P. D. A. (1992). Hay mow and silo fires. Ministry of Agriculture Food and Fisheries. British Columbia.

Kabiri, K., H. Omidian, et al. (2003). "Synthesis of fast-swelling superabsorbent hydrogels: effect of crosslinker type and concentration on porosity and absorption rate." European Polymer Journal **39**(7): 1341-1348.

Kirshenbaum, N. W. (1967). Transport and handling of sulphide concentrates: problems and possible improvements, [Stanford, Calif] : Stanford University, Dept. of Mineral Engineering.

Kocabag, D. and M. R. Smith (1985). The effect of grinding media and galvanic interactions upon the flotation of sulfide minerals, Metall. Soc.

Kwong, Y. T. J., G. W. Swerhone, et al. (2003). "Galvanic sulphide oxidation as a metal-leaching mechanism and its environmental implications." Geochemistry: Exploration, Environment, Analysis **3**(4): 337-343.

Lowson, R. T. (1982). "Aqueous oxidation of pyrite by molecular oxygen." Chem. Rev. Chemical Reviews **82**(5): 461-497.

Lukaszewski, G. M. (1973). Sulphides in underground mine filling operations. Jubilee Symposium on Mine Filling Mt Isa**:** 87-96.

McGuire, M. M. and R. J. Hamers (2000). "Extraction and Quantitative Analysis of Elemental Sulfur from Sulfide Mineral Surfaces by High-Performance Liquid Chromatography." Environmental Science & Technology **34**(21): 4651-4655.

Mehta, A. P. and L. E. Murr (1983). "Fundamental studies of the contribution of galvanic interaction to acid-bacterial leaching of mixed metal sulfides." Hydrometallurgy **9**(Copyright (C) 2012 American Chemical Society (ACS). All Rights Reserved.): 235-256.

Mielke, R. E., D. L. Pace, et al. (2003). "A critical stage in the formation of acid mine drainage: Colonization of pyrite by Acidithiobacillus ferrooxidans under pH-neutral conditions." Geobiology **1**(1): 81-90.

Mycroft, J. R., G. M. Bancroft, et al. (1990). "Detection of sulphur and polysulphides on electrochemically oxidized pyrite surfaces by X-ray photoelectron spectroscopy and Raman spectroscopy." Journal of Electroanalytical Chemistry Journal of Electroanalytical Chemistry **292**(1-2): 139-152.

Mycroft, J. R., H. W. Nesbitt, et al. (1995). "X-ray photoelectron and Auger electron spectroscopy of air-oxidized pyrrhotite: Distribution of oxidized species with depth." Geochimica et cosmochimica acta. **59**(4): 721.

Nelson, M. I. and X. D. Chen (2007). "Survey of experimental work on the self-heating and spontaneous combustion of coal." The Geological Society of America - Reviews in Engineering Geology **XVIII**.

Ninteman, D. J. (1978). Spontaneous oxidation and combustion of sulfide ores in underground mines : a literature survey. [Washington], Dept. of the Interior, Bureau of Mines : For sale by the Supt. of Docs., U.S. Govt. Print. Off.

Nordstrom, D. K. and G. Southam (1997). "Geomicrobiology of sulfide mineral oxidation." Reviews in Mineralogy and Geochemistry **35**(1): 361-390.

Norris, P. R., D. A. Clark, et al. (1996). "Characteristics of Sulfobacillus acidophilus sp. nov. and other moderately thermophilic mineral-sulphide-oxidizing bacteria." Microbiology **142 (Pt 4)**(Copyright (C) 2012 U.S. National Library of Medicine.): 775-783.

Nowak, P., E. Krauss, et al. (1984). "The electrochemical characteristics of the galvanic corrosion of sulfide minerals in short-circuited model galvanic cells." Hydrometallurgy **12**(Copyright (C) 2012 American Chemical Society (ACS). All Rights Reserved.): 95-110.

Ott, J. B. and J. Boerio-Goates (2000). Chemical thermodynamics : principles and applications. London, UK; San Diego, Academic Press.

Pankratz, L. B. (1984). Thermodynamic properties of halides. [Washington], U.S. Dept. of the Interior, Bureau of Mines : For sale by the Supt. of Docs., U.S. G.P.O.

Payant, R., F. Rosenblum, et al. (2012). "The self-heating of sulfides: Galvanic effects." Minerals Engineering **26**(0): 57-63.

Pfeiffer, J. B., I. American Chemical Society. Division of, et al. Sulfur removal and recovery from industrial processes, Washington, American Chemical Society.

Powell, A. V., P. Vaqueiro, et al. (2004). "Structure and magnetism in synthetic pyrrhotite Fe~7S~8: A powder neutron-diffraction study (12 pages)." Physical review. B, Condensed matter and materials physics. **70**: 014415.

Pratt, A., I. Muir, et al. (1994). "X-ray photoelectron and Auger electron spectroscopic studies of pyrrhotite and mechanism of air oxidation." Geochimica et Cosmochimica Acta Geochimica et Cosmochimica Acta **58**(2): 827-841.

Rao, S. R. and J. Leja (2004). Surface chemistry of froth flotation. New York, Kluwer Academic/Plenum Publishers.

Rohwerder, T. and W. Sand (2007). "Oxidation of Inorganic Sulfur Compounds in Acidophilic Prokaryotes." Engineering in Life Sciences **7**(4): 301-309.

Rosenblum, F., J. Nesset, et al. (2001). "Evaluation and control of self-heating in sulphide concentrates." CIM bulletin. **94**(1056): 92.

Rosenblum, F. and P. Spira (1981). Self-heating of sulphides. The Thirteenth Annual Meeting of the Canadian Mineral Processors. Ottawa**:** 34-49.

Rosenblum, F. and P. Spira (1995). "Evaluation of hazard from self-heating of sulphide rock." CIM bulletin **88**(989).

Rosenblum, F., P. Spira, et al. (1982). Evaluation of hazard from backfill oxidation. XIV International Mineral Processing Congress. Toronto, Ontario, Canadian Institute of Mining and Metallurgy.

Shaw, S. C., L. A. Groat, et al. (1998). "Mineralogical study of base metal tailings with various sulfide contents, oxidized in laboratory columns and field lysimeters." ENVIRONMENTAL GEOLOGY -BERLIN- **33**(2/3): 209-217.

Shuai, X. and A. Meisen (1995). "New correlations predict physical properties of elemental sulfur." Oil & Gas Journal **93**(42): 50-50.

Smith, J. M., H. C. V. Ness, et al. (2005). Introduction to chemical engineering thermodynamics. Boston, McGraw-Hill.

Somot, S. (2006). High self-heating rate of a pyrrhotite-rich material: H2S as a fuel? The 38th Annual Meeting of the Canadian Mineral Processors. Ottawa, Ontario, Canada**:** 83-92.

Somot, S. and J. A. Finch (2010). "Possible role of hydrogen sulphide gas in self-heating of pyrrhotite-rich materials." Miner. Eng. **23**(Copyright (C) 2012 American Chemical Society (ACS). All Rights Reserved.): 104-110.

Stachulak, J. S. (1994). "Inco's design and protection against underground fires." CIM bulletin **87**(58-63).

Steger, H. F. (1976). "Determination of the elemental sulphur content of minerals and ores." Talanta **23**(5): 395-397.

Steger, H. F. (1982). "Oxidation of sulfide minerals: VII. Effect of temperature and relative humidity on the oxidation of pyrrhotite." Chemical Geology **35**(3–4): 281-295.

Steger, H. F. and L. E. Desjardins (1978). "Oxidation of sulfide minerals, 4. Pyrite, chalcopyrite and pyrrhotite." Chemical Geology Chemical Geology **23**(1-4): 225-237.

Steudel, R. and B. Eckert (2004). "Solid Sulfur Allotropes." ChemInform **35**(14): no-no.

Suzuki, I., C. W. Chan, et al. (1994). "Oxidation of inorganic sulfur compounds by thiobacilli." ACS Symp. Ser. **550**(Copyright (C) 2012 American Chemical Society (ACS). All Rights Reserved.): 60-67.

Thomas, J. E., R. S. C. Smart, et al. (2000). "Kinetic factors for oxidative and non-oxidative dissolution of iron sulfides." Minerals Engineering **13**(10–11): 1149-1159.

Tremblay, G. (2011). Environmental challanges and opportunities for the mining industry. Short Course on Mineral Processing Systems. McGill University, Natural Resources Canada.

Tributsch, H. and H. Gerischer (1976). "The oxidation and self-heating of metal sulphides as an electrochemical corrosion phenomenon." Journal of Applied Chemistry and Biotechnology **26**(1): 747-761.

UnitedNations (2008). Manual of Tests and Criteria. PART III - Classification procedures test methods and criteria relating to Class 3, Class 4, Division 5.1 and Class 9.

UnitedNations (2011). Recommendations on the Transport of Dangerous Goods. Seventeenth revised edition.

Vaughan, D. J., E. J. Schwarz, et al. (1971). "Pyrrhotites from the Strathcona Mine, Sudbury, Canada; A Thermomagnetic and Mineralogical Study." Economic Geology Economic Geology **66**(8): 1131-1144.

Wang, X. (2007). Exploring conditions leading to self-heating of pyrrhotite-rich materials. Mining and Materials Engineering. Montreal, McGill University. **M.Eng**.

Wang, X., F. Rosenblum, et al. (2009). Oxidation, Weight Gain and Self-Heating of Sulphides. The 41st Annual Meeting of the Canadian Mineral Processors. Ottawa.

Weast, R. C. and Editor (1984). CRC Handbook of Chemistry and Physics. 64th Ed, CRC Press, Inc.

Weintraub, S. (2002) Demystifying silica gel. Object Specialty Group Postprints **9**,

Wu, C., Z.-j. Li, et al. (2001). "Investigation of chemical suppressants for inactivation of sulfide ores." J. Cent. South Univ. Technol. (Engl. Ed.) **8**(Copyright (C) 2012 American Chemical Society (ACS). All Rights Reserved.): 180-184.

Wu, C. and Z. Li (2005). "A simple method for predicting the spontaneous combustion potential of sulphide ores at ambient temperature." Mining Technology **114**(2): 125-128.

Yanful, E. K. and A. Verma (1999). "Oxidation of flooded mine tailings due to resuspension." Canadian geotechnical journal. Revue canadienne de géotechnique. **36**(5): 826.

Yang, F., C. Wu, et al. (2011). "Investigation of the propensity of sulfide concentrates to spontaneous combustion in storage." Journal of Loss Prevention in the Process Industries **24**(2): 131-137.

Appendix

Table A1: Summary of Self-Heating Rates and Self-Heating Capacities

Sample Name	Hygroscopic Reagent	Method of Introduction	Self-Heating Rate (^{o}C/hr) Stage A	Self-Heating Rate (^{o}C/hr) Stage B	Self-Heating Capacity (J/g) Stage A	Self-Heating Capacity (J/g) Stage B
SJ6-02	Control	N/A	337.80	336.9	50.67	50.54
SJ5-03	Control	N/A	325.80	377.60	48.87	56.64
SJ6-04	Control	N/A	357.60	324.70	53.64	48.71
SJ5-05	Sodium Chloride (9.57g)	Saturated solution mixed homogenously	353.70	372.90	53.06	55.94
SJ6-06	Sodium Chloride (9.57g)	Mixed homogenously	373.90	404.80	56.09	60.72
SJ6-07	Sodium Chloride (50g)	Mixed homogenously	109.50	287.20	16.43	43.08
SJ5-08	Sodium Hydroxide (50g)	Mixed homogenously	232.00	411.70	34.80	51.76
SJ5-10	Sodium Chloride (100g)	Mixed homogenously	26.40	90.90	3.96	13.64
SJ5-11	Calcium Oxide (50g)	Mixed homogenously	227.40	64.40	34.11	9.66
SJ4-12	Silica Gel (50g)	Mixed homogenously	239.70	85.60	35.96	12.84
SJ6-13	Silica Gel (100g)	Mixed homogenously	131.60	42.80	19.74	6.42
SJ5-14	Calcium Oxide (100g)	Mixed homogenously	190.70	63.60	28.61	9.54
SJ4-15	Silica Gel (100g)	Layered on top	86.20	0.01	12.93	0.01
SJ5-16	Poly (acrylic acid sodium salt) (100g)	Mixed homogenously	0.01	0.01	0.01	0.01
SJ6-17	Drierite (100g)	Mixed homogenously	372.20	340.50	55.83	51.08
SJ5-18	Poly (acrylic acid sodium salt) (50g)	Mixed homogenously	2.30	4.60	0.35	0.69
SJ6-19	F-150 (50g)	Mixed homogenously	6.00	88.10	0.90	13.22
SJ5-20	F-150 (50g)	Layered on top	19.50	215.60	2.93	32.34
SJ6-21	F-150 (31.9g)	Mixed homogenously	0.01	65.60	0.01	9.84

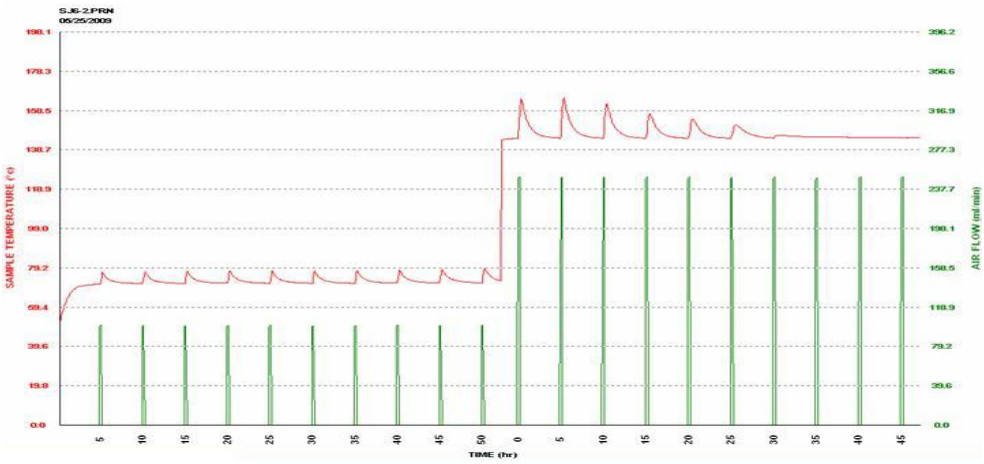

Figure A1: Computer output of control (SJ6-02)

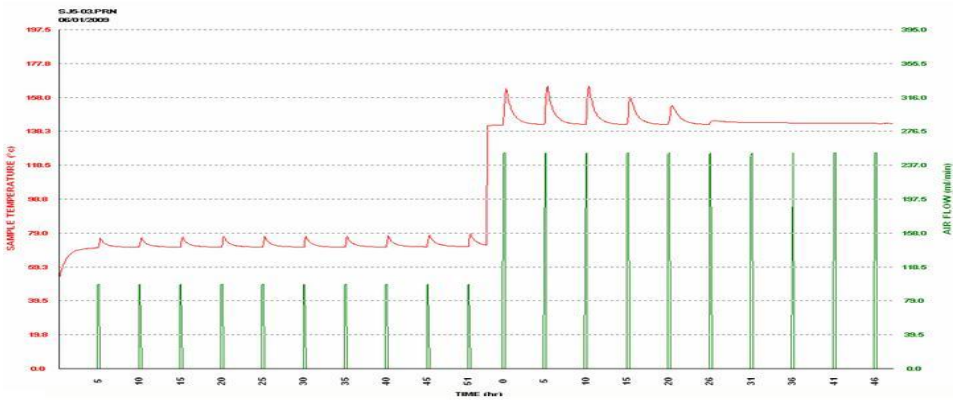

Figure A2: Computer output of control (SJ5-03)

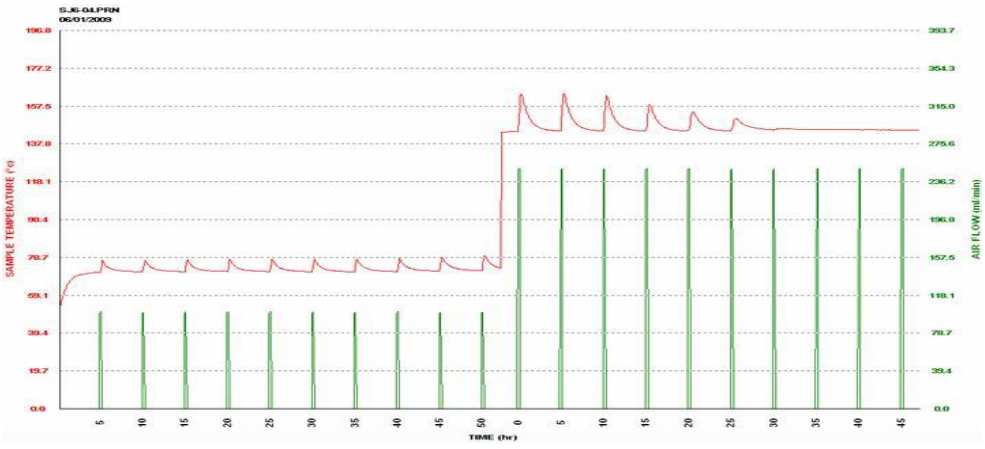

Figure A3: Computer output of control (SJ6-04)

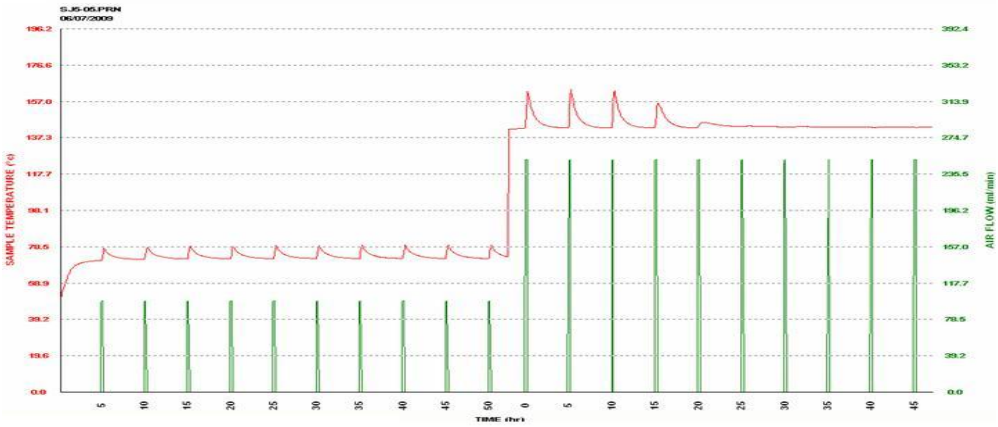

Figure A4: Computer output of sample with 9.57g saturated Sodium Chloride solution (SJ5-05)

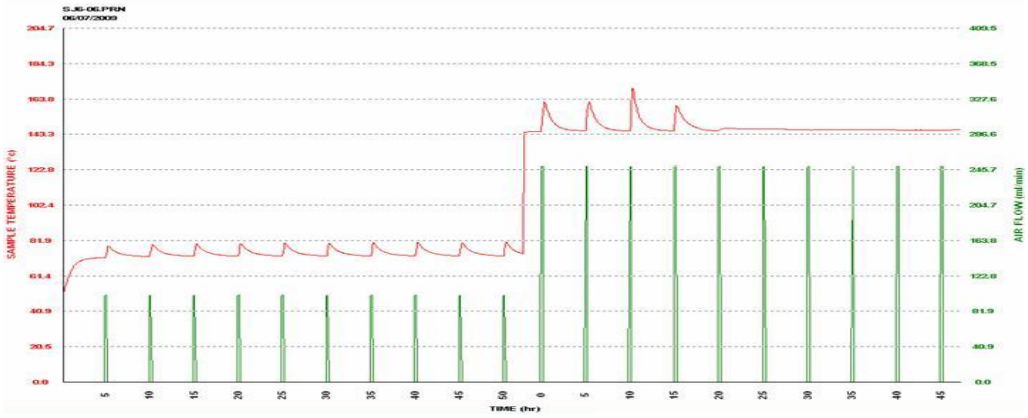

Figure A5: Computer output of sample with 9.57g Sodium Chloride (SJ6-06)

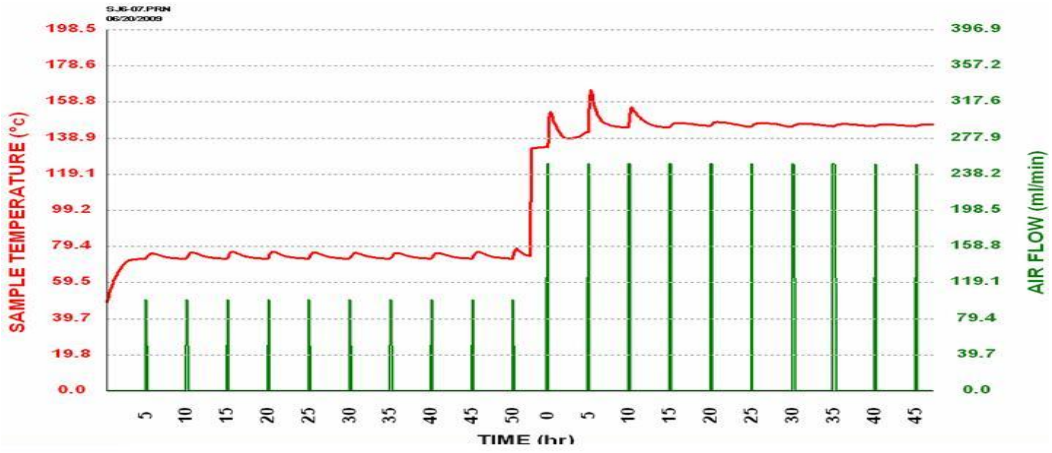

Figure A6: Computer output of sample with 50g Sodium Chloride (SJ6-07)

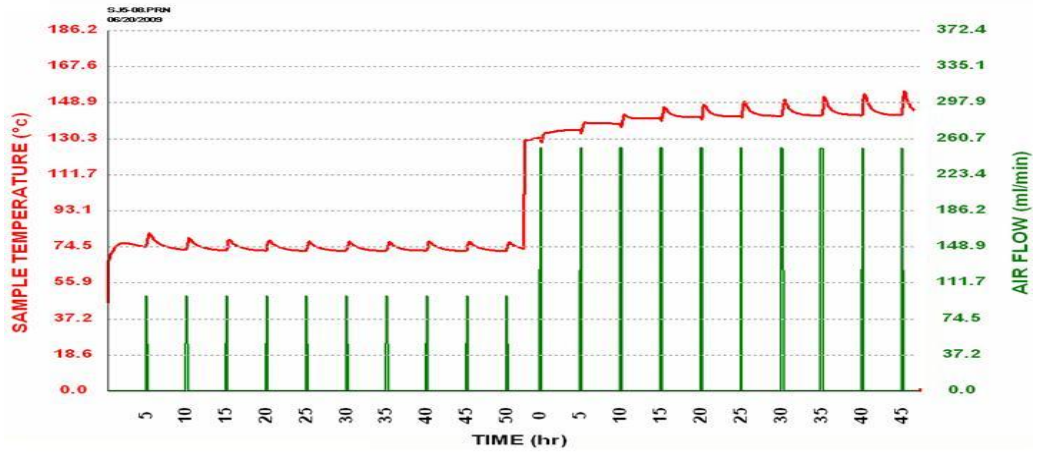

Figure A7: Computer output of sample with 50g Sodium Hydroxide (SJ5-08)

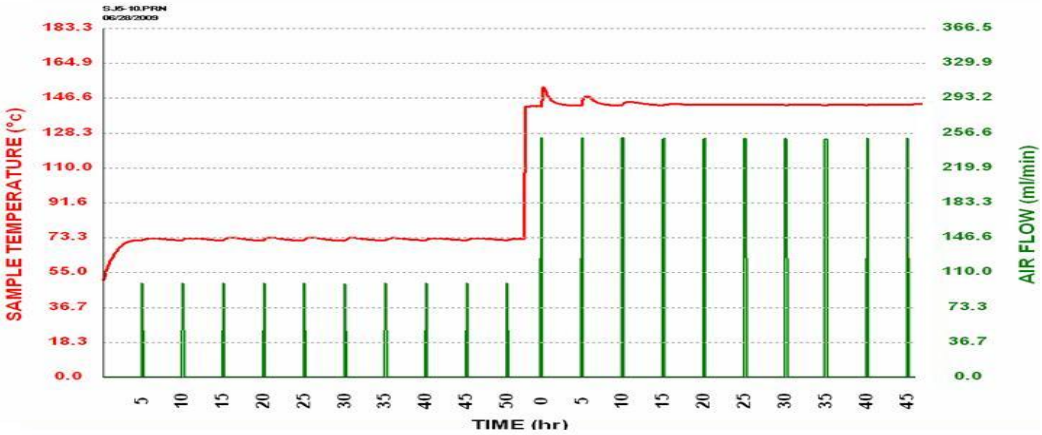

Figure A8: Computer output of sample with 100g Sodium Chloride (SJ5-10)

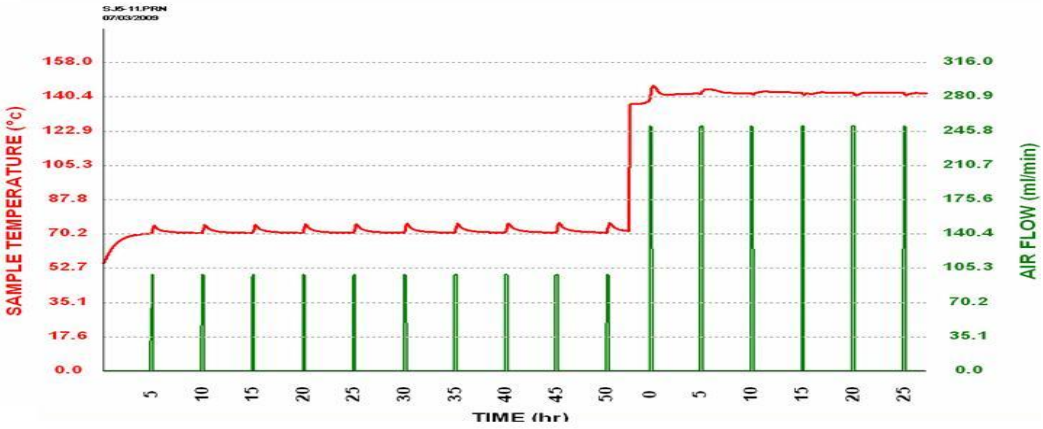

Figure A9: Computer output of sample with 50g Calcium Oxide (SJ5-11)

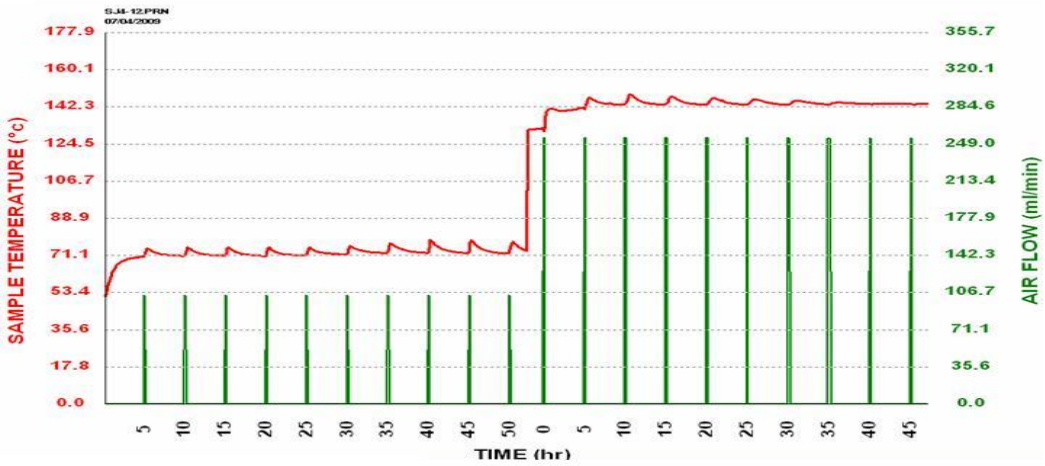

Figure A10: Computer output of sample with 50g Silica Gel (SJ4-12)

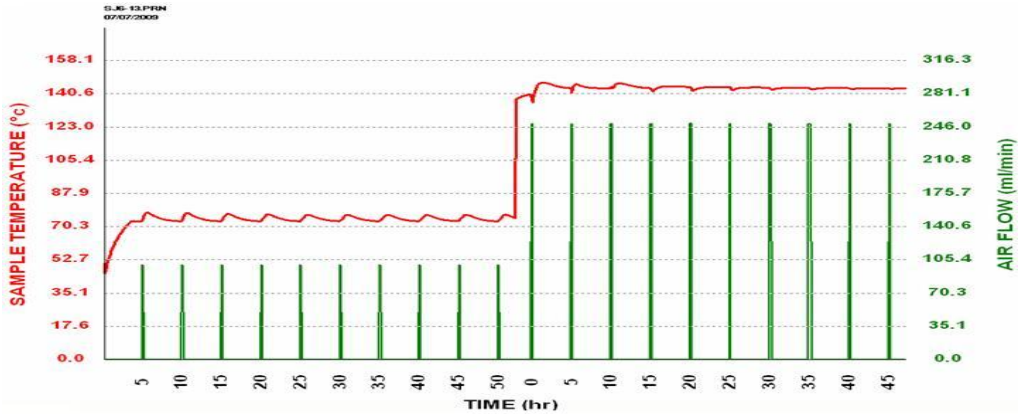

Figure A11: Computer output of sample with 100g Silica Gel (SJ6-13)

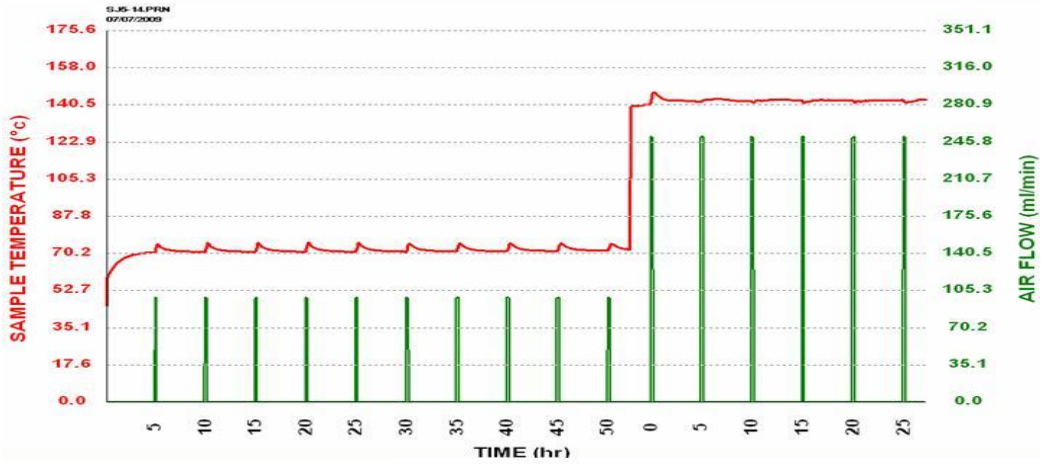

Figure A12: Computer output of sample with 100g Calcium Oxide (SJ5-14)

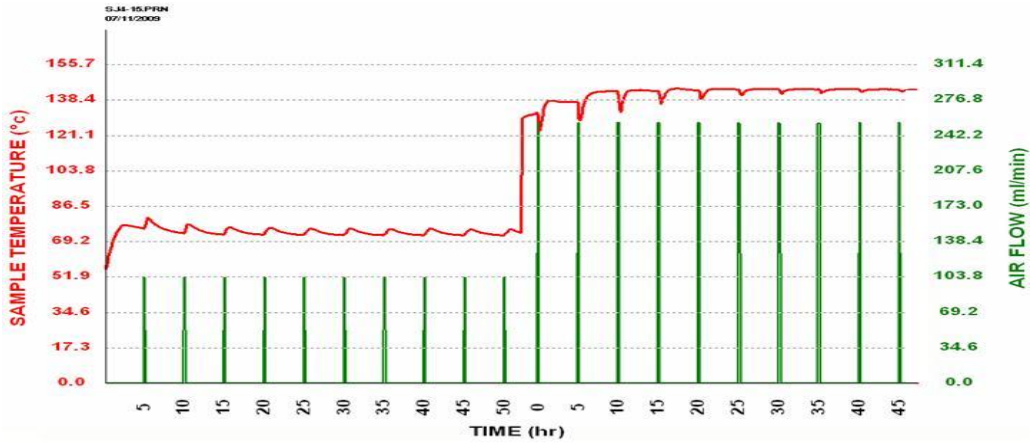

Figure A13: Computer output of sample with 100g Silica Gel layered on top (SJ4-15)

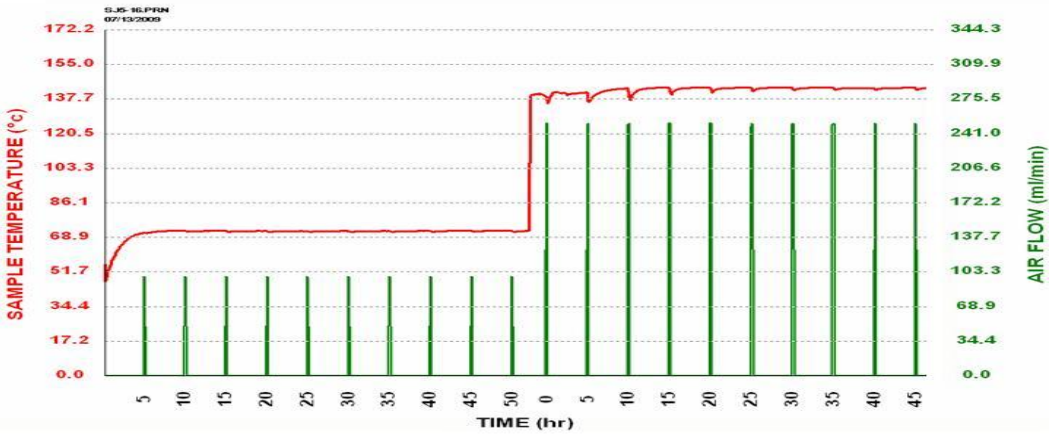

Figure A14: Computer output of sample with 100g Poly (acrylic acid sodium salt) (SJ5-16)

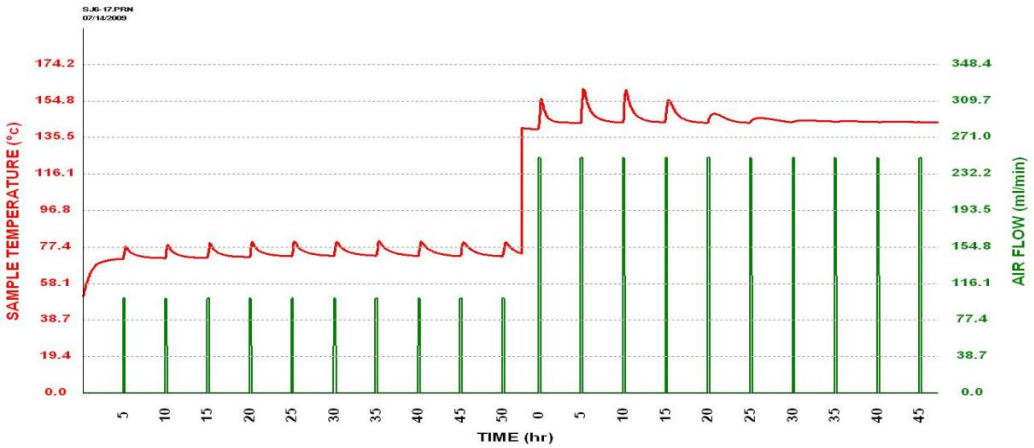

Figure A15: Computer output of sample with 100g Drierite (SJ6-17)

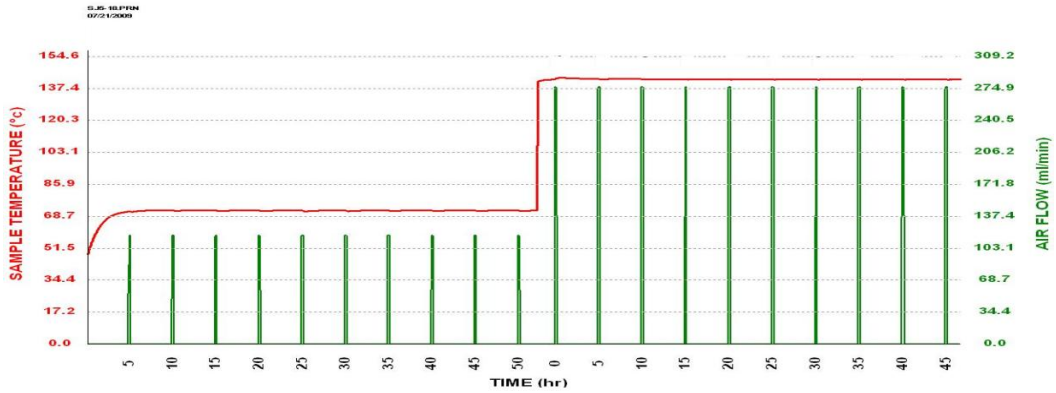

Figure A16: Computer output of sample with 50g Poly (acrylic acid sodium salt) (SJ5-18)

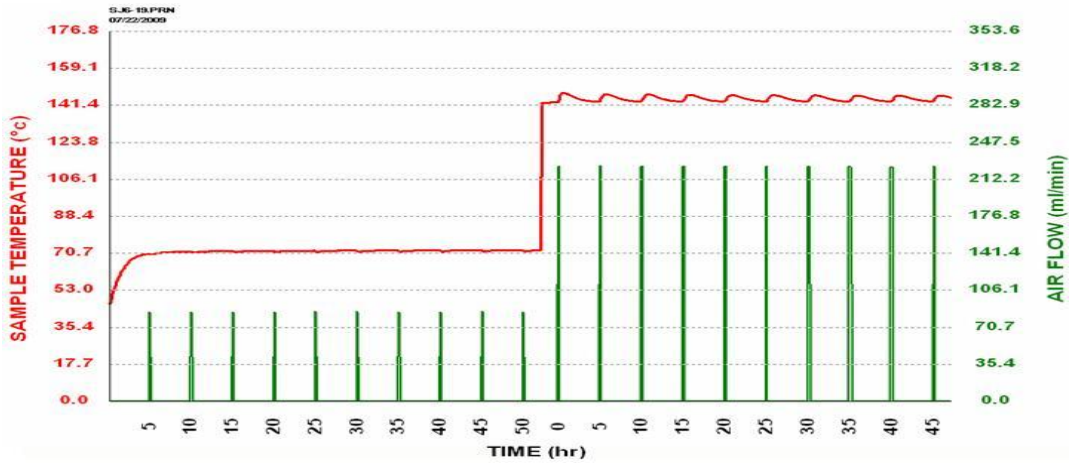

Figure A17: Computer output of sample with 50g F-150 (SJ6-19)

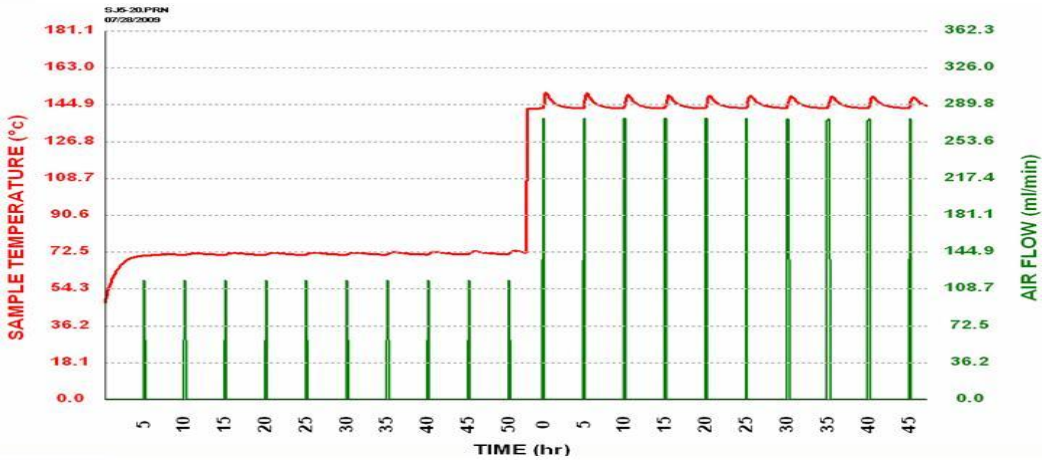

Figure A18: Computer output of sample with 50g F-150 layered on top (SJ5-20)

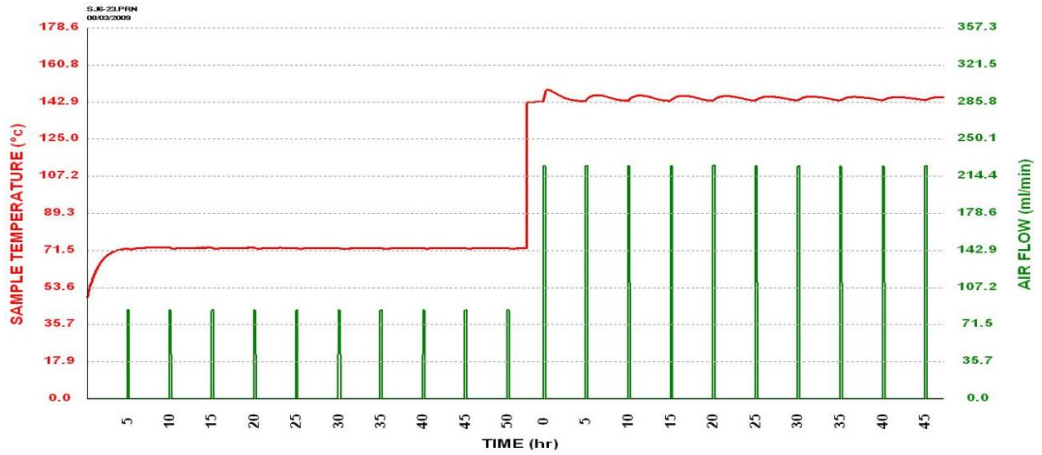

Figure A19: Computer output of sample with 6 weight% F-150 (SJ6-21)

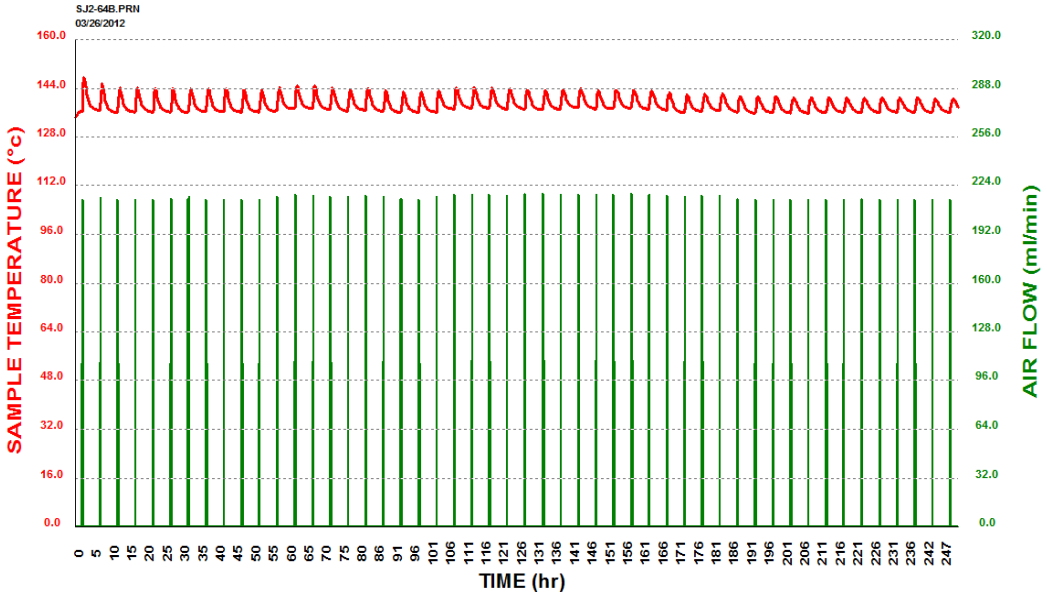

Figure A20a: Stage B computer output RH = 100%, T = 40 ^{o}C (SJW11-20)

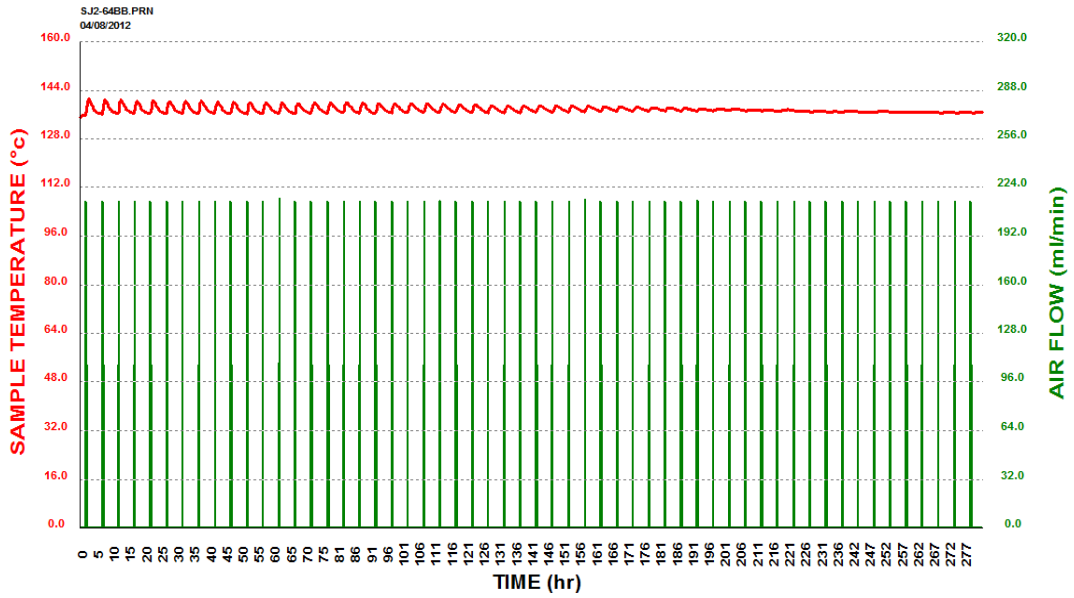

Figure A20b: Stage B computer output RH = 100%, T = 40 °C (SJW11-20)

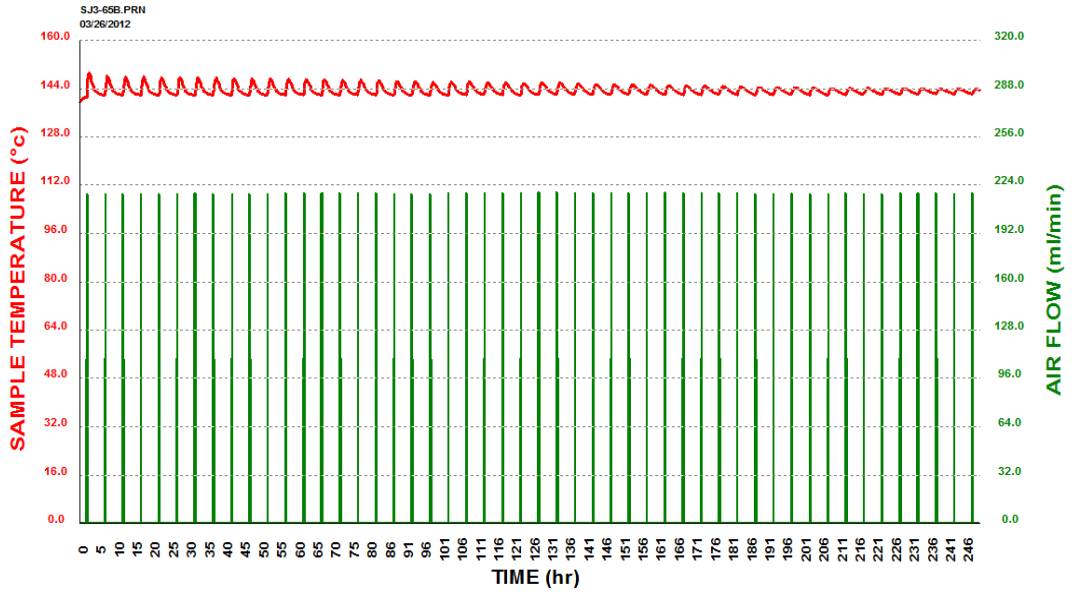

Figure A21a: Stage B computer output RH = 100%, T = 60 °C (SJW22-21)

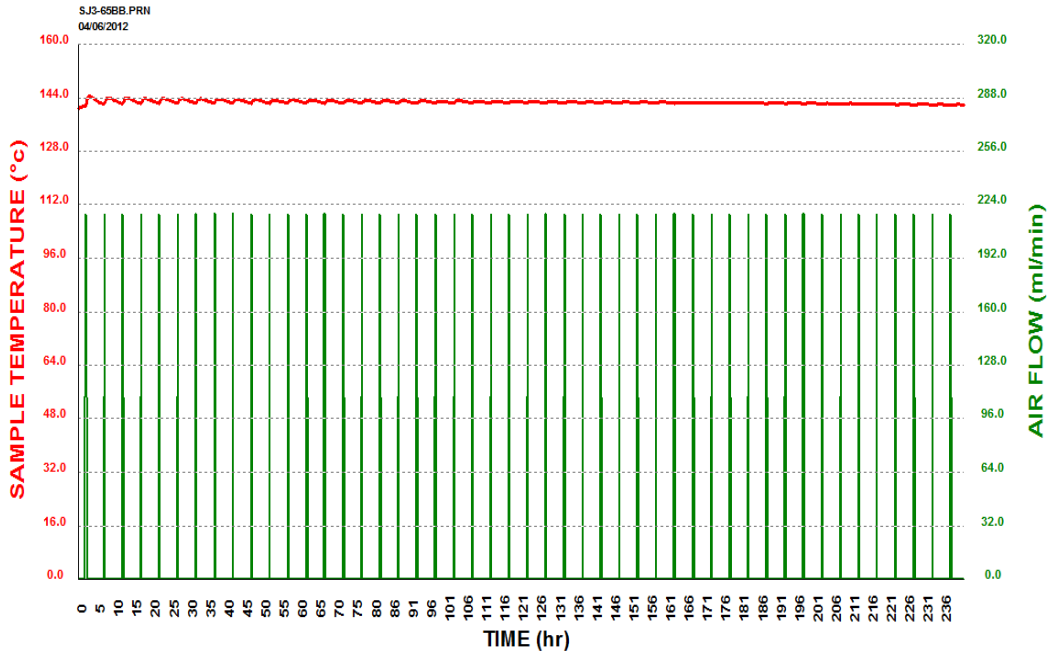

Figure A21b: Stage B computer output RH = 100%, T = 60 °C (SJW22-21)

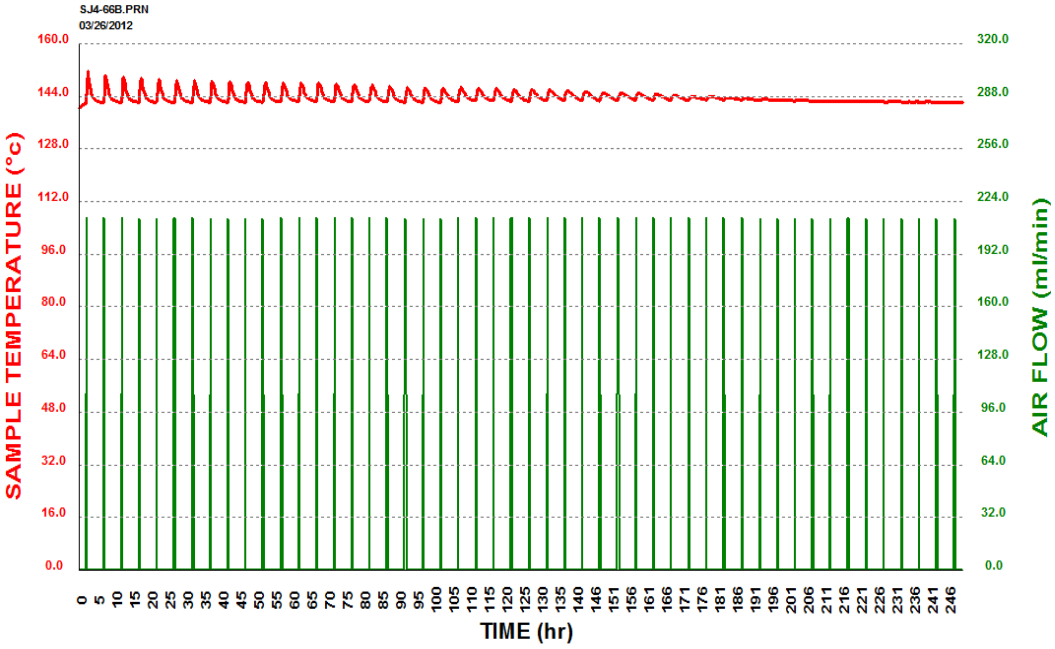

Figure A22: Stage B computer output RH = 30%, T = 40 °C (SJW33-22)

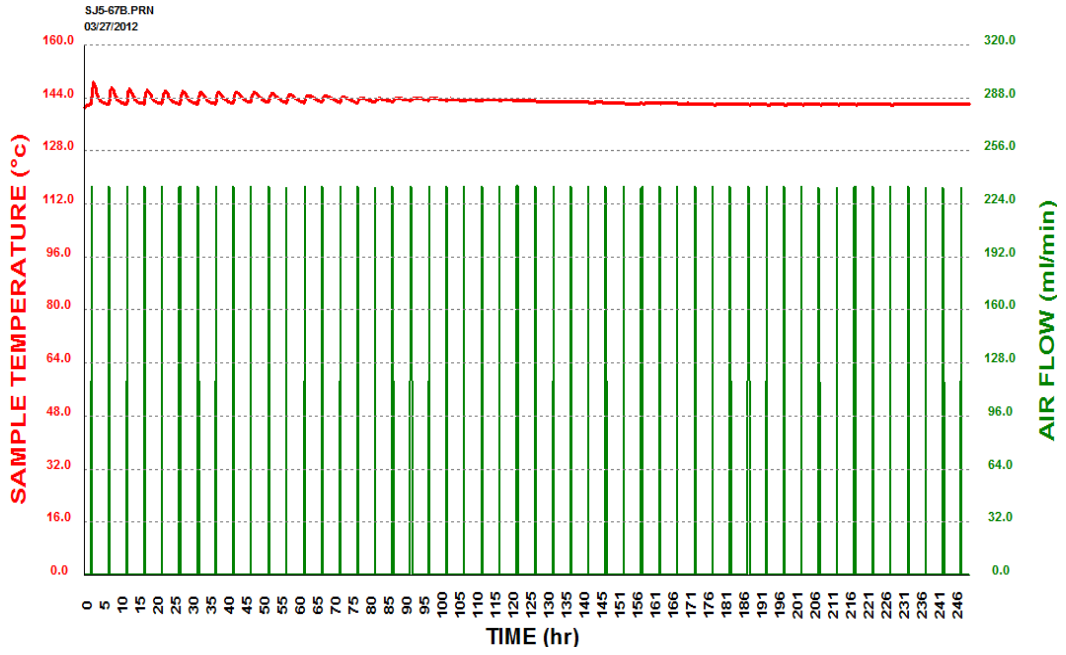

Figure A23: Stage B computer output RH = 30%, T = 60 °C (SJW44-23)

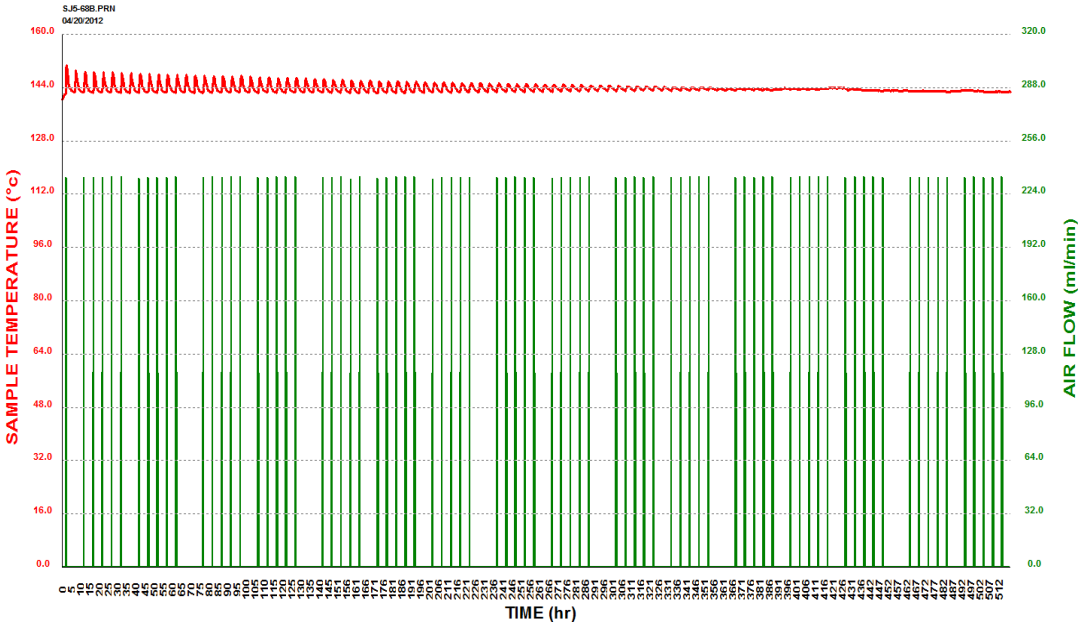

Figure A24: Stage B computer output RH = 70%, T = 40 °C (SJW55-24)

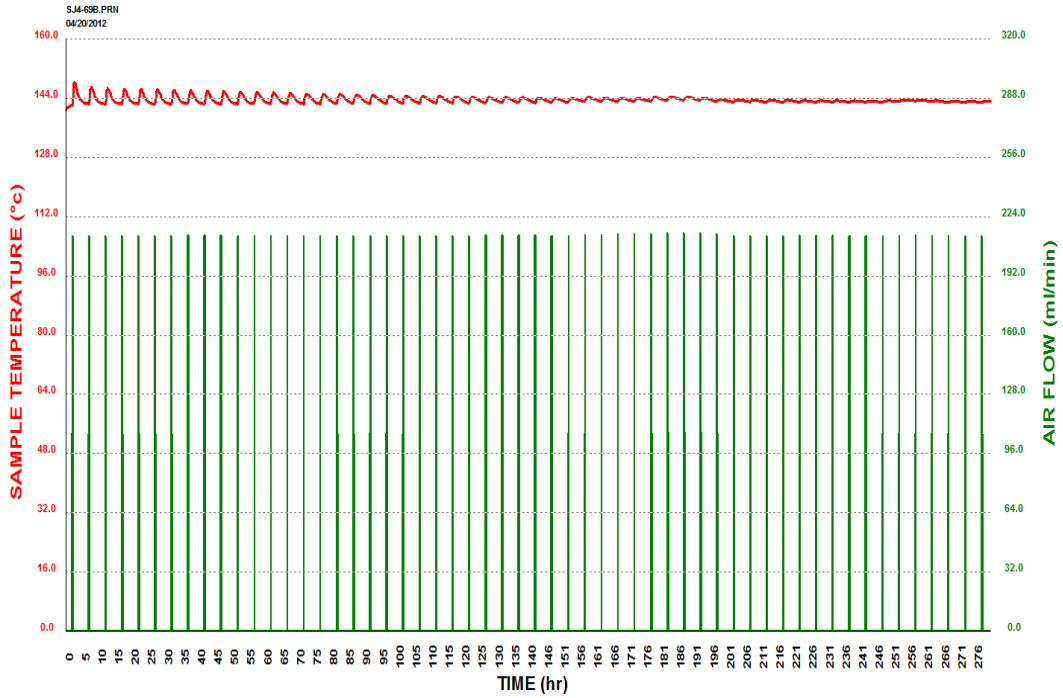

Figure A25: Stage B computer output RH = 70%, T = 60 ^{o}C (SJW66-25)